Ultrasonic Investigation of the Elastic Properties and Liquid Fragility of Bulk Metallic Glasses in the Supercooled Liquid Region

Thesis by

Mary Laura Lind

In Partial Fulfillment of the Requirements

for the Degree of

Doctor of Philosophy

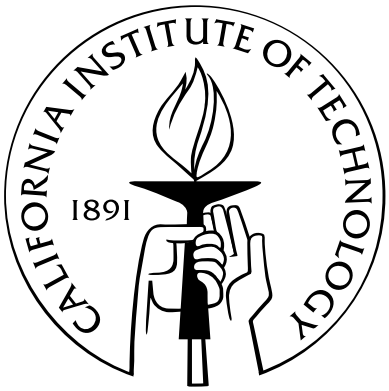

California Institute of Technology

Pasadena, California

2008

(Defended 15 October 2007)

To my family, for their unconditional love, support, and guidance.

Acknowledgements

First I would like to thank Professor Johnson for his great support and inspiration throughout the last 5 years. Professor Johnson's deep understanding, love, and enthusiasm for the subject matter have provided a constant source of inspiration. I thank him for his guidance; he is truly a man of science. Secondly, I would like to acknowledge my thesis committee for their time and input.

Next, I would like to thank all of the members of the Johnson Group, past and present. In particular, I would like to thank my office-mate Gang Duan for fighting with me for our 3rd floor office, for many helpful discussions, and for generally putting up with me for the past 3 years. Dr. Haien Choi-Yim taught me how to use much of the equipment in our laboratory when I first arrived at Caltech, and for this I am very grateful. Dr. Dale Conner also taught me much about the lab as well as graciously allowing me to use both his temperature controller and copper-block heating setup. Jin-Yoo Suh performed all thermal expansion measurement results presented in this thesis. Annelen Kahl joined me at the end of my thesis research and helped me complete many of the last crucial experiments. Joe Schramm was very patient with me. Chris Veazey always had a smile and helpful comment. I'd like to thank Dr. Paul Kim for having my first gigantic batch of Vitreloy-4 alloyed at Liquidmetal. Stewart

Youngblood, a high schooler who only worked in our lab for one month, proved to be incredibly independent and hard working and helped dramatically increase my productivity as I finished the experiments in this thesis. Glenn Garrett: thanks for taking over group meeting duties (and going surfing occasionally). Doug Hoffman's assertiveness was entertaining and motivating. Lastly, from my lab, I would like to thank Dr. Marios Demetriou for just being there.

Many of the experiments I performed in this thesis would not have been possible without the expert machining skills of Mike Vondrus, Mike Gerfen, and Rodney Rojas. In addition to putting up with my difficult requests, they each offered insightful ideas and produced finely machined parts. Pam Albertson helped everything run smoothly from the moment I arrived at Caltech and I thank her for that.

Additionally, I would like to thank Dr. Jan Schroers (now a professor at Yale) for supplying me with the platinum-alloy; and Professor Konrad Samwers for many insightful discussions and his enthusiasm about my research. I would like to thank Dr. Tracy Kidd from G. Ravichandran's group for teaching me the basics of ultrasonic measurements and allowing me to use her equipment until we purchased our own. Dr. Ricardo DiSalvo, of LIGO, has been a joy to talk to and work with. He is incredibly skilled at fixing equipment, and during my second year saved me weeks of down-time by helping me fix the leaking power supply for silver boat.

I would like to thank all of my friends beyond the lab at Caltech who have had an enormous impact both academically and socially. They have truly made this a wonderful experience.

First, many thanks to Max Kresch, my very first friend at Caltech, for allowing me to practically live on his couch our first year of grad school. Without Max's help and study-group organization, I never would have survived classes the first year. I would also like to thank him for being my thesis writing buddy, and suppling me with many delicious meals over the years. Next, I would like to thank Kenji Sasaki whose friendship and smarts have been rock-solid throughout these past 5 years. Kenji helped me connected my experimental apparatus to the computer, and spent many hours fighting with LabView for me. Demetri Spanos is a brilliant guy, and helped me out many times with Matlab, in particlar he helped me with the program to overlap the wavefunctions that is presented in Chapter 2.

Alice has been a great friend and taught me how to make banana bread. The C-boys proved a great outlet for fun beyond work, and I've never enjoyed feeding any group of people more!

I'd like to thank Joanna Dodd for her friendship, lunches at the Ath, helping me create our "SuperMonkey" basketball team, and going to the 2007 Pac-10 Tournament.

Anne Hergarden and Jillian Dempsey have been great friends and great workout buddies, and I know we will keep up the activities even when I leave Caltech.

Many thanks to Nathan Lundblad for watching Duke basketball with me (and converting to be a Duke fan) as well as attending the 2003 Pac-10 tournament with me. Additionally, Lundblad provided much advice and help in using Matlab and La-tex.

I'd like to acknowledge Robb Walters for being authoritative in words and a good friend; Jen Ruglovsky and Jane K. for grounding me with fun activities outside of the lab; and Megan Eckert for swimming, surfing, and biking. Additionally, thanks to all of my friends who I did not mention here: you have all made Caltech a special place.

Emily Hyde and Adam Mutchler have been excellent friends since college, and they were very awesome to hike the JMT with me this summer and provided much guidance in selecting my post-caltech path.

Thanks to my entire family for supporting me throughout all of my education. From keeping me supplied in scuppernoggs to taking me to Greece, I am thankful for every moment.

Finally, Dan Fisher has taught me more than he will ever realize and has been a source of constant inspiration and challenge. Hopefully, our adventures will continue for years to come.

This research was supported by the Materials Research Science and Engineering Center under awards DMR-0080065 and DMR-0520565.

Abstract

In this thesis new methods for accessing the ultrasonic properties of supercooled liquid region in bulk metallic glass forming liquids are presented. Additionally, an extensive examination of the relationship between the elastic properties of metallic glasses and liquid fragility has been undertaken.

In Chapter 2 the novel experimental techniques that have been developed are introduced. The fundamental governing equations for ultrasonic measurements and relationships to the elastic properties, as well as benefits and limitations of the various methods are discussed.

Annealing relaxation experiments were the first method developed for accessing the elastic properties of the supercooled liquid region. Chapter 3 presents the results of annealing experiments from two different alloy systems, Vitreloy-4 (Vit-4) $Zr_{46.75}Ti_{8.25}Cu_{7.5}Ni_{10}Be_{27.5}$ and PdNiCuP - $Pd_{43}Ni_{10}Cu_{27}P_{20}$. In addition to exploring the temperature dependence of the elastic properties of the undercooled liquid and determining the isoconfigurational shear modulus, a relationship between the viscosity and shear modulus was established. It is also shown that the temperature dependence of the shear modulus is, percentage-wise, much stronger than the temperature dependence of the bulk modulus. It is shown that it is possible to accurately

predict the viscosity from the shear modulus. The Angell fragility parameters calculated from previously performed viscosity experiments are compared with the Angell fragility predicted from these new shear modulus measurements.

Chapter 4 explores the application of *in situ* ultrasonic methods utilizing a delay line to measure the elastic properties of low-T_g glasses. Results from the recently discovered series of gold-based glasses are presented.(1)

In situ ultrasonic methods utilizing a novel notched sample geometry are discussed in Section 2.4 and are applied to a variety of metallic glass forming systems with a range of Angell fragilities in Chapter 5. Two of the systems studied were also studied via the *ex situ* annealing methods. The results from both types of measurement compared favorably; thus supporting the claim that we are truly measuring the properties of the equilibrium supercooled liquid. Additionally, a cooperative shear model for the viscosity model and the corresponding "Johnson indices" are presented in Chapter 3.

Chapter 6 discusses two experiments. In the first the possibility of controlling material properties of metallic glasses by varying the cooling rate is examined. It was determined that many other factors come into play. The second experiment was originally designed to measure the *in situ* ultrasonic properties of the organic glass, glycerol. This proved to be beyond our capabilities, however led to an attempt to explore cavitation behavior in glycerol.

Finally, in Chapter 7 concluding thoughts are presented, and the experiments in this thesis are put into a larger context. Future research topics for exploration using the techniques presented in this thesis are discussed.

Contents

List of Figures

List of Tables

Chapter 1

Introduction

1.1 Metallic Glass Overview

Traditional crystalline metallic alloys consist of periodically ordered atoms. Amorphous metals, on the other hand, are essentially "frozen" liquids and have been cooled in such a way that crystallization is bypassed. The resulting metals have no long-range periodic order and many desirable mechanical properties. The first of these materials, $Au_{75}Si_{25}$, was found and reported at The California Institute of Technology in 1960 by Pol Duwez.(10) Later, the first bulk metallic glass (BMG), defined as having a minimum casting thickness of 1 mm was found by Chen.(11) Since then many alloy systems based on various elements (Pd, La, Mg, Pt, Zr, Cu) have been found.(12, 13, 14, 15, 16, 17)

Now, metallic glasses are used for a variety of commercial applications, including medical devices, sporting goods, and thin casings for electronics. One of the long-range goals for metallic glasses is to use them as structural materials. BMGs are much stronger and have much better elastic energy transfer than their crystalline counterparts; this is largely due to the lack of crystalline grain boundaries in the

glassy alloys which, in crystalline alloys, behave as energy sinks. However, one of the major downfalls of metallic glasses is that they tend to fail in a non-graceful, catastrophic manner akin to the way a wine glass shatters.

1.1.1 The Glass Transition

The glass transition phenomenon is an important feature distinguishing glasses from other metallic alloys and is intimately tied in with the unique properties of metallic glasses. This phenomenon exists both in metallic and non-metallic glasses, and is the point/region that distinguishes the solid from the supercooled liquid.

The (rheologic) glass transition temperature, T_g, is defined as the temperature at which the viscosity of the melt is $10^{12} Pa - s$. At this viscosity the time-scale for flow in the amorphous solid is on the laboratory scale. At temperatures well below T_g all glasses are essentially solid for human lifetime and applications. The thermodynamic concept of the glass transition can be seen in Figure 1.1, which demonstrates the temperature dependence of the volume (or enthalpy) of a liquid at a constant pressure. It can be seen that by rapid cooling the liquid can be cooled below the melting temperature. The liquid bypasses crystallization and when the molecular motion of the atoms slows down enough (at T_g) the rate of change of volume (enthalpy) changes sharply and the liquid is essentially "frozen". At T_g both the thermal expansion coefficient and isobaric heat capacity change abruptly but continuously; since none of these things change discontinuously the glass transition is not a true phase transition. This heat capacity anomaly can be seen upon heating a glassy sample at a constant

rate in a Differential Scanning Calorimeter (DSC)

However, there is some difficulty associated with the thermodynamic/calorimetric definition of the glass transition. Different heating rates can yield different glass transition temperatures for the same alloy; in the literature most DSC curves are taken at a rate of 10 or 20 K/s. However, the apparent glass transition temperature can shift due to different heating rates — typically a lower heating rate corresponds to a lower T_g. This is largely related to the idea of frequency dependence of measurements, a concept that will be discussed in more detail throughout this thesis. Different heating rates correspond to different characteristic-length (in distance and time) atomic vibrations/rearrangements in the alloy, thus the transition from solid-like to liquid-like occurs at different temperatures.

In the late 1940s - early 1950s Turnbull predicted that the "reduced glass transition temperature", T_{rg}, was an important parameter characterizing glass forming ability. T_{rg} is defined as the ratio of T_g to the liquidus temperature, and he hypothesized that as this ratio approached 2/3 that homogeneous nucleation of crystals should proceed very slowly on the laboratory time scale.(18, 19) To date, this "Turnbull criterion" is still a quite accurate rule of thumb in the glass community.

Physically, at temperatures above the glass transition region, the viscosity drops very rapidly. Figure 1.2 shows the viscosity of Vitreloy-4 from the glass transition region through crystallization; and the steep drop in viscosity above the glass transition region is apparent. Much of the interesting, and not completely understood, physics of glassy systems occurs in the Supercooled Liquid Region (SCLR), which is

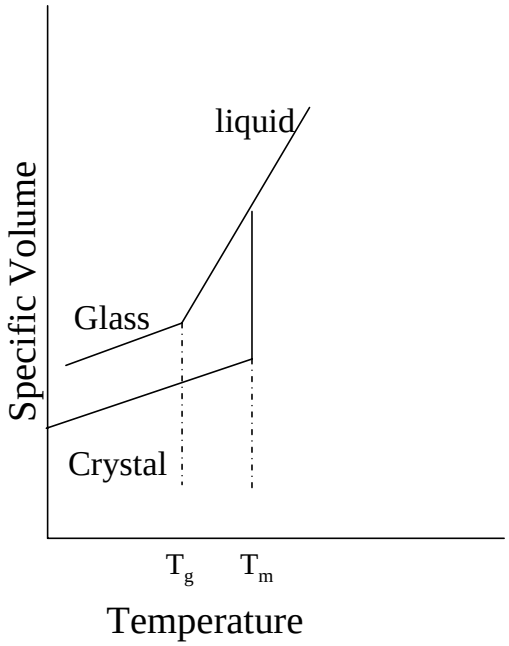

Figure 1.1: The Glass Transition

the region above T_g and below the crystallization temperature (T_x). In the SCLR, due to the decreasing viscosity and thus increasing fluidity, glasses are able to be processed similarly to plastics and can be "net shaped" formed.(20, 21)

1.2 Elastic Properties

Elastic properties are a means for classifying material and comparing material responses to different applied stresses and strains. They provide useful information for predicting how a material will behave under certain conditions and when and how they might fail. Thus, a solid understanding of the elastic properties of a material allows us to choose the appropriate material for a selected application.

For BMGs, the most commonly discussed elastic parameters are the bulk modulus, B, the shear modulus, G, Young's modulus, E, and the Poisson ratio, v. The bulk modulus is a measure of a material's response to a uniform pressure change. The shear modulus measures a material's resistance to shearing. The Young's modulus measures the material's response to uniaxial strain (below the yield strength). The Poisson ratio is a ratio of transverse to axial strain when pulling or pushing on a material; by definition it has an upper limit of .5 (for a perfectly incompressible elastic material).

These properties can either be measured in a destructive manner, using INSTRON-type machines, or in a non-destructive manner utilizing ultrasonics. Within ultrasonics there are two main types of measurements: contact and non-contact. In this thesis we only use and discuss contact methods. Since bulk metallic glasses have no

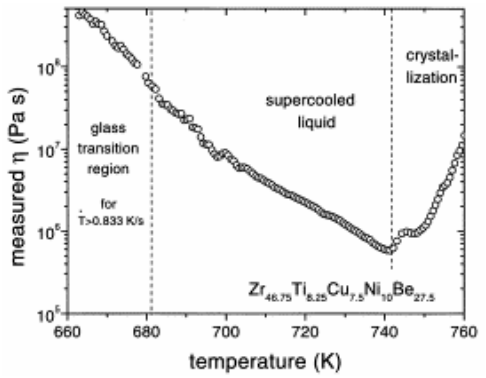

Figure 1.2: Vitreloy-4 plot reproduced from (2), depicting the temperature dependence of viscosity of Vitreloy-4 in the Supercooled Liquid Region through crystallization; this is typical of the viscosity of metallic glasses in the Super Cooled Liquid Region. Note, by definition the glass transition temperature is where the viscosity is $10^{12} Pa - s$, thus the actual initiation of the glass transition temperature is not displayed on this graph.

long-range periodic ordering of the atoms, the elastic properties are considered to be isotropic (the same in every direction). The detailed governing equations for ultrasonic measurements and their relation to elastic constants in isotropic materials are given in Section 2.1.1.

1.2.1 Ultrasonic Measurements

Ultrasonic waves are sound waves that are beyond the frequency that humans are able to hear ($\geq\sim$ 20 kHz). At the simplest level, ultrasonics are a way of studying elastic properties by measuring the time it takes for a sound wave to travel through a sample of known thickness. In 1880, the Curie brothers discovered that crystals could convert ultrasonic energy to electrical energy; and in 1881 the inverse of this, the piezoelectric effect, the ability of a crystal to convert electrical signals to mechanical impulses, was discovered by Lippman. By the mid-1910s, ultrasonics were used to detect underwater objects, and by the 1930s ultrasonic methods had been developed and applied to testing materials.(22) It is possible to use ultrasonics to measure the material properties discussed in Section 1.2. More of the details of the ultrasonic methods employed in this thesis can be found in Chapter 2. A review of previous contributions of ultrasonic techniques to the field of metallic glasses is given in Section 1.4.

1.3 Motivation and Objectives

The main goal of this research is to measure *in situ* elastic properties, particularly the shear modulus, of bulk metallic glasses in the supercooled liquid region (SCLR). The dynamics and rheology of deeply undercooled liquids is a fertile area of condensed matter physics. Much academic debate swirls around the form of the shear modulus (G) versus temperature (T) curve in the supercooled liquid region for metallic glasses.

1.3.1 The Potential Energy Landscape and Cooperative Shear Model

In glass physics there exists the concept of the Potential Energy Landscape (PEL) or corresponding Potential Energy Surface (PES). This is a multi-dimensional function describing the potential energy of a system of N (point-like) particles in 3N coordinates.(23, 24, 25, 26, 27, 28, 29) The PEL itself is not dependent on temperature, but when locally exploring parts of the PEL a physical system will exhibit a strong temperature dependence. PEL formalism is defined by the local minima, and their distribution in energy and their corresponding surrounding potential energy surface. Local minima are separated by potential barriers. Stillinger and Weber introduced a formal exact partitioning of configuration space into distinct basins, or inherent states (IS). A basin consists of all points in space that are connected to the local minimum by the steepest descent path. Sufficiently large thermal fluctuations will allow transitions over the potential barriers to occur, and the system can change its energetic inherent state. Figure 1.3 is reproduced from Debenedetti and Still-

inger's 2001 Nature paper and is a schematic representation of the PEL. From this figure one can get a sense of the "basins" as well as an idea of the barriers between different basins.

For metallic glasses, the yield strength is thought to be determined by the cooperative shear motion of atomic clusters.(30, 31, 32, 33, 34) These clusters are called Shear Transformation Zones (STZs).(30) The STZs, are localized atomic clusters, that can undergo stress-induced transformations that release stored elastic energy.

Recently, combining aspects of PEL/IS theory, the concept of STZs, and the Frenkel analysis of shear strength for solids, Johnson and Samwer have developed a Cooperative Shear Model (CSM) to describe plastic yielding of metallic glasses in the glassy state below T_g.(35) A scaling relationship is constructed between the barrier to shear flow, a critical yield strain (that is determined to be a universal constant), and the isoconfigurational shear modulus. This relationship is discussed in more detail in Section 3.1.

Since the CSM predicts that W, the barrier to shear flow is temperature dependent, it is natural to study the temperature dependence of the components that contribute to the barrier. Thus, since $W \propto G$ it is logical to study the temperature dependence to G.

Using the Johnson-Sawmer barrier the shear modulus, G, of the super-cooled liquid of the glass is related to the viscosity, η. The details of this are given in Section 3.1.5. Also, a relationship between G, η, and the Angell fragility parameter is also discussed.(36, 37) In this section new parameters, including the reduced "elastic

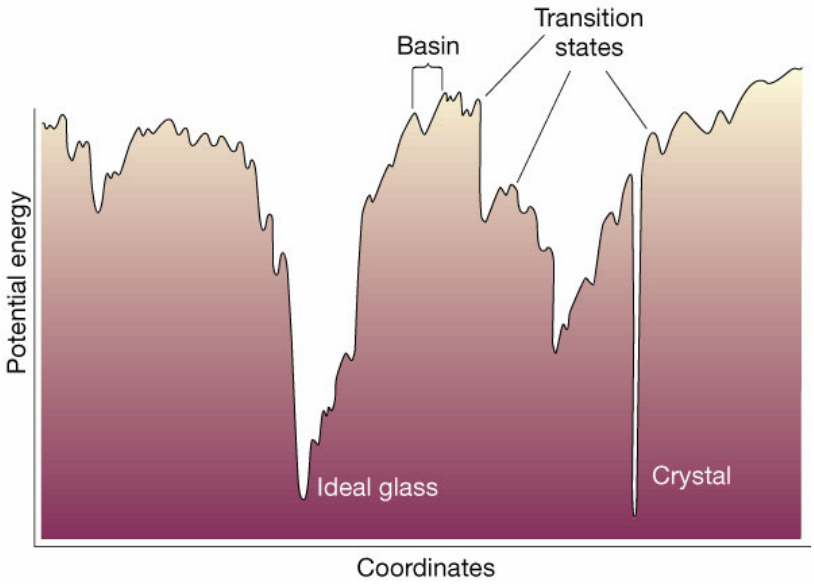

Figure 1.3: Schematic illustration of a Potential Energy Landscape where the x-axis represents all configurational coordinates reproduced from Stillinger(3) (copyright 2001 Nature).

fragility" (n) and "cooperative shear zone fragility" (p) indices are introduced. Later, Johnson et. al. further refined the model relating shear modulus, viscosity, and Angell fragility and found experimentally that for most glasses, $n = p$. (6)

Thus, motivated to try and further understand the Johnson-Samwer barrier, the challenge is to successfully access and measure the elastic properties in the SCLR and determine the shape of the G vs. T curve above T_g.

1.3.2 Viscosity and Fragility

Glasses are considered to be viscoelastic materials. They have time-dependent responses to applied mechanical stresses and strains (38) This viscoelastic response can be described by the Maxwell model

$$\tau_s = \frac{\eta}{G} \tag{1.1}$$

where τ_s is the shear stress relaxation time, η is the viscosity, and G is the shear modulus. Using the definition of viscosity at the glass transition and the fact that G is on the order of GPa at the glass transition, the relaxation time at T_g is on the order of hundreds of seconds.(39) For reference, the viscosity of water at room temperature and pressure is $\sim 10^{-3}$ Pa-s. In the high temperature limit, glasses are expected to approach the viscosity predicted by the Plank limit ($\sim 4 * 10^{-5}$ Pa-s for Vit-4).

Experimentally, there are two main techniques used to measure the viscosity of a metallic glass: parallel plate rheometry and beam bending. In Figure 1.2 parallel plate rheometry was used to measure the viscosity of Vit-4 through the supercooled

liquid until crystallization of the sample. The viscosity of different glasses "falls off" above T_g at different rates.

The Angell fragility parameter, m, was introduced as a way to classify glasses based on their viscosities.(37) It has become a widely used parameter in the glass literature.(40) By plotting the log of the viscosity vs. the dimensionless temperature, T_g/T, the deviation from Arrhenius-like behavior can be assessed by evaluating the derivative of this function at the glass transition temperature. This yields the parameter known as the "Angell fragility parameter", m. This refers to the "kinetic" fragility of an alloy: less-fragile alloys, such as the Zirconium-based alloys, have a lower m≈30 while more fragile alloys such as Pd-based alloys have m≈50

Equation 1.2 is a formal definition of the Angell fragility, where $y = \frac{T_g}{T}$.

$$m = \left[\frac{dln(n(y))}{dy}\right]_{y=1} \tag{1.2}$$

In 1999 Perera performed an analysis of 21 metallic glass forming alloys and found that those with lower critical cooling rates tended to have lower fragility parameters, or in other words to be kinetically "strong".(41) Attempts have been made to correlate the fragility of liquids with elastic properties, mentioned in Section 1.2, of their corresponding glasses.(42) Figure 1.4 is an Angell-type plot of typical metallic and non-metallic glasses reproduced from Busch et al.(4) As can be seen in the plot, metallic glasses fall within a wide range between the prototypical "strong" liquid (SiO_2) and "fragile" liquid (o-terpheynl).

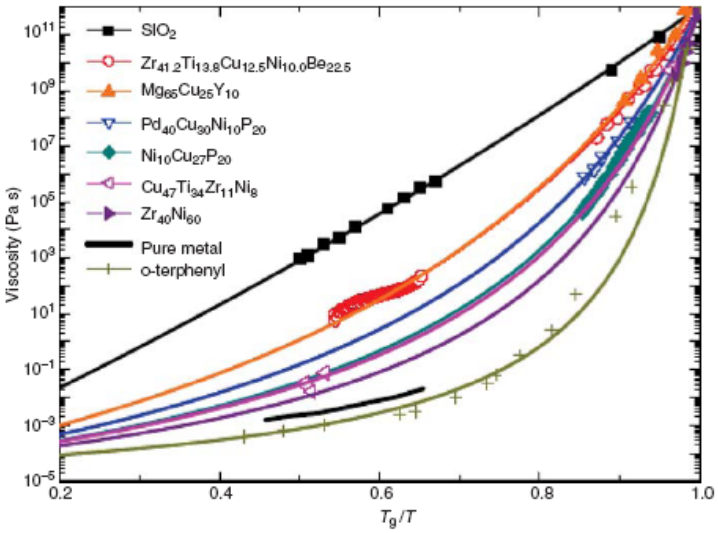

Figure 4. Angell plot comparing the viscosities of different types of glass-forming liquids.[6–8,15,37] Data on the nonmetallic liquids are taken from Reference 20.

Figure 1.4: Angell plot reproduced from (4).

1.3.3 Frequency Dependence of Elastic Properties

A prime example of the frequency dependence of elastic properties is the behavior of the children's toy "silly putty" — a viscoelastic polymer. When silly putty is slowly pulled on (a low frequency event) the material can be stretched to extraordinary lengths. However, when quickly pulling on the same sample of silly putty at the same temperature (a high frequency event), it will hardly stretch at all and quickly "snaps" into two pieces. Thus, depending on the frequency at which we are looking at the material properties, they appear to behave differently.

Returning to the Maxwell model of viscoelastic solids and Equation 1.1, we see that the time-scale for viscoelastic relaxation at the rheologic glass transition temperature is on the order of 100s of seconds at the glass transition temperature. Depending upon the measuring frequency with which we are looking at a property, it may yield different results due to the various time-scale relaxation processes in the material. In glasses there are the "fast" relaxation processes, or those with relaxation times shorter than the Maxwell relaxation time, and "slow" processes. In order to achieve an accurate picture of instantaneous (or isoconfigurational properties) of the glass, we need to measure using instruments that probe more rapidly than the timescale on which the "fast" relaxation occurs.

1.4 Review of Past Ultrasonic Contributions to Metallic Glasses

Ultrasonic studies through non-contact methods (such as Electromagnetic Acoustic Resonance (EMAR)) have been performed on metallic and non-metallic glasses. Elastic properties can also be measured by studying the vibration characteristics through Brillioun scattering. However, this thesis focuses exclusively on contact ultrasonic methods.

Most of the work using ultrasonics to study metallic glasses done prior to the year 2000 was to either study the room-temperature characteristics of a series of alloys of varying compositions or to measure the low-temperature (from 4K to 300K) temperature behavior of the properties. H.S. Chen and collaborators measured the room temperature sound velocities and hardness of a series of Pd- and Pt- based glasses and correlated the Poisson ratios' with the composition of these glasses. They also noted that the alloys with higher Poisson ratios tended to be more ductile.(43) Egami et al. utilized a torsional pendulum to measure the shear modulus of thin ribbons of metallic glass in 1984, studying the effect of structural relaxation on the shear modulus of the glass.(44) In 1986, Lambson et al. studied the low-temperature dependence of the elastic properties of $Pd_{40}Ni_{40}P_{20}$.(45)

More recently, the temperature dependence of the elastic properties of lanthanum gallogermanate glasses was studied by Hwa et al.(46) While they present results over a very large temperature range, they only take data points on the order of every

70–100 degrees. They utilize a "specially designed high temperature piezoelectric transducer," but when contacted gave no response upon where/how to get/fabricate such a transducer.

Ichitsubo et al. use EMAR techniques at relatively low-frequencies (300–1500KHz) to study the elastic properties of Zr and Pd-based glasses. They claim that the ultrasonic vibration instigates early crystallization in the alloys.(47, 48, 49)

The W.H. Wang group has done numerous studies investigating the *in situ* pressure dependence of the elastic properties of glasses.(50, 51, 52) They have also done stepwise annealing of glasses near the glass transition temperature until they crystallize.(53)

Most recently, in 2007, studies by Inoue have measured *in situ* elastic properties of BMGs via ultrasonics. However, in the these measurements the shear sound velocity is not measured directly from a shear signal sent into the sample, but by measuring the "trailing" pulse of a longitudinal wave and using mode conversions to calculate the shear sound velocity.(54) In this thesis all of the shear sound velocities were measured directly using a shear sound wave. Additionally, the measuring frequencies used by Inoue et al. are a factor of 2 lower than the measuring frequencies used in most of the experiments presented in this thesis.

1.5 Key Contributions

The key contributions made in this thesis were the development of new methods for accessing the ultrasonic properties of supercooled liquid region in bulk metallic glass

forming liquids. Additionally, an extensive examination of the relationship between the elastic properties of metallic glasses and liquid fragility has been undertaken.

In Chapter 2 the novel experimental techniques that have been developed are introduced. The fundamental governing equations for ultrasonic measurements and relationships to the elastic properties as well as benefits and limitations of the various methods are discussed.

Annealing Relaxation experiments were the first method of accessing the elastic properties of the supercooled liquid region that were developed. Chapter 3 presents the results of annealing experiments from two different alloy systems, Vitreloy-4 (Vit-4) $Zr_{46.75}Ti_{8.25}Cu_{7.5}Ni_{10}Be_{27.5}$ and PdNiCuP - $Pd_{43}Ni_{10}Cu_{27}P_{20}$. In addition to exploring the temperature dependence of the elastic properties of the undercooled liquid and determining the isoconfigurational shear modulus, a relationship between the viscosity and shear modulus was established. It is also shown that the temperature dependence of the shear modulus is, percentage-wise, much stronger than the temperature dependence of the bulk modulus. It is shown that it is possible to accurately predict the viscosity from the shear modulus. The Angell fragility parameters calculated from previously performed viscosity experiments are compared with the Angell fragility predicted from these new shear modulus measurements.

Chapter 4 explores the application of *in situ* ultrasonic methods utilizing a delay line to measure the elastic properties of low-T_g glasses. Results from the recently discovered series of gold-based glasses are presented.(1)

In situ ultrasonic methods utilizing a novel notched sample geometry are discussed

in Section 2.4 and are applied to a variety of metallic glass forming systems with a range of Angell fragilities in Chapter 5. Two of the systems studied were also studied via the *ex situ* annealing methods. The results from both types of measurement compared favorably; thus supporting the claim that we are truly measuring the properties of the equilibrium supercooled liquid. Additionally, a cooperative shear model for the viscosity model and the corresponding "Johnson indices" are presented in Chapter 3.

Chapter 6 discusses two experiments. In the first the possibility of controlling material properties of metallic glasses by varying the cooling rate is examined. It was determined that many other factors come into play. The second experiment was originally designed to measure the *in situ* ultrasonic properties of the organic glass, glycerol. This proved to be beyond our capabilities. We also attempted to explore cavitation behavior in glycerol.

Finally, in Chapter 7 concluding thoughts are presented. Future research topics for exploration using the techniques presented in this thesis are discussed.

Chapter 2

Introduction to Ultrasonic Measurements and Experimental Apparatus

Ultrasonic measurements are utilized for a variety of applications, from finding defects and flaws in metallic parts to imaging human internal organs. In addition to being relatively simple, ultrasonic measurements have the added benefit of being nondestructive.(22) There are a variety of methods, either contact or non-contact, of introducing an ultrasonic signal into a sample. In this thesis, only contact methods have been employed.

2.1 Experimental Setup

The basic system needed to perform ultrasonic measurements consists of a transducer, an oscilloscope, and an electrical pulser/reciever (PR). The PR generates pulsed electronic wavepackets which the piezoelectric transducer converts into mechanical oscillations that are sent into a sample. The oscilloscope allows the monitoring and recording of these electrical signals. Ninety percent of the ultrasonic measurements

presented in this thesis were performed with Ultran 25 MHz transducers, a tektronix 1500 oscilloscope, and a Panametrics 3500 pulser/reciever. Some measurements were done with 5 MHz transducers from Panametrics.

There are two basic types of transducers: those that generate shear waves and those that generate longitudinal waves. Longitudinal waves produce oscillations in the direction of propagation of the wave while shear waves produce oscillations perpendicular to the direction of wave propagation. In order to obtain a complete picture of the elastic properties of the material it is necessary to have both types of transducer. Both types of transducers send and receive signals. The 25 MHz Ultran transducers have built-in delay lines: the shear transducers have a quartz delay line with a delay time of 10.6 μs, while the longitudinal transducers have a plastic-based delay line with a delay time of 5.6 μs. There is no built-in delay line for the 5 MHz Panametrics transducers.

In addition, a method of digital signal acquisition and processing was developed. The oscilloscope was connected to a Windows-based personal computer through a GPIB interface. A labview program was created to interface with the oscilloscope allowing the computer to digitally capture and save data points for the various signals. Later analysis, through a Matlab program, of these captured signals yields the transit time taken for the different types of sound waves to traverse the sample.

2.1.1 Governing Equations

For elastic waves in an isotropic medium, the following equations hold:

$$C_t = \sqrt{\frac{\mu}{\rho}} = \sqrt{\frac{G}{\rho}} \tag{2.1}$$

$$C_l = \sqrt{\frac{\lambda + 2\mu}{\rho}} = \sqrt{\frac{3K + 4G}{3\rho}}. \tag{2.2}$$

In these equations, C_t is the transverse, or shear, sound velocity; the shear wave propagates through a sample with the direction of material motion perpendicular to the direction of wave propagation. C_l is the longitudinal sound velocity, in which the material motion is parallel to the direction of wave propagation (this is also called a compressional or pressure-wave). Lamé parameters, μ and λ, are commonly used in elasticity theory, ρ is the density of the material, G is the shear modulus, and K is the bulk modulus. By measuring C_t, C_l, and ρ, Equations D.3 and 2.2 can be solved for G and K or λ and μ.

Another, slightly more intuitive, physical way to think of the shear and bulk modulii are as follows:

$$G = \frac{\delta\tau}{\delta\gamma} \tag{2.3}$$

where τ is the shear stress and γ is the shear strain. The thermodynamic definition of bulk modulus is as follows:

$$K = -V\left(\frac{\delta P}{\delta V}\right). \tag{2.4}$$

As a rule of thumb, as first determined by MD simulations and later by experiments, the bulk modulus of a glassy metal is $K \approx .95K_{crystalline}$ while the shear modulus of a glassy meal $G \approx .7G_{crystalline}$.(36)

The Poisson ration is a combination of both the shear and bulk modulii and is defined as follows:

$$\nu = -\frac{\epsilon_{lateral}}{\epsilon_{longitudinal}} = \frac{\lambda}{2(\lambda+\mu)} = \frac{1}{2}\left[\frac{3-2\frac{G}{K}}{3+\frac{G}{K}}\right] \tag{2.5}$$

In theory the Poisson ratio can range from negative to .5, most rubbers have a Poisson ratio of .45 while cork has a Poisson ratio close to 0. In the limit where G approaches 0, the Poisson ratio approaches .5, corresponding to a material with conservation of volume upon deformation. Recently, in the glass physics community, the Poisson ratio has been correlated with the liquid fragility as well as the fracture toughness and ductility of glassy alloys.(55, 56, 57)

Young's Modulus may also be calculated from these measured values.

$$E = 2G(1+\nu) \tag{2.6}$$

2.1.2 Pulse-Echo Vs. Through Transmission

There are two major types of ultrasonic measurements used in this work: pulse-echo and through transmission. The majority of the measurements in this thesis were performed with the pulse-echo technique. Each technique has specific benefits and drawbacks.

In pulse-echo measurements the acoustic signal is sent and received with a single transducer. Successive reflections off of the "back-wall" of the sample are overlapped, and thus the time delay for the signal to travel two lengths of the sample is calculated. Pulse-echo measurements are considered the standard type of measurement in the ultrasonic world. With pulse echo measurements it is often easy to see defects and other non-uniformities within samples. See Figure 2.1 for a sample pule-echo measurement reflection train and echo overlap. Also see Appendix E for the Matlab code used in processing pulse-echo data.

In through-transmission measurements the acoustic signal is generated in one transducer and received by a second transducer. The signal passes once through the length of the sample. Prior to sample measurement, the intrinsic time delay of the signal to pass from the first to the second transducer is measured and then subtracted from the time measured with the sample. Through-transmission measurements are useful for materials that have strong acoustic-attenuation. In this thesis this type of measurement has been used to measure very thin ($\sim$.2 mm) samples.

Ultrasonic waves generally travel with low attenuation through metallic materials, due to the high density and uniformity of the material. In contrast, ultrasonic waves do not propagate well through porous or mechanically "soft" materials.

2.2 Room Temperature Measurements

To perform simple ultrasonic measurements on metals at room temperature the most important things are (1) to have a sample of the proper size and shape with highly

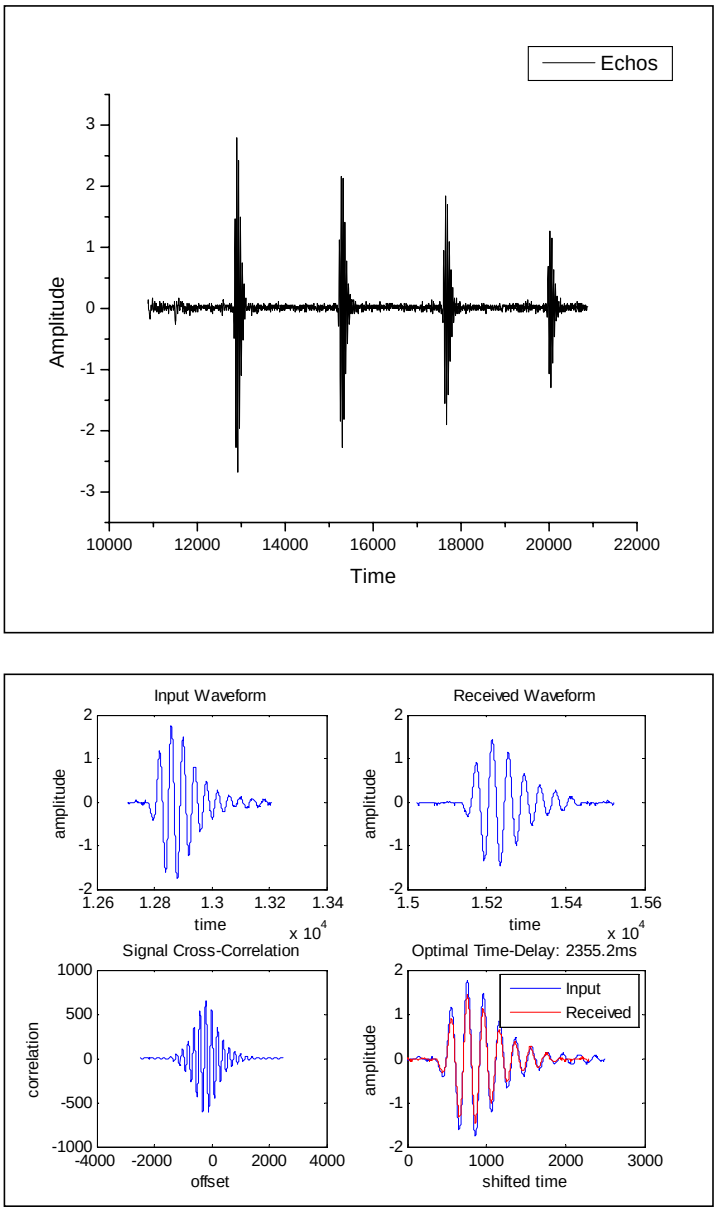

Figure 2.1: Top: sample pulse-echo wave train captured via labview. Bottom: overlap of pulse-echo reflections via Matlab. Note, the scale of the input and received waveforms are different time-scales, in the top figures of (b), but as can be seen in the lower right corner of (b) they are of essentially the same pulse-width and amplitude.

polished surfaces and (2) a transducer of the proper frequency. Equally as important as the sample preparation and geometry is the method of coupling the transducer to the sample. In particular the couplant for shear waves needs to be viscous enough to support the shear wave, while at the same time fluid enough to wet and form good contact between the face of the transducer and the sample. There are commercially available shear wave couplants from companies such as Panametrics, but we have found that simple honey works as well and is much less expensive. The longitudinal couplant used was Paker Aquasonic 100 Gel.

Precise measurement of both sample density and sample thickness are vital to obtaining accurate results. If these measurements are sloppy, large errors will propagate through the calculation of the elastic properties from the sound velocities. Density was measured according to American Society for Testing of Materials (ASTM) standard C-693. Sample thicknesses were measured multiple times using a micrometer.

2.3 Delay Line Measurements

Performing in-situ measurements above or below room temperature poses a challenge. Generally it is not possible to subject the transducers to extreme temperatures (less than 0C or greater than 70C). To avoid this but still enable the sample to be cooled or heated, a "delay line" was introduced.(58) The delay line, or buffer rod, is not a novel idea, but its use with metallic glasses is. In the experimental setup at hand, quartz was chosen as the ideal delay-line material: not only because the built-in delay-line of the shear transducers is quartz (and thus there is minimal impedance mismatch

between the transducer and the delay), but also because quartz has a relatively low thermal conductivity and thus will not rapidly conduct heat to the transducer. Care was taken when selecting the length of the delay line so that the reflections from the delay line would not overlap or be confused with reflections from the built in delay of the transducer. Additionally, it was necessary to have a highly polished surface on both ends of the delay line. At room temperature honey and aquasonic gel worked to couple the transducer to the delay line and ultimately to the sample. However, the above couplants failed at both low and high temperatures. Many different mechanisms of coupling the delay line to the sample were tested (see Appendix B for complete results of both successful and unsuccessful methods).

Ultimately, it was found that Varian Torr-Seal 2-part vacuum sealer was capable of both transmitting the acoustic signal and maintaining the bond between the sample and the delay line at temperatures as low as liquid nitrogen. The 2-part torr seal solution was mixed and within 5 minutes a small dab was applied to the cleaned and polished sample surface, the sample was then slowly twisted onto the end of the polished delay line. The sample was rotated such that the thinnest possible, but still complete layer of Torr-Seal connected the two parts. The part was then allowed to air-dry at room temperature for a minimum of 1 hour and up to 24 hours to ensure adequate bonding. After use, the sample could be removed from the delay line by a combination of mechanical force and acetone.

While a successful means to couple the delay line to the sample was found for low-temperature measurements, a simple solution for high-temperature measurements was

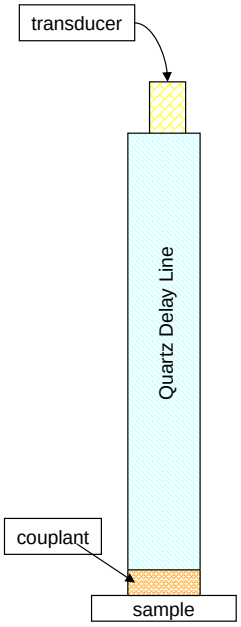

Figure 2.2: Schematic of delay line concept, note that the figure is not to scale — the thickness of the couplant layer is extremely exaggerated

not found as easily. Again, many different types of adhesives and cements were tested to see if they would both resist high temperatures and transmit the acoustic signals. A major problem for high-temperature measurement is that most good glass formers that we are studying have T_gs greater than 200C, while most organic adhesives begin to break down around 100-150C.

It was eventually discovered that Big-Swell High Quality S-250A Clear Sanding Resin with catalyst (primarily used for home-repair of fiberglass surfboards) was capable of transmitting an acoustic signal from a quartz delay line into a metallic sample at temperatures up to 150C. However, to date, no adhesive has been found that supports the shear wave above 150C.

2.4 "Notched" Sample Measurements

In the 1980s in Britain, DP Almond and S Blairs created an apparatus to measure the sound velocities of liquid metals. They successfully employed a long silica delay line to measure *in situ* sound velocities in liquid indium and liquid mercury.(58) Both of these metals have melting points below 160C. This apparatus precisely measured the height of the delay line in the liquid, and by changing this height they were able to obtain very accurate measurements. While interesting, this method was not readily applicable to our metallic glass systems. In the temperature range we desire to study, the viscosity of the alloys changes from solid-like to liquid-like.

Finally I unearthed a paper by JT Krause, published in 1961, attacking this problem from a different point of view. In this paper the concept of differential path

length was introduced.(59) A long rod of the desired material is made and at one end a notch is cut and removed. This lower part of the sample is then placed into a heat sink/source while the opposite end of the sample is kept out of the furnace at room temperature, thus allowing contact via honey of the transducer to the sample. See Figure 2.3 for a visual of how this powerful concept works. I discovered that it was not necessary to completely remove the notched section from the sample, but that a simple clean, straight cut (forming the top of the notch) parallel to the end face of a metallic or organic glass rod was usually sufficient to produce high quality reflections from the "notch surface". When creating the notch it is important that the position at which the notch is placed is carefully chosen, so as not to overlap with one of the built-in reflections (if using 25 MHz transducers).

For both delay-line and notched measurements the transducer is held in-line with the delay line or rod-sample through an aluminum fixture, as well as slight pressure. In addition to holding the transducer in place and allowing for the tracking of one ultrasonic signal through the heat-up and cool down process, the applied axial pressure also helps improve the coupling of the signal to the sample.

As the temperature of the experiment increases (and the gauge section passes) through the glass transition temperature, the viscosity of the glass decreases rapidly. This decrease in viscosity coupled with the pressure applied to maintain the inline positioning of the transducer tends to cause the sample to slowly flow and deform. Thus, design of an appropriate sample holder with the ability to prevent the sample from significantly deforming was critical. Additionally, because the viscosity of the

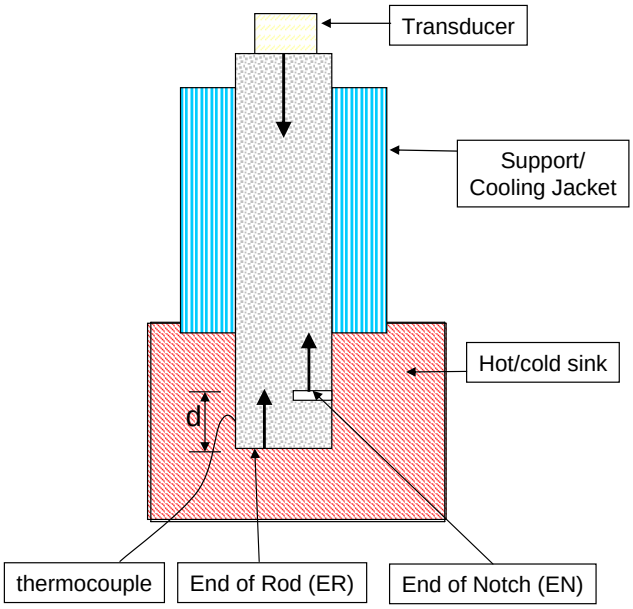

Figure 2.3: Notched sample geometry. The transducer and one end of the rod is kept at room temperature. The delay time for the signal to travel between EN and ER, over the distance d, is measured. The lower portion of the sample is kept at the desired temperature by submersion in either a cold bath or in a copper heat sink.

sample decreases rapidly above T_g and because there is slight applied pressure to form contact between the transducer and the rod, the cut notch is prone to collapse by pressure-induced flow. Therefore it was also necessary to insert a quartz-chip within the notch to maintain the integrity of the notch during heating and measurement.

2.5 Hot/Cold Sinks

To create uniform temperatures for the samples both attached to the end of delay lines and the "notched" region of the rods during in-situ measurements, hot and cold sinks were devised.

The hot sink consists of two 8 x 4 x .5 inch copper blocks, with two holes drilled through the length of each. These holes allowed 150-watt heating cartridges to be inserted directly into the block. The heating cartridges were wired to a 5-Ampere DC power supply that allowed the current level to be manually adjusted to obtain a block temperature with an accuracy of one degree Celsius. A 13-mm diameter hole was drilled completely through the thickness of the top copper block and halfway through the thickness of the bottom block; thus allowing a sample to be in contact with the large heat reservoir of high thermal conductivity; this ensured temperature uniformity of the blocks. Additionally, the blocks were insulated with fire brick and/or pipe insulation. A thermocouple was brought between the top and bottom block, and into direct contact with the sample to accurately record the temperature of the sample in the gauge system during measurement. Small cylindrical samples with polished flat surfaces were attached to the end of the quartz-delay-lines were in direct contact with

the bottom copper block. Split copper molds were designed to encase the notched rod samples: they have interior flat bottoms and inner diameters of either 5 or 7 millimeters, and are held tightly closed around the samples by set screws. The molds are sized to slip-fit into the central hole in the copper blocks to ensure excellent physical contact and heat transfer.

The cold sink consisted of an aluminum stand placed in the center of an insulating cup. Methanol was then poured in the cup to a level that completely covered the sample (or region of the sample to be measured). A thermocouple is placed into the cup touching the area to be measured. The temperature could then be controlled very precisely by adding small amounts of crushed dry-ice to the methanol and allowing the mixture to come to a metastable equilibrium; methanol and dry ice reach a stable equilibrium at -77 C.

Chapter 3

Relaxation Experiments in Glasses

Prior to getting the *in-situ* high-temperature experiment to work, we determined the best way to access the super-cooled liquid was to anneal and quench the samples from temperatures in the super-cooled liquid region and then measure the properties at room temperature. The first study of this type was performed on Vitreloy-4 $Zr_{46.75}Ti_{8.25}Cu_{7.5}Ni_{10}Be_{27.5}$ and the second on $Pd_{43}Ni_{10}Cu_{27}P_{20}$. Vit-4 was chosen because it has a large supercooled liquid region and is robust to phase-separation in the undercooled liquid.(2) The Pd-based alloy was chosen for its large supercooled liquid region and resistance to crystallization and oxidation.

3.1 Isoconfigurational Elastic Constants and Liquid Fragility in Vitreloy-4

3.1.1 Abstract

Samples of $Zr_{46.75}Ti_{8.25}Cu_{7.5}Ni_{10}Be_{27.5}$ (Vit-4) were isothermally annealed around the glass transition temperature, from 567 to 671K, and subsequently water quenched.

The acoustic and elastic properties of the annealed samples were studied via the pulse-echo overlap technique. The shear modulus G of the annealed samples shows a strong reversible dependence on varying annealing temperatures and correspondingly on the specific configurational potential energy of the equilibrium liquid. In contrast, the low-temperature dependence (from 78K to 298K) of the elastic modulii of the configurational frozen glasses show weakly linear temperature dependence as expected from Debye-Gruneisen theory. The T-dependence of G in the super-cooled equilibrium liquid state is directly related to the viscosity of the liquid and more specifically the liquid fragility.

3.1.2 Introduction

In the undercooled melt, Zr-based alloys exhibit "strong" liquid behavior with a Vogel-Fulcher "fragility" parameter of D≈20 or Angell Fragility of m≈30.(60, 2) The enthalpy recovery method was used in relaxation experiments to determine the enthalpy of the equilibrium liquid $h_L(T)$ in the neighborhood of the glass transition temperature.(37, 61) According to the Potential Energy Landscape (PEL)/Inherent State (IS) theory of Stillinger and Weber and later refinements, the liquid enthalpy consists of separate vibrational and configurational contributions, $h_L = h_V + h_C$.(62, 25) The glass transition can be identified with the configurational freezing of Inherent States. The glass/liquid heat capacity anomaly at $T_g, c_P = c_{P_L} - c_{P_G}$, can be directly associated with the configurational enthalpy $h_{C(T)}$ such that

$$h_C(T) = h_C(T_g) + c_P(T - T_g) + higherorderterms. \tag{3.1}$$

By contrast, the vibrational enthalpy is expected to vary smoothly and linearly as the glass transition is traversed with a slope given by the Dulong-Petit heat capacity of $3K_B$ per atom. Recently, Johnson and Samwer have developed a Cooperative Shear Model (CSM) to describe plastic yielding of metallic glasses in the glassy state below T_g.(35) In the CSM, the barrier, W, for shear flow is related through a scaling law to a universal critical yield strain γ_{CO}, the shear modulus G for a fixed-glass configuration, and the effective volume of the cooperative shear zones $\Omega_{\text{effective}} = \zeta\Omega$

$$W = \frac{8}{\pi} G\gamma_{CO}\zeta\Omega \tag{3.2}$$

In Equation 3.2 the core volume of a Cooperatively Shearing Zone (CSZ) is Ω and ζ is an "Eshelby" factor which corrects for matrix confinement of the CSZ.(35) This relation predicts that the barrier height for shear flow for a given glass or liquid configuration should be proportional to the shear modulus for a given glass configuration. For an equilibrium liquid near and above T_g, the IS configuration and corresponding configurational enthalpy depend on T. It is natural to inquire how the shear modulus of the liquid depends on the liquid configuration, or on h_C(T). This can be obtained by studying the temperature dependence of the liquid shear modulus. Previous ultrasonic studies have investigated the pressure dependence of the elastic properties of BMGs while torsional pendulum experiments have been used to study G.(50, 53, 44)

3.1.3 Experimental

Ingots of Vit-4 were prepared via arc-melting from the mixture of the elements of purity ranging from 99.5% to 99.999%. These ingots were cast into rods by melting in a resistance furnace in an 8-mm diameter stainless steel tube for 3 minutes under vacuum and 2 minutes under positive-pressure argon. Subsequently the entire tube was water quenched. Then the steel tube and a thin reaction layer with the Vit-4 were removed by machining. The amorphicity and homogeneity of the cast rod were verified through X-ray diffraction and by differential scanning calorimetry. The glass transition temperature, T_g, was found to be 627K with a delta T of 100K. The rod was cut into 3.2-mm-thick slices which were polished with flat and parallel surfaces with a finish of 2 microns.

Ultrasonic measurements performed at a frequency ω in the mega-hertz regime measure the "isoconfigurational" (or unrelaxed) shear modulus G_∞ for an IS, provided that the α-relaxation (or fast relaxation) time of the liquid, $\tau = \eta(T)/G$, is much greater than the inverse of the measuring frequency; where $\eta(T)$ is the viscosity. This condition is in fact easily satisfied for temperatures from below the laboratory T_g to substantially above T_g. Only when T falls below $\sim 10^6$ Pa-s ($\sim$ 150C or more above T_g for Vitreloy-4) is this condition violated. Thus Ultrasonic measurements can be used to probe the instantaneous or "isoconfigurational" G for IS of the liquid from T_g far into the undercooled liquid state. As a first step toward investigating the dependence of G on the configurational state of the liquid, we measured the longitudinal and transverse sound velocities of Vit-4 following thermal relaxation to the equilibrium liq-

uid state at temperatures ranging around the laboratory glass transition temperature (T_g). Following relaxation, the samples were configurationally quenched to ambient temperature where ultrasonic measurements could be conveniently performed.

We report results from an ultrasonic study of G[T], or G[e(T)]. We show that the low-temperature dependence of the elastic modulii is roughly independent of configuration state. In the equilibrium liquid, obtained from the reversible variation of G with annealing temperature the isothermal relaxation of $G_L(T)$, at a given annealing temperature T_A is found to follow stretched exponential time dependence, similar to isothermal viscosity relaxation.[5] Cycling between two T_As results in reversible changes in G showing that the relaxed G is indeed an equilibrium liquid property. For a fixed-glass configuration, we find a weakly linear dependence of G(T) on T, as expected from a Debye-Gruinesen model. Additionally, the implications for the temperature dependence of the liquid viscosity are examined.

3.1.4 Relaxation and Reversibility

The samples were isothermally annealed in sealed quartz tubes under an argon environment in a resistance furnace at a variety of annealing temperatures (T_As) around T_g, and then water quenched after each aging treatment. The total annealing time at each temperature was chosen to be less than the time to the onset of detectable crystallization as determined by the Time-Temperature-Transformation (TTT) for Vit-4 to be comparable to the previously determined time for viscosity relaxation to occur.(2, 63) This ensured that the samples are in a fully relaxed, glassy state.

Through rapid water quenching, the relaxed liquid at T_A can be configurationally captured provided the quenching time is short compared to the α-relaxation time at T_A. When these conditions are met, the acoustical properties at ambient temperature are characteristic of the equilibrium liquid at T_A.

The pulse-echo overlap technique with piezoelectric transducers with a center frequency of 25 megahertz was used to measure the shear and longitudinal wavespeeds at room temperature T_{RT} for each of the quenched samples.(64) Additionally, *in situ* low-temperature measurements were performed from 78K to 298K, on samples that were quenched from $T_A = 567$ and 665. The low-temperature measurements were performed *in situ* using the methodology of the quartz delay line with Varian Torr-Seal as a couplant, as described in Section 2.3. The density of all of the samples post-annealing was measured by Archimedean technique according to American Society for Testing of Materials (ASTM) standard C 693-93.

To ensure that the quenched samples were truly representative of the equilibrium liquid the samples were cycled between a low and a high annealing temperature. From this cycling the reversibility of the elastic modulii was demonstrated. Figure 1 depicts the shear sound velocity C_s relaxation of a sample at 567K. This sample was initially relaxed and quenched from a temperature of 652K. After the initial relaxation at 652K the sample was isothermally annealed at 567K, with measurements initially taken every 15 minutes and then taken every one to two hours. This isothermally relaxed sample exhibits stretched exponential relaxation towards a unique equilibrium value. This relaxation follows the same form that Busch, Bakke, and Johnson demonstrated

for isothermal viscosity relaxation for Vit-4. (2)

$$C_s(t) = C_{S,0} + \Delta C_S[1 - exp^{-(\frac{t}{\tau})^{\beta}}] \tag{3.3}$$

where C_S(t) is the shear sound velocity at time t, $C_{S,0}$ is the initial modulus, ΔC_S is the total shear modulus change during relaxation into the final equilibrium state, t is the elapsed annealing time in seconds, τ is the characteristic shear flow relaxation time, and β is the stretching exponent. Upon completion of the low-temperature first relaxation the same sample was "cycled" back to 652 K, where C_S was found to relax back to the same value it had prior to the lower temperature annealing. This demonstrates that the measured equilibrium values of the samples annealed and quenched from high temperatures are truly representative of the equilibrium liquid, and have no residual irreversible effects. This can be seen in Figure 3.1.

Figure 3.2 shows the temperature dependence of the G and bulk modulus K for equilibrium Vit-4 liquid together with in-situ data from 78K to 298K on the quenched glass from samples annealed at 567K and 665K. The glass samples annealed at different temperatures have different but fixed configurational entropy states, but the linear fits to the low temperature modulus data have essentially the same slope. This demonstrates that the low-temperature modulii T-dependence is independent of the configurational state. This is the expected Debye-Gruinesen (DG) effect of thermal expansion on elastic constants at a fixed glass configuration. The average bulk modulus DG slope was found to be, $\frac{dK}{dT}DG = -.006815(+/-.0016)[\frac{GPa}{K}]$, and the average DG shear modulus slope $\frac{dG}{dT}DG = -.009115(+/-.00033)[\frac{GPa}{K}]$. This thermal

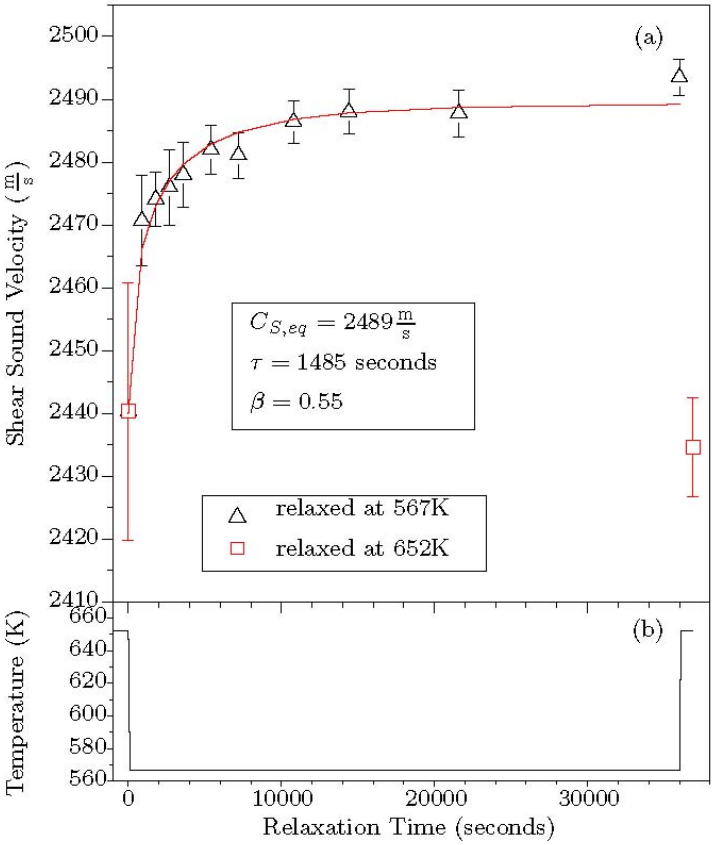

Figure 3.1: Relaxation of Vit-4 CS at 567K. Open squares represent the sample annealed and quenched from 652K. The fitting parameters are for Equation 3.3. After completion of relaxation at 567K, the sample was annealed at 652K and the shear modulus came back to the value initially measured from 652K.

expansion effect on the elastic properties was taken into account when analyzing the data measured at room temperature for the samples annealed and quenched from temperatures around T_g. The trend in the modulii measured from the quenched samples at room temperature is representative of the trend that the values should have if they were to be measured in-situ. To determine the modulii at the actual annealing temperature, the measured room temperature data should be corrected with the DG effect. It is expected that the measured low-temperature DG dependence of the modulii is a component of the temperature dependence at all temperatures. The data measured at room temperature for a sample annealed at T_A should then be corrected by $T_A - T_{RT}\frac{dG}{dT}DG$ to obtain the actual value of G(T_A). This correction was included in all of the liquid data shown in Figure 3.2 and Figure 3.3.

3.1.5 The Energy Dependence of The Shear Modulus

At ambient temperature in the "as-cast" sample G was 35.02 GPa while K was 110.34 GPa; the room temperature properties of a fully crystallized sample increased significantly over the glassy material, G increases nearly 26% to 44.21 GPa while K increases 6.5% to 117.5 GPa. In the equilibrium liquid around T_g there is a strong linear correlation between both G and K and temperature: [dG/dT]L = - 0.035 GPa/K and [dK/dT]L = - 0.0422 GPa/K. Although the absolute value of the change of K around T_g is larger than that of G, the relative change in G is much larger. Around T_g, G undergoes relatively greater configurational "softening" than K. G decreases by nearly 9.3% over the 100K interval from 567 to 671K, while K only decreases by 2.4% over

the same 100K interval. In summary, the configurational excitation of IS in the liquid with increasing T leads to a dramatic softening of the shear modulus in the liquid with temperature $G_L(T)$. The T-dependence is much greater than the DG thermal expansion effect for a fixed glass configuration $\left[\frac{dG}{dT}\right]_{DG}$.

Combining our data for G_L(T) with earlier data for H_L(T) obtained by Busch, we can obtain the energy (enthalpy) dependence of G on the configurational enthalpy of the liquid. Specifically, the isoconfigurational shear modulus G of the equilibrium relaxed liquid should be a unique function of pressure, P, and temperature, T—or equivalently, of P and h_C(T). From Busch's enthalpy recovery experiments on Vit-4 $\delta h_C(T)/\delta T$ was found to be 17 J (mol*K)$^{-1}$.(65) Using the definition of enthalpy, $h_C(T) = e_C + Pv$, and the fact that the experiments were performed at constant pressure, taking the partial derivative with respect to temperature gives $\delta h_C/\delta T = \delta e_C/\delta T$. Combining $\delta h_C/\delta T$ with the experimental shear modulus data yields that $\delta G/\delta e_C = -2.05 GPa/(KJ/mol)$ over the temperature range studied around T_g. This result expresses the dependence of G on the specific configurational potential energy of the Inherent States of the liquid. This demonstration that $G_L(T)$ falls steeply above T_g suggests that the energy barrier for configurational hopping between inherent states and the related viscosity may be related to $G_L(T)$.

3.1.6 Viscosity Model

Considering the energy barrier W(T), from Equation 3.2 for configurational hopping, one would expect that the liquid viscosity would be of the form:

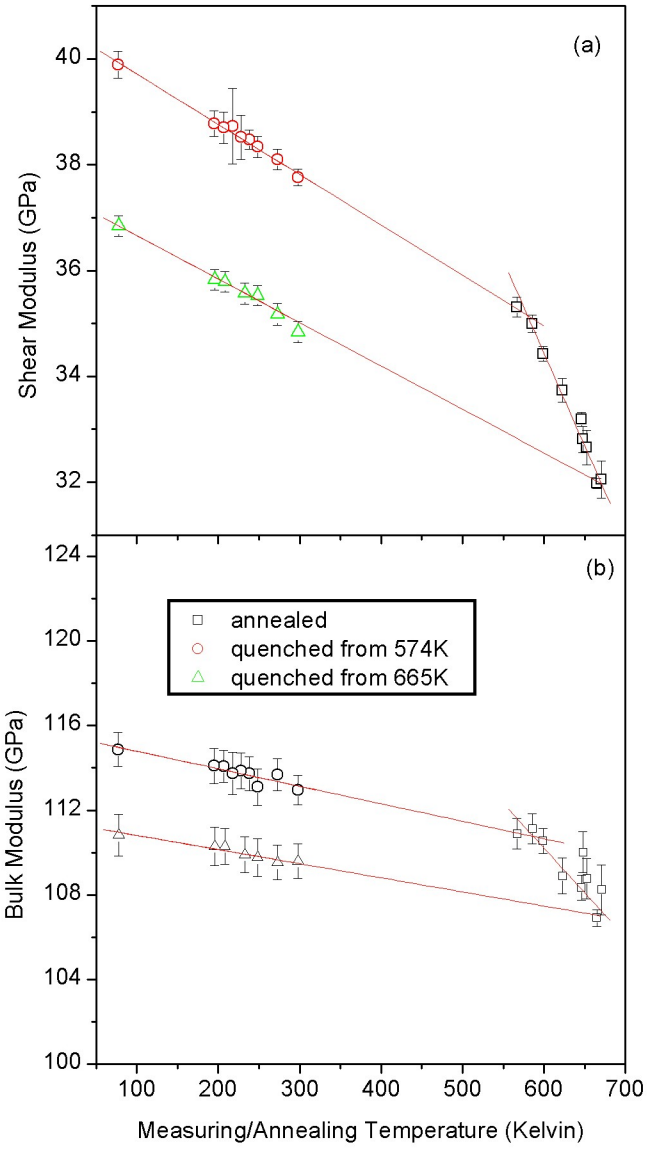

Figure 3.2: (a),(b) The Shear and Bulk Modulii of Vit-4 as measured *in situ* from -78 to 298K and measured from samples quenched from the equilibrium liquid around T_g. Open circles represent samples annealed at 567K, open triangles samples annealed at 665K. Samples annealed at different temperatures, thus having different configuration states, have the same low-temperature slopes. This demonstrates that the low-temperature dependence of the elastic modulii is independent of configuration state.

$$\frac{\eta}{\eta_o} = exp\left[\frac{W(T)}{k_B T}\right] \tag{3.4}$$

where η is the viscosity at temperature T, η_o is the high-temperature limit of the viscosity, k_B is Boltzmann's constant, and T is temperature in Kelvin. By using the dimensionless term y= T_g/T , Equation 3.4 can be recast as:

$$ln(\frac{\eta}{\eta_o}) = \frac{yW(T)}{k_b T_g} \tag{3.5}$$

by definition at T_g $\eta = 10^{12}$ Pa s and in the high-T (Plank) limit $\eta_o = 4 * 10^{-5}$ Pa s. Thus evaluating Equation 3.5 at T_g yields 37.8, a value that should be nearly constant for all glasses. Angell defined liquid fragility as:

$$m = \left[\frac{dln(n(y))}{dy}\right]_{y=1} = \frac{W(1)}{2.303 k_B T}\left[1 + \left[\frac{dln(W(y))}{dy}\right]_{y=1}\right] = 16.4\,[1+i] \tag{3.6}$$

where i is a reduced liquid fragility index related to the logarithmic derivative of W(y) evaluated at T_g. According to Equation 3.2, the temperature dependence of W(y) should include $G(T)$ or $G(y)$. Following Johnson and Samwer, we assume γ_{CO} to be independent of y. Thus only the CSZ effective volume $\Omega_{eff}(y) = \Omega\zeta$ has a possible temperature dependence; allowing for this, Equation 3.6 becomes $m = 16.4[1+i] = 16.4[1+n+p]$ where n and p are reduced "elastic fragility" and "CSZ volume fragility" indices:

$$n = \left[\frac{dln(G(y))}{dy}\right]_{y=1} = -\frac{T_g}{G(T_g)}\left[\frac{dG(T)}{dT}\right]_{T_g} \tag{3.7}$$

$$p = \left[\frac{dln(\Omega_{eff}(y))}{dy}\right]_{y=1} = -\frac{T_g}{\Omega_{eff}(T_g)}\left[\frac{d\Omega_{eff}(T)}{d_T}\right]_{T_g}. \tag{3.8}$$

Figure 3.3 is an Angell plot depicting the Newtonian viscosity for Vit-4 calculated from the shear modulus as outlined above, and measured by parallel plate rheometry and three-point beam bending.(2) The measured viscosity yields an Angell fragility parameter of $m = 33(\pm 1.5)$ and fragility index $i = 1.0$. Later data of Masuhr that includes high-T Couette viscometry measurements yields $m \sim 37$, or $i = 1.3$.(66) Applying Equations 3.7 and 3.8 to the present data for $G_L(T)$, we obtain $n = 0.65$ and an Angell fragility of $m = 28.6(+/-1.1)$. Comparing the reduced fragility indices calculated from the measured G with those from viscosity measurements, there is a discrepancy between i and n of 0.35–0.65. Thus, the steep temperature dependence of $G_L(T)$ found in this study does not account solely for the entire reduced fragility index of Vit-4; perhaps the difference should be attributed to the temperature dependence of the effective volume. From PEL studies, one expects as temperature is increased, the characteristic CSZ barrier-crossing events will involve atomic clusters of decreasing volume and thus decreasing cooperativity.(67) The present data suggest that a power law behavior of the form y^p with p 0.35–0.65 may provide an apt description of this dependence in Vit-4; however the exact functional form above $1.2T_g$ has yet to be experimentally measured. This model relating viscosity to shear modulus is similar

to the "shoving" model put forth by Dyre et al; the main difference between them is in the details of the functional form taken for the energy barrier to configurational hopping or a flow event.(68)

3.1.7 Conclusion About Vit-4

In conclusion, in the limited temperature range around T_g that was studied, the temperature dependence of the liquid shear modulus G_L for Vit-4 was found to be linear and much stronger than that of the bulk modulus K. The temperature dependence of G_L in the liquid state is much steeper than the DG dependence of the configurationally frozen glass. The dramatic change in the slope of G from glass to liquid corresponds to a strong dependence of G on configurational potential energy of the liquid. This finding provides support for the idea that the barrier height for configurational change in the liquid PEL scales with shear modulus. Using a simple model, we compared the rheological fragility measured for Vitreloy 4 with that predicted from the temperature dependence of the shear modulus utilizing the CSZ model of Johnson and Samwer. The experimentally determined slope of $G_L(T)$ and corresponding elastic fragility index n=0.65 accounts for most, but not all, of the liquid fragility index i=1.0–1.3. This suggests that the remaining part of i arises from the decrease in size of CSZs with increasing temperature. To explain our data, a "volume fragility index" of p 0.35-0.65 is required.

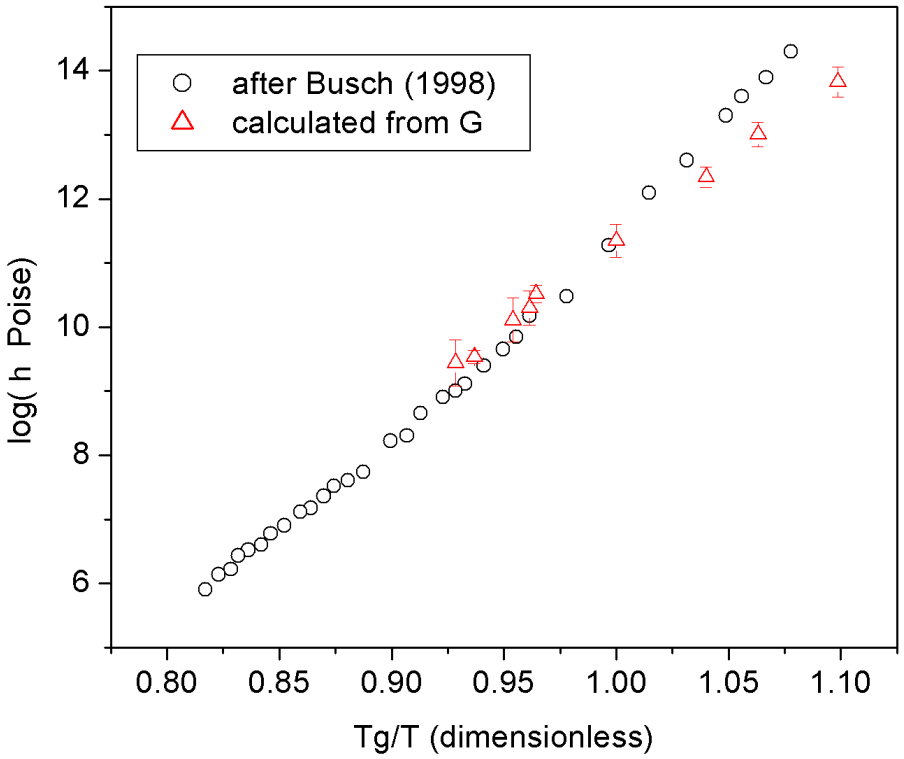

Figure 3.3: Angell plot of the viscosity of Vit-4 as measured by Busch (2) (open circles), and calculated from the measured shear modulus following Equation 3.4. Above T_g the viscosities match very well.

3.2 Elastic Constants in $Pd_{43}Ni_{10}Cu_{27}P_{20}$

Annealing experiments similar to the ones performed in Vitreloy were performed in a Pd-based alloy. The alloy $Pd_{43}Ni_{10}Cu_{27}P_{20}$ was selected for its relatively low T_g, large ΔT, and resistance to oxidation.(13, 14) This alloy was also selected due to its accessibility for inelastic neutron scattering experiments used to obtain phonon Density of States for the glasses. These experiments will not be discussed here, but were performed on the samples in collaboration with Rebecca Stevens of the Dr. Brent Fultz's group.

3.2.1 Palladium Experimental

One-mm-thick, by one-cm-wide, by three-cm-long samples were cast via copper-mold casting with Argon-pressure in a vacuum. Amorphicity and homogeneity were determined by XRD and DSC. T_g was found to be 585K, T_x 716 K, and T_f 802K.

3.2.2 Relaxation and Reversibility

Similar to the Vitreloy-4 study, a stretched exponential relaxation was noted in the Pd-alloy. Figure 3.4 shows this phenomenon in the Pd-based alloy. In Figure 3.4 the reversibility of the shear and longitudinal sound velocities between 531K and 597K can be seen, demonstrating that the annealed and quenched samples are representative of the equilibrium liquid.

In Figure 3.6 there is data from samples that were annealed and quenched at temperatures around the calorimetric glass transition temperature and then measured

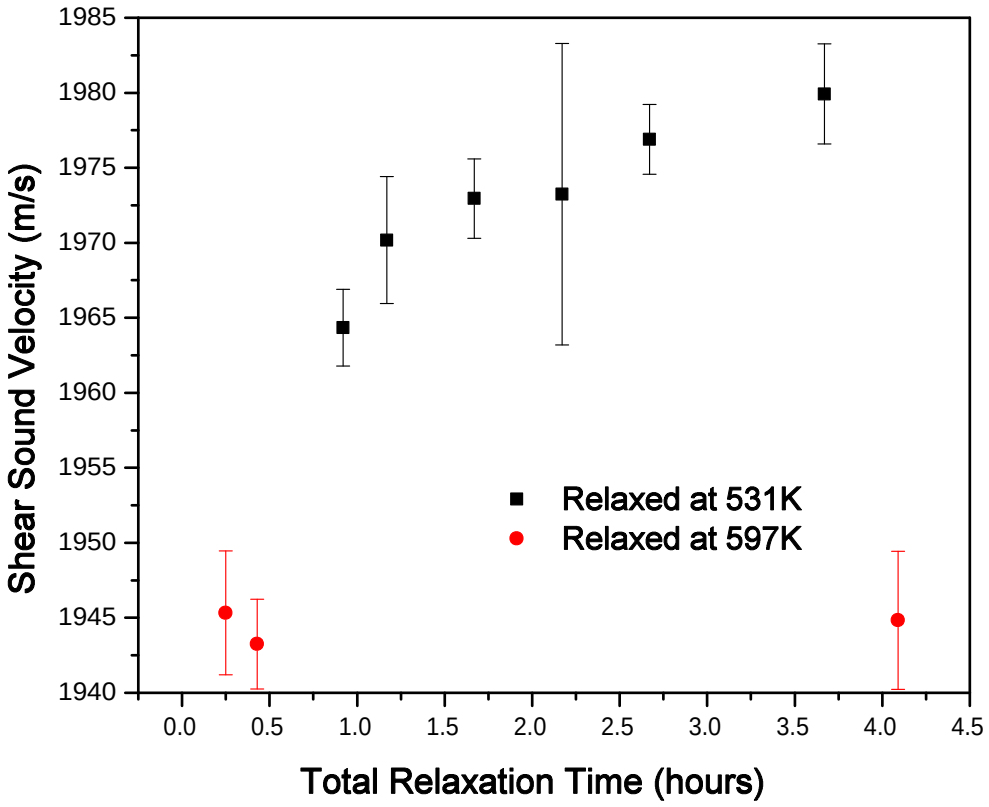

Figure 3.4: Reversibility of $Pd_{43}Ni_{10}Cu_{27}P_{20}$ glass shear sound velocity

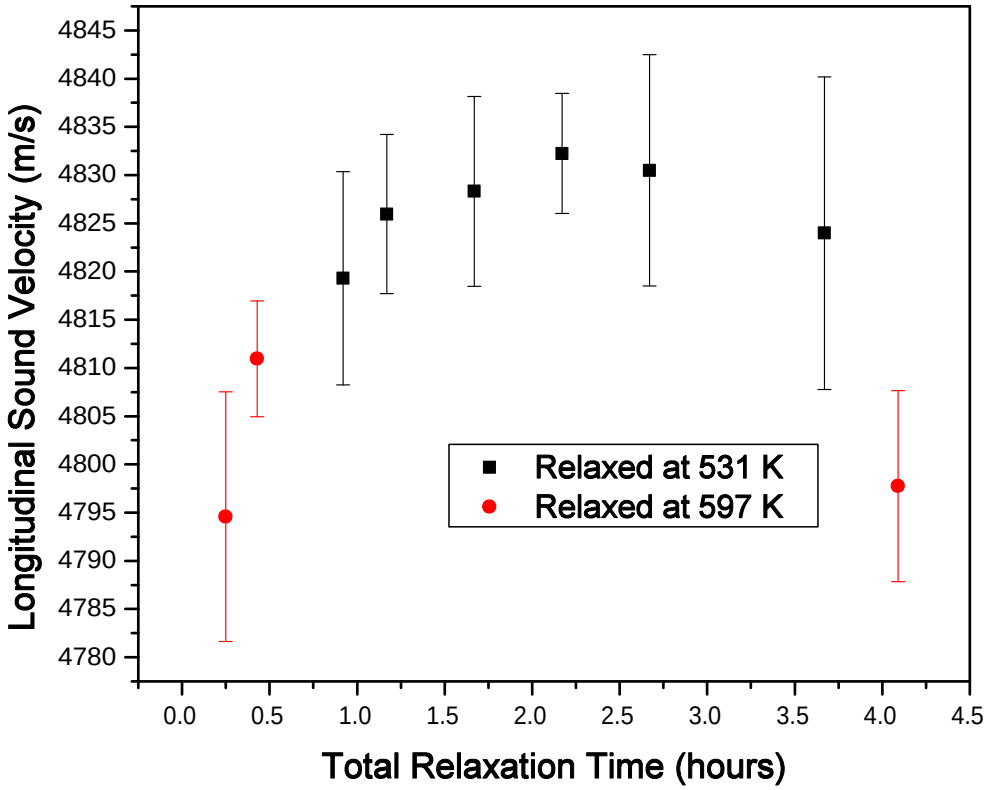

Figure 3.5: Reversibility of $Pd_{43}Ni_{10}Cu_{27}P_{20}$ glass longitudinal sound velocity

ex situ. Additionally, samples quenched from both 300C and 350C were measured *in situ* at temperatures below room temperature in order to determine the Debye-Gruinesen effect.

region	$\frac{dG}{dT}$	error	coeff
quenched around T_g	-0.0455	0.002	.993
below RT, quenched from 300 C	-0.0129	4.86e-4	.988
below RT, quenched from 350 C	-0.0127	8.56e-4	.96

Table 3.1: Summary of fitting data to $Pd_{43}Ni_{10}Cu_{27}P_{20}$ relaxation measurements in Figure 3.6

Table 3.1 contains the fitting results to the various regions of the Pd-relaxation data. The slopes of the *in situ* measurement below room temperature of the samples quenched from two different temperatures are very similar, as in the Vit-4 experiment; thus further supporting the idea that the temperature dependence of the shear modulus below the calorimetric glass transition temperature is essentially due to thermal expansion.

Figure 3.7 has viscosity data from Fan et al. (5) along with viscosity calculated from the shear modulus data of samples annealed and quenched around T_g. Clearly, there is not a strong fit between the viscosity measured by Fan and that calculated from G. This inconsistency can be attributed to a few things. First there are two distinct regions of data from the previously performed viscosity measurements, these are due to measurements that were done by two different methods (parallel plate rheometry and beam bending). Additionally, as the viscosity model stands it does not currently account well for the temperature dependence of the volume of the Shear Transformation Zones.

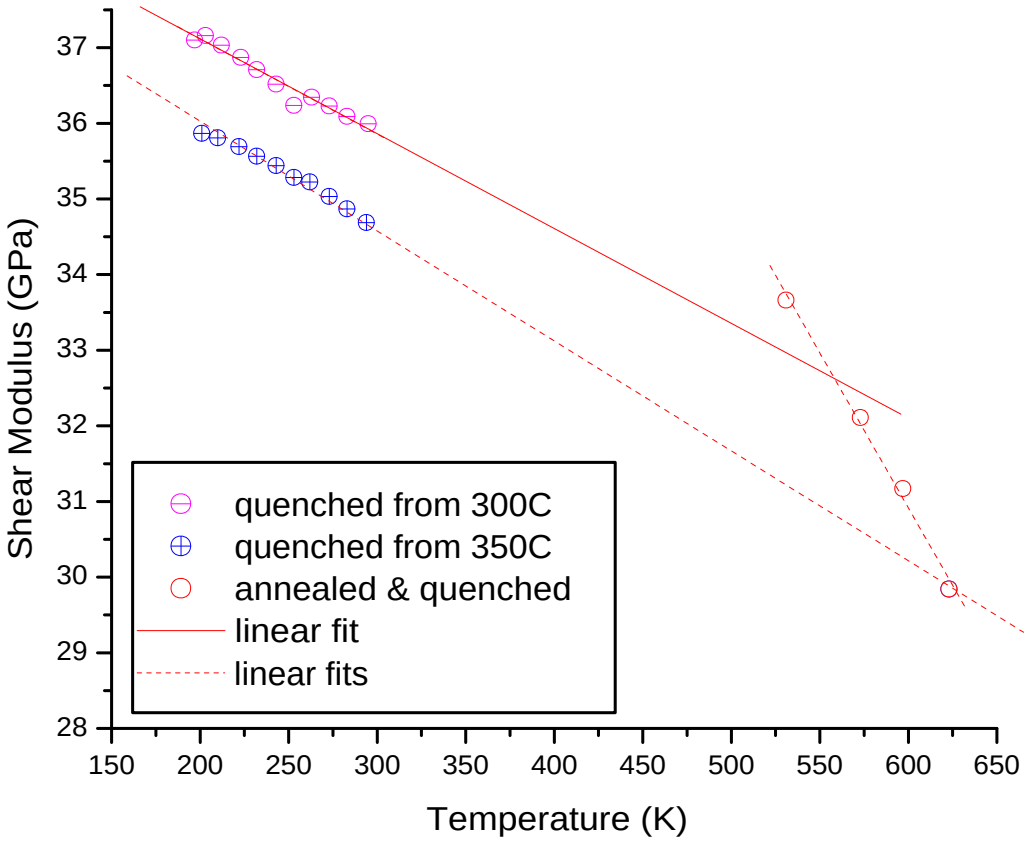

Figure 3.6: Low-temperature *in situ* measurement of $Pd_{43}Ni_{10}Cu_{27}P_{20}$ samples quenched from 300 and 350C, high-temperature annealing and quenching

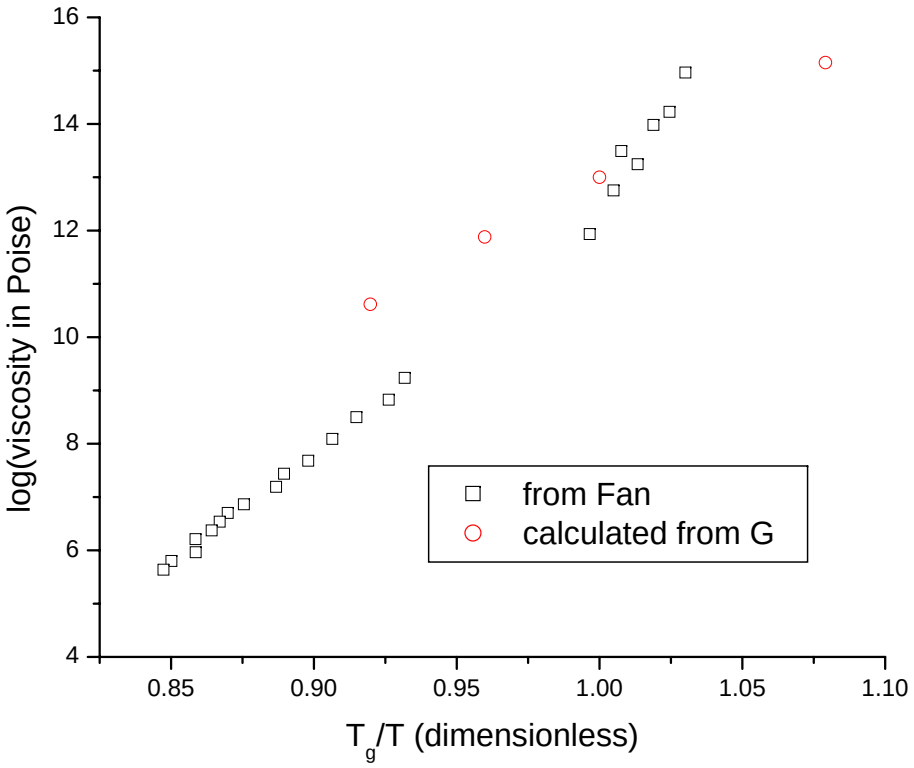

Figure 3.7: $Pd_{43}Ni_{10}Cu_{27}P_{20}$ viscosity, open circles calculated from G, open squares from Fan (5)

Using Equation 3.7, n for the Pd-alloy can be calculated. It is found to be: $n \approx .81$ From the Fan viscosity data $m \approx 58$ or $i \approx 2.47$. Using the n from the shear modulus data and the p from the previously measured viscosity data yields a $p \approx 1.66$. However, the fragility parameter calculated directly from the shear modulus data, $m \sim 28.26$, is quite a bit lower than that from the measured viscosity data. Additionally, the apparent $\frac{dG}{dT}$ seen from the *in situ* measurements presented later in Chapter 5, and also seen in other *ex situ* annealing experiments on the same alloy, is larger than that measured in this section.(7) This discrepancy may be explained either by not-completely-relaxed samples at 531K or possibly by crystallization in the samples annealed above T_g. Not-fully-relaxed samples *below* T_g have the effect of "pulling down" the overall slope of the T_g region, as their effective shear modulii are lower than expected. Partially crystallized samples at and above T_g also have the effect of "pulling down" the $\frac{dG}{dT}$ in the T_g, region because partially crystallized alloys present higher elastic properties than their glassy counterparts (noted in Chapter 2).

Chapter 4

In situ Experiments in Low-T_g Glasses Using a Delay Line

As discussed in Chapter 2, two methods were developed that allowed for *in situ* measurement of the shear and longitudinal sound velocities in bulk metallic glasses at temperatures beyond room temperature. All measurements that are discussed in this chapter were performed with a polished quartz delay line and adhesive as shown in Figure 2.2. Below 300K Varian Torr-Seal was utilized, and from 300K to 450K Surf Resin was used. All of the low-temperature data presented in Chapter 3 was also performed by the delay line technique. While this technique was not discussed extensively in Chapter 3 it was integral to the adjustment of the *ex situ* data from the samples around T_g. The low-temperature data yielded the Debye-Gruinesen correction factor by which all *ex situ* annealing data was adjusted to get an accurate representation of the equilibrium isoconfigurational shear modulus around T_g. In this chapter low-temperature results on $Pt_{57.5}Ni_{5.3}Cu_{14.7}P_{22.5}$ that were used by Harmon et al. are presented.(69, 70) Additionally, *in situ* shear modulus data from glasses with $T_g s$ below 150C are discussed. Updates to the viscosity model of Chapter 3 are

presented.

4.1 Measurements in $Pt_{57.5}Ni_{5.3}Cu_{14.7}P_{22.5}$

The first low-temperature measurements in this thesis performed with the use of a delay line and couplant were those presented for Vitreloy-4 and PdNiCuP in Chapter 3. With the concept refined, proven, and tested, measurements were performed for other members in the Johnson research group.

To facilitate a series of experiments and analysis very similar to those of the isoconfigurational shear modulus presented in Chapter 3, samples of $Pt_{57.5}Ni_{5.3}Cu_{14.7}P_{22.5}$ were measured utilizing the *in situ* techniques described in detail in Chapter 2. These results are presented in Figure 4.1. The Debye-Gruinesen slope was found to be -12.7$\frac{MPa}{K}$ $\pm$.541$\frac{MPa}{K}$.

4.2 History and Development of Gold-Based Bulk Metallic Glasses

Duwez et al. found the first metallic glass in 1960 in the Au-Si system.(10) However, the alloy found by Duwez could only be formed into thin films at very high cooling rates ($10^6 - 10^8 K/s$). Since Duwez's discovery, many good metallic glass formers have been found. While good glass forming systems based on other "precious metal" systems such as Pd and Pt have been found, it was not until recently that good glass formers in gold-based systems were discovered.(1, 71) This recent push to develop

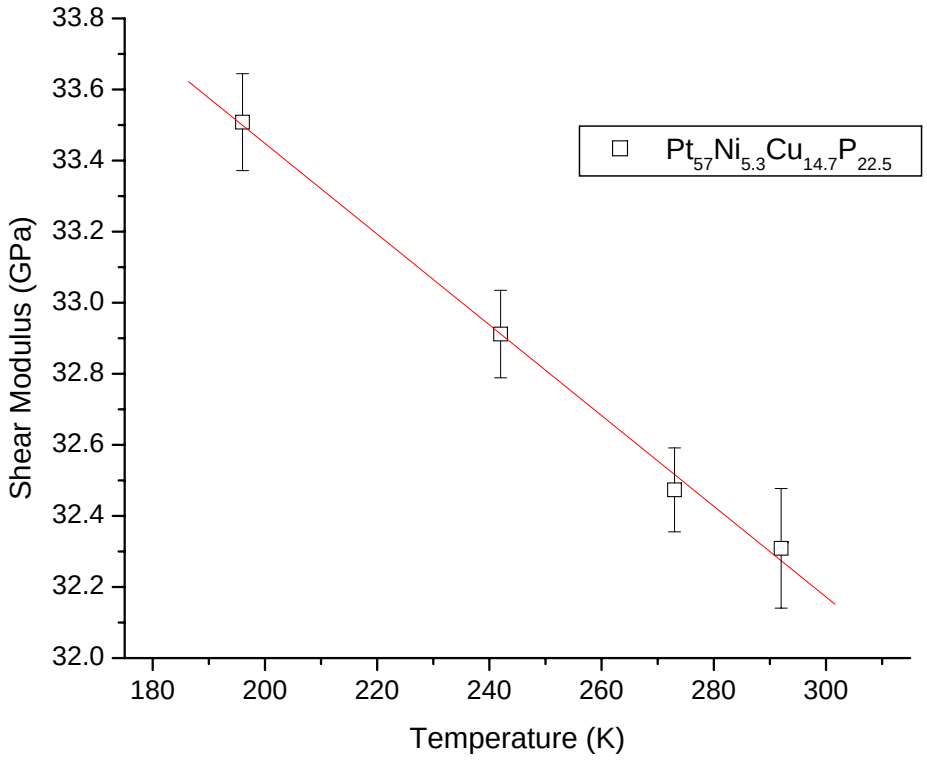

Figure 4.1: *In situ* low-temperature measurement of $Pt_{57.5}Ni_{5.3}Cu_{14.7}P_{22.5}$ by delay line technique of Section 2.3

a good gold-based BMG was spurred by the desire for a high-Poisson-ratio alloy, as well as the desire to find new gold alloys for jewelry applications. In addition to being good glass formers, the newer Au alloys also have relatively low glass transition temperatures.

To be able to perform *in situ* shear modulus measurements with the quartz delay line and the "high temperature" adhesive, the T_g of the glasses studied needed to be low. Thus, the series of gold-based alloys discovered by B. Lohwongwatana in collaboration with employees of Liquidmetal Technologies in Lakeforest, CA were chosen.(1) This series of gold alloys has T_gs ranging from 348–403K, ΔTs of 25–58K, and critical casting thicknesses from .5-5mm. There are other metallic glasses with very low glass transition temperatures (some less than the boiling point of water), however these alloys (cerium-based, or gold-lead) are neither as good glass-formers nor as easy to handle as the newer gold-based alloys.

4.3 Gold-Based Glass Sample Preparation and Experimental

A .63mm sample of slightly off-composition $Au_{55}Cu_{25}Si_{20}$ (Au-1) alloy was alloyed and cast at Liquidmetal Technologies in Lakeforest, CA. The $T_g = 363$K and $T_x = 393$K were determined by DSC (with a heating rate of 20K/min) and ρ was found to be 14.34 g/cm^3. As can be seen in the X-ray diffraction pattern in Figure 4.3, there is a small crystallization peak around 2θ of 36 degrees, however, despite these small

crystals, the sample was mainly amorphous; it is possible that this small peak could have been due to surface oxidation.

The sample was then attached to the quartz delay line with Torr- Seal. After the low temperature *in situ* measurements were performed, the torr seal attachment was severed and the sample was attached on the other side with surf resin. The *in situ* heating rate was 4 K/min.

A 1.5-mm sample of $Au_{52}Pd_{2.3}Cu_{29.2}Si_{16.5}$ (Au-2) was cast under vacuum with argon pressure in the casting box at Caltech. The amorphocity and homogeneity were determined by XRD and DSC. At a heating rate of 20 K/min in the DSC T_g was found to be 120 C and T_x 152 C. The low- and high-temperature measurements were performed in the same manner as with the previous gold alloy.

4.4 Gold-Based Glass Results and Discussion

In Figure 4.2 the results of the *in situ* shear sound velocity measurement for Au-1 can be seen. As seen both in the figure and in Table 4.4 there is a distinct change in slope from the Debye-Gruinesen region to the region immediately above the glass transition temperature. However since this alloy only has a small undercooled liquid region before the onset of crystallization occurs, the data collection in the SCLR was limited. According to the calorimetric data, the crystallization temperature at a heating rate of 20 K/min is approximately 393K. As can be seen in Figure 4.2, the shear modulus begins to increase dramatically above 389K, representing the nucleation and growth of crystals. Above 423K the Surf Resin used to attach the sample to the delay line

begins to significantly break down and no longer transmits the ultrasonic signal, thus no data was taken above 387K.

Figure 4.4 displays the *in situ* results from Au-2. There is the expected obvious change of slope around the glass transition temperature, as the dependence of the shear modulus on temperature turns from a purely thermal-expansion dependence to more of a configurational dependence.

	region	dG/dT	error	R^2
$Au_{55}Cu_{25}Si_{20}$	below T_g	-0.0262	0.0022	0.9328
	above T_g	-0.0989	0.0056	0.9856
$Au_{52}Pd_{2.3}Cu_{29.2}Si_{16.5}$	below T_g	-0.0146	.00069	0.961
	above T_g	-0.0549	0.00598	0.977

Table 4.1: Summary of linear regression slopes and correlation coefficients for $Au_{55}Cu_{25}Si_{20}$ and $Au_{52}Pd_{2.3}Cu_{29.2}Si_{16.5}$ *in situ* measurement above and below T_g

4.4.1 Updated Viscosity Model

In Section 3.1.6 a viscosity model was introduced that utilized the energy barrier of the Cooperative Shear Model.(35) More recently, aspects of the model were updated.(6) Particularly, it was determined that for most metallic glasses a reasonable approximation to make is that the "elastic fragility" (n) and "cooperative shear zone fragility" (p) are equal. Or in other words assume that i, the reduced liquid fragility index, is equal to 2n ($i = n + p = 2n$).

Using the Johnson-Samwer barrier, rearranging Equation 3.2 (essentially normalizing to the barrier at the glass transition temperature) yields:

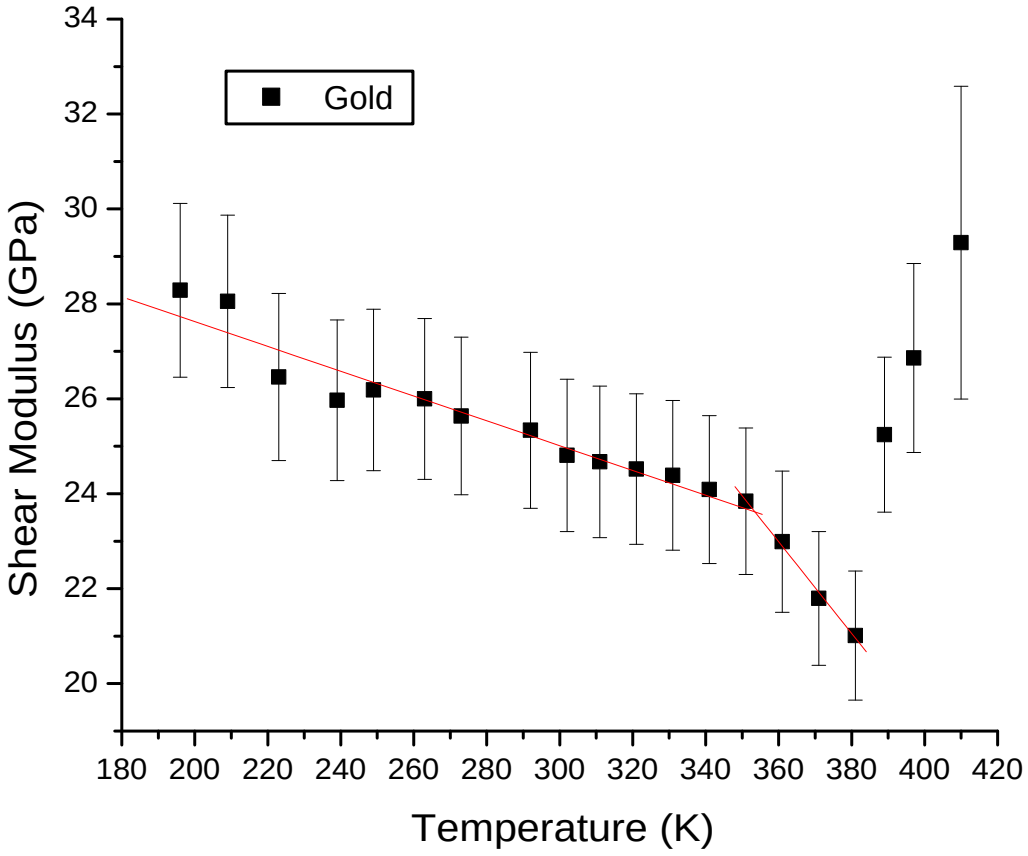

Figure 4.2: *In situ* measurement of $Au_{55}Cu_{25}Si_{20}$, above 393K G dramatically increases indicating crystallization

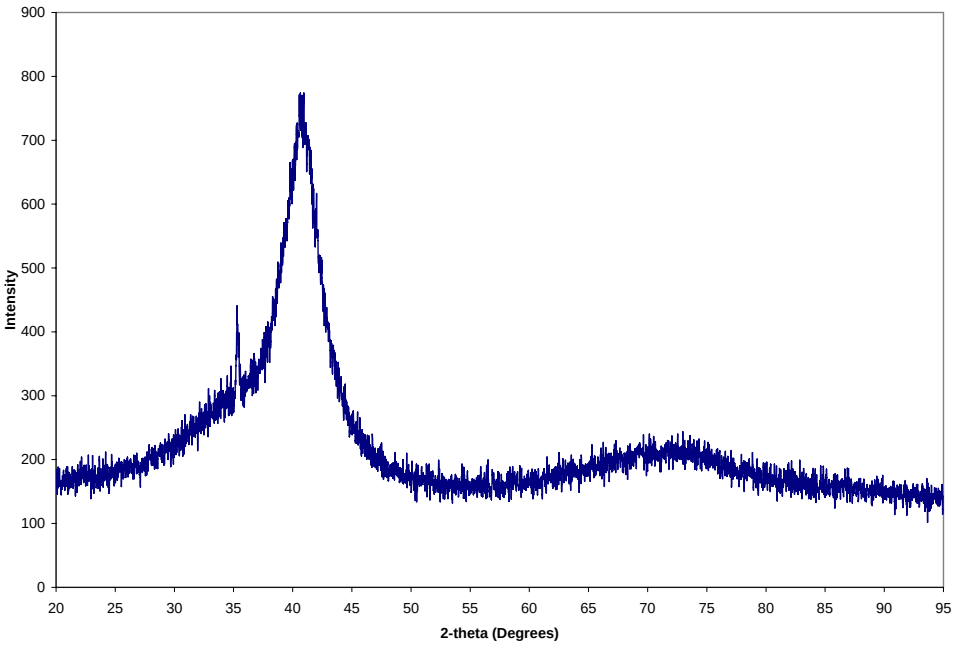

Figure 4.3: X-ray diffraction pattern of $Au_{55}Cu_{25}Si_{20}$. Note the small peak around 2-theta of 36 could be due to surface oxidation of the sample.

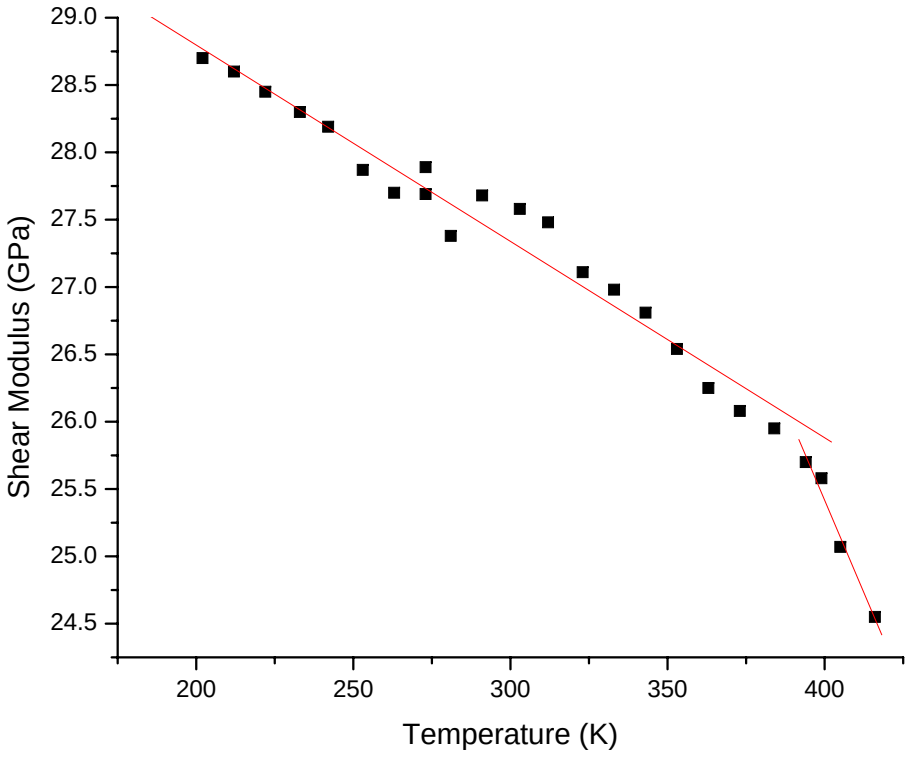

Figure 4.4: *In situ* G data from $Au_{52}Pd_{2.3}Cu_{29.2}Si_{16.5}$

$$W = W_g \left(\frac{G}{G_g}\right)\left(\frac{\Omega}{\Omega_g}\right). \tag{4.1}$$

Since G is a much easier quantity to measure experimentally than Ω (the size of the Cooperative Shear Zone), the following approximation is made,

$$\left(\frac{G}{G_g}\right)^n = \left(\frac{\Omega}{\Omega_g}\right)^p. \tag{4.2}$$

Then, the general viscosity equation formulated with the Johnson-Sawmer barrier given in Equation 3.4 can be reworked with the "new" barrier of Equation 4.1, the relation of Equation 4.2, and the assumption that n=p yielding:

$$\frac{\eta}{\eta_o} = exp\left(\frac{W}{k_B T}\right) = exp\left[\frac{W}{k_B T}\left(\frac{G}{G_g}\right)^{1/q}\right] \tag{4.3}$$

where $q = n/(n+p)$ (or in the case of $n = p$ then $q = 1/2$).

Considering Newtonian flow as simply thermally activated flow, the Newtonian viscosity would be determined by the shear modulus of the equilibrium state, G_e.(6) It is expected that G_e will decay with increasing temperature in an approximately exponential fashion. So, using the following exponential decaying relationship similar to that used previously(70, 72):

$$\frac{G_e(T)}{G_g} = exp\left[n\left(1 - \frac{T}{T_g}\right)\right] \tag{4.4}$$

Equation 4.4 can be substituted into Equation 4.3, and viscosity data can be fit to determine n; or if G has been measured directly as a function of temperature, Equation

4.4 can be used to fit the results and determine the "n", elastic fragility parameter. Johnson et al. have determined the correlation between the Johnson, n, parameter and the Angell fragility, m, (discussed in Section 1.3.2) to be $m = (1+2n)log(\eta_g/\eta_\infty)$, where η_g is the viscosity at the glass transition temperature and η_∞ is the high temperature limit of the viscosity.

In Figure 4.5 only the equilibrium shear modulus data from the Au-1 supercooled liquid is utilized and fit by the method described above. Figure 4.6 displays only the data around/above the calorimetric glass transition temperature and the fit by the Johnson theory for Au-2.

	n	R^2	m
$Au_{55}Cu_{25}Si_{20}$	1.6 ±0.10	.9838	67.2
$Au_{52}Pd_{2.3}Cu_{29.2}Si_{16.5}$	.95 ±0.118	.93194	47.5

Table 4.2: Summary of linear regression slopes and correlation coefficients for $Au_{55}Cu_{25}Si_{20}$ and $Au_{52}Pd_{2.3}Cu_{29.2}Si_{16.5}$ *in situ* measurement above and below T_g

As can be seen in Table 4.2 the Au-1 alloy has a much larger n-parameter than the Au-2 alloy. Accordingly the Au-1 alloy has a much higher Angell fragility parameter, and can be considered a very "fragile" liquid. Although no experimental viscosity data is available for either of these alloys, their n-parameters and associated Angell fragilities place them as some of the most fragile glasses (in Chapter 5 they will be compared with other data). From experience in the laboratory these alloys are very fragile. When casting in the casting box, an extremely small nozzle must be used so that the alloy will not fall prematurely into the mold.

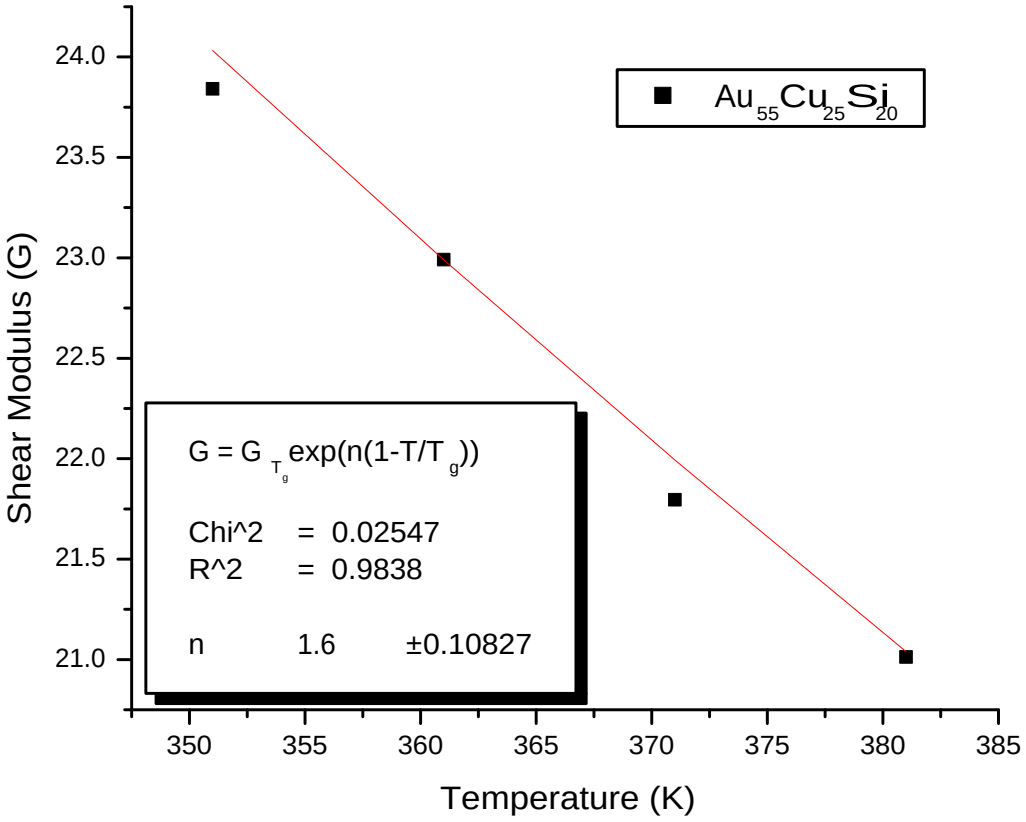

Figure 4.5: *In situ* G data of $Au_{55}Cu_{25}Si_{20}$ from T_g to just before the onset of crystallization. The data is fit to the model relating viscosity and G discussed in Section 4.4.1.

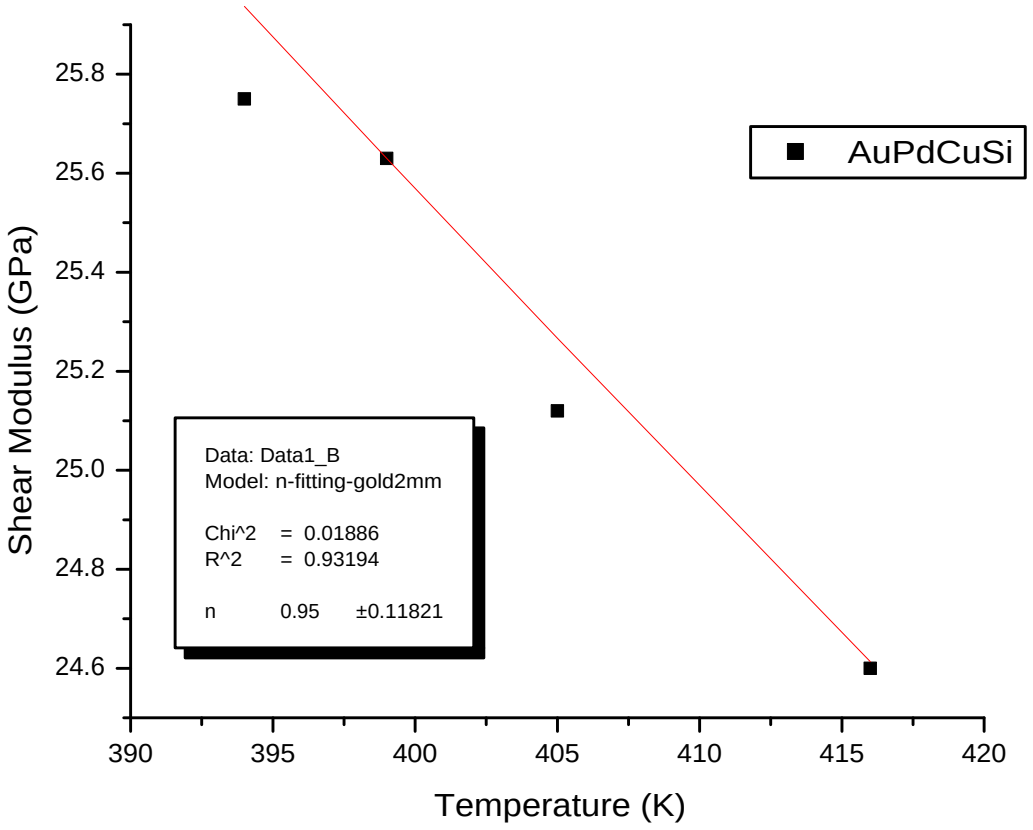

Figure 4.6: *In situ* G data of $Au_{52}Pd_{2.3}Cu_{29.2}Si_{16.5}$ above T_g fit by the Johnson viscosity model discussed in Section 4.4.1

4.5 Conclusions of Gold-Based Glasses

It is interesting to note that while both alloys, $Au_{55}Cu_{25}Si_{20}$ and $Au_{52}Pd_{2.3}Cu_{29.2}Si_{16.5}$, exhibit the expected change in temperature dependence of G around the glass transition temperature, that above their respective calorimetric T_gs $Au_{55}Cu_{25}Si_{20}$ has a much steeper slope than $Au_{52}Pd_{2.3}Cu_{29.2}Si_{16.5}$. The fall off of $Au_{55}Cu_{25}Si_{20}$ above T_g is nearly twice as fast as that of $Au_{52}Pd_{2.3}Cu_{29.2}Si_{16.5}$; additionally the "n parameter" of the former is much larger (1.6) than that of the latter (0.95). Even though AuCuSi is apparently much more fragile than AuPdCuSi, it is a much worse glass former. In fact, it was impossible to probe more than 25 K into the supercooled liquid region without nucleating crystals in Au-1. Rough correlations between the glass forming ability and the liquid fragility have been made: more fragile alloys tend to be worse glass formers. (4) This trend apparently holds true with these two gold-based alloys: while Au-1 is much more fragile than Au-2, the latter is a much better glass former.

Chapter 5

In situ Experiments in High-T_g Glasses Using "Notched" Samples

5.1 Abstract

Novel in situ *shear ultrasonic measurements using a unique measurement setup have been performed on a series of bulk metallic glass forming systems with a variety of Angell fragilities:* $Zr_{46.75}Ti_{8.25}Cu_{7.5}Ni_{10}Be_{27.5}$ *(Vit-4),* $Pd_{43}Ni_{10}Cu_{27}P_{20}$*,* $Pt_{50}Ni_{17.7}Cu_{8}P_{24.3}$*,* $Au_{55}Cu_{25}Si_{20}$ *(Au-1), and* $Au_{52}Pd_{2.3}Cu_{29.2}Si_{16.5}$ *(Au-2). The new* in situ *data corroborates previously measured* ex situ *data. Additionally, using the Cooperative Shear Model (CSM) the correlation between fragility and shear modulus is thoroughly investigated and discussed.*

5.2 Introduction

Many multi-component alloy systems that form bulk metallic glasses (BMGs) have been found in the past twenty years.(12, 73, 16, 1) The Angell fragility is a way of indexing the apparent deviation from Arrhenius-like behavior of the temperature de-

pendent viscosity of the supercooled liquid in glasses.(37) "Kinetically strong" glasses (e.g., Vitreloy-type glasses) have lower fragility parameters and less deviation from Arrhenius behavior while "kinetically fragile" glasses (e.g., Pt-based glasses) have higher fragility parameters and more deviation. A rough correlation exists between the glass forming ability and fragility: stronger liquids tend to be better glass formers.(4) Thus, having a sense of the liquid fragility of an alloy is valuable in both developing new alloys and characterizing existing ones.

Using the concept of the Potential Energy Landscape (PEL) or Inherent State (IS) theory(62, 25), Johnson and Samwer developed a Cooperative Shear Model (CSM) that describes the plastic yielding of bulk metallic glasses utilizing the constructs of the Shear Transformation Zone (STZ) and barrier height (W) to configurational change (which is hypothesized to be directly proportional to the shear modulus, G). A rheological model was developed using G as a thermodynamic parameter and relates the equilibrium shear modulus directly to viscosity at various temperatures in the supercooled liquid (see Equation 5.1 for the model).(35) A fitting parameter, n, is introduced in this viscosity model, from which the Angell fragility can be predicted. The method of measuring the shear modulus in the supercooled liquid that is presented in this paper, coupled with the previously introduced viscosity model, provides a simpler way of determining the fragility than measuring viscosity directly.

It has previously been shown through *ex situ* ultrasonic measurements that in the supercooled liquid region of Vit-4 the shear modulus has a much stronger temperature dependence than the bulk modulus, and that the shear modulus is directly related

to the configurational state of the alloy.(36) Also, in the CSM for plastic deformation of glasses, the shear modulus was identified as one of the primary controlling parameters to the barrier to shear flow.(35) This strong configurational dependence of G on T also has been shown through Molecular Dynamics simulations.(74) Thus, in this chapter we focus exclusively upon the shear sound velocity and shear modulus. We present new *in situ* ultrasonic data for $Zr_{46.75}Ti_{8.25}Cu_{7.5}Ni_{10}Be_{27.5}$ (Vit-4), $Pd_{43}Ni_{10}Cu_{27}P_{20}$, $Pt_{50}Ni_{17.7}Cu_{8}P_{24.3}$, $Au_{55}Cu_{25}Si_{20}$ (Au-1), and $Au_{52}Pd_{2.3}Cu_{29.2}Si_{16.5}$ (Au-2).(1) We show that the *in* and *ex situ* data corroborate one another, proving that both are accurate representations of the supercooled equilibrium liquid. Additionally, the shear modulus and the liquid fragility are discussed in terms of the viscosity model that was introduced and refined by Johnson et al.(6, 36)

5.3 Alloy Selection

The three alloys selected for *in situ* measurement via the "notch" technique were chosen for the following reasons: the primary reason the Pt-glass was selected was due to its relatively low T_g (220 C). In addition to having a very low T_g, the Pt-glass has a large super-cooled liquid region ($\sim$ 100C), is highly resistant to oxidation, and is recyclable. Despite having less than ideal oxidation-resistance behavior in air, Vitreloy-4 was chosen for direct comparison between the new *in situ* results with the previously presented *ex situ*. $Pd_{43}Ni_{10}Cu_{27}P_{20}$ (studied *ex situ* in Section 3.2) was also studied for comparison with *ex situ* results, as well as for its oxidation-resistance and recyclability. Additionally, both the Pd-based and V-4 alloys have extensive viscosity

data available in the literature.

In a recent study the *in situ* elastic properties of BMGs have been measured via ultrasonics through mode conversion calculations of a "trailing shear wave" following a longitudinal pulse.(54) However, in the these measurements the shear sound velocity is not measured directly from a shear signal sent into the sample. Additionally, the measuring frequencies used by are a factor of two lower than the measuring frequencies used in the following experiments. Measurements have also been done on the pressure dependence of the elastic properties of BMGs; torsional pendulum experiments have been used to study G.(50, 44)

5.4 Experimental

In situ shear ultrasonic pulse-echo measurements were performed on five alloys from liquid nitrogen temperature to temperatures 20–70 degrees above the calorimetric glass transition temperature. An ultrasonic measuring frequency of 25 MHz was employed. This measuring frequency allows for the measurement of the "isoconfigurational" (or unrelaxed) shear modulus G_∞ of an Inherent State (IS) of the liquid, provided that the α-relaxation (or fast relaxation) time of the liquid, $\tau = \eta(T)/G$, is much greater than the inverse of the measuring frequency; where $\eta(T)$ is the viscosity. This condition is easily satisfied for temperatures from below the laboratory T_g to substantially above T_g. Only when (T) falls below $\sim 10^6$ Pa-s ($\sim$150 C or more above T_g for Vit-4) is this condition violated.

Rods of Vit-4 approximately 76 mm long and 8 mm in diameter were prepared and

cast via the method described elsewhere.(36) The Pd-based and Pt-based rods of the same length, ranging from 5–8 mm in diameter, were cast via melting in a quartz tube in an induction furnace under an argon environment and then water quenching. The gold-based samples were made by copper-mold casting in an argon environment. The amorphicity and homogeneity of all of the samples were confirmed by X-ray diffraction and differential scanning calorimetry and the coefficients of thermal expansion were measured by differential thermal analysis; this data is presented in Table 5.1.

The ultrasonic properties of "as-cast" rods were measured at and below room temperature. The rods were then annealed at temperatures near T_g to put them into a defined configurational entropic state. The ends of the rod were polished to be plane parallel and flat to a surface finish of 2 microns. Due to the low glass transition temperatures and ease of crystallization the gold-based alloys were not annealed prior to measurement. The density of the "as cast" and annealed rods and gold samples were measured by Archimedean technique according to American Society for Testing of Materials (ASTM) standard C 693-93. In the subsequent calculations of G from the sound velocities both the lengths and densities used were adjusted by the appropriate factor utilizing the measured thermal expansion coefficient.

The inspiration for the *in situ* experimental design for the measurements above room temperature came from J.T. Krause's seminal 1961 paper which utilized a "differential path method" to measure sound velocities in glass rods.(59) In the rods, notches .2 mm thick and approximately one-third of the diameter of the rods were cut into the sample. Each notch was cut such that the gauge length, d, between the

top of the notch and the end of the sample was approximately 20 mm; additionally, the notch was plane parallel to both ends of the rod. A .2-mm-thick piece of quartz glass was placed in the cut notch to prevent collapse of the notch upon heating. The rod was placed in a split copper mold held tightly together with set screws. This mold slip fit into a larger copper heat sink that was heated by four 250-watt cartridge heaters controlled by a 5-ampere DC power supply. A thermocouple was fitted into the heat sink and contacted the split copper mold. The ultrasonic pulse sent from the transducer is reflected back from both the top of the notch and the end of the rod and the time difference between these two pulses is measured and used to calculate the elastic properties. There is a large temperature gradient from the portion of the rod outside of the copper heat sink to the top of the rod in contact with the transducer, however this gradient effectively can be ignored since it is the same for both the reflection from the top of the notch and the bottom of the rod. See Figure 5.1(b) for a schematic of the experimental setup and notch design. The Au-based samples were measured through the use of a quartz delay line.

The samples were heated and cooled at a rates ranging from 4–10 K/min. Upon reaching the point where the ultrasonic signal was attenuated to have no amplitude (the order of the measuring frequency was on the same timescale as the fast relaxation in the liquid), the heating was stopped. In Figure 5.2 the results of the *in situ* heating and cooling cycles are shown. As can be seen from this figure it is virtually impossible to distinguish between the heating and cooling cycles, thus demonstrating the reversibility of the measurement and supporting the claim that we are measur-

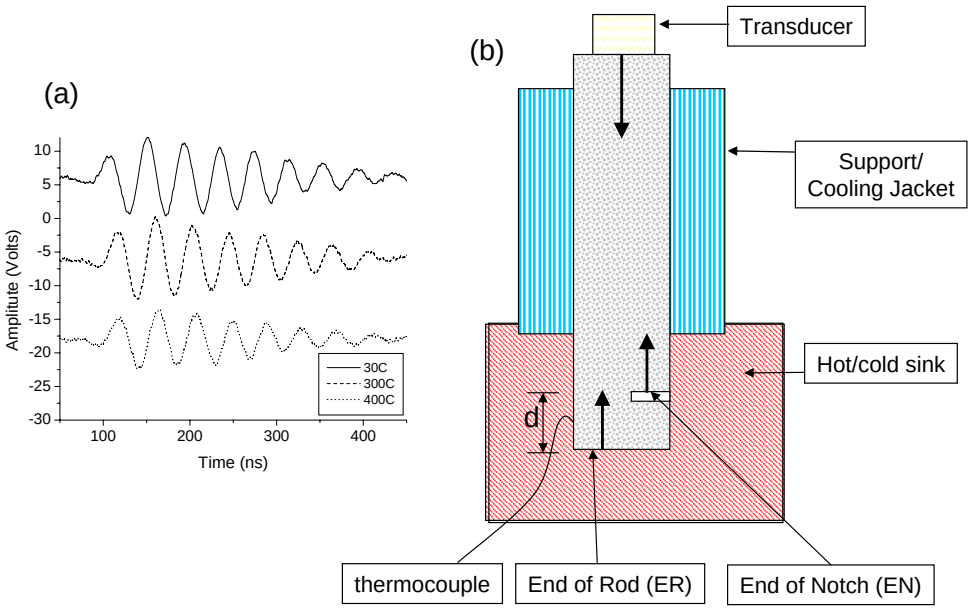

Figure 5.1: Schematic of *in situ* experimental measurement setup. The ultrasonic pulse was sent from the transducer and reflected from both the End of Notch (EN) and End of Rod (ER). The gauge section of length, d, from EN to ER was kept entirely in the copper hot/cold sink. The temperature was measured with a thermocouple that penetrates through the copper heat sink in direct contact with the sample. The Cu hot/cold sink was kept well insulated with thermal fire-bricks.

ing the elastic properties of the supercooled liquid *in situ*. Also in Figure 5.2, the sharp increase in the shear modulus above 381K for Au-1 is due to crystallization of the sample. The error in the shear modulii calculated from the ultrasonic data is approximately 5%.

5.5 Results and Discussion

parameter	Vit-4	Pd-based	Pt-based	Au1	Au2
T_g (K)	623	573	493	363	393
T_x (K)	733	716	591	393	425
CTE (/K)	$8.6 * 10^{-6}$	$13.0 * 10^{-6}$	$10.8 * 10^{-6}$		$19.7 * 10^{-6}$
dG/dT quenched from LT, DG region	-0.0087	-0.0129	ND	ND	ND
dG/dT quenched from HT, DG region	-0.0094	-0.0127	ND	ND	ND
dG/dT *in situ* below T_g (DG region)	-0.0099	-0.0118	-0.0124	-0.0262	-0.0135
dG/dT quenched from above T_g *ex situ*	-0.0352	-0.0455	ND	ND	ND
dG/dT *in situ* above T_g	-0.0350	-0.0527	-0.057	-0.0989	-0.0546
n	0.753 ($\pm$0.079)	1.045 ($\pm$0.105)	1.176 ($\pm$0.099)	1.510 ($\pm$0.087)	0.869 ($\pm$0.106)
Angell fragility calculated from n	40.1	49.4	53.6	64.3	43.8

Table 5.1: Summary of calorimetric data, linear regression slopes to different regions (all correlation coefficients are greater than .9 for the regressions). ND = no data available.

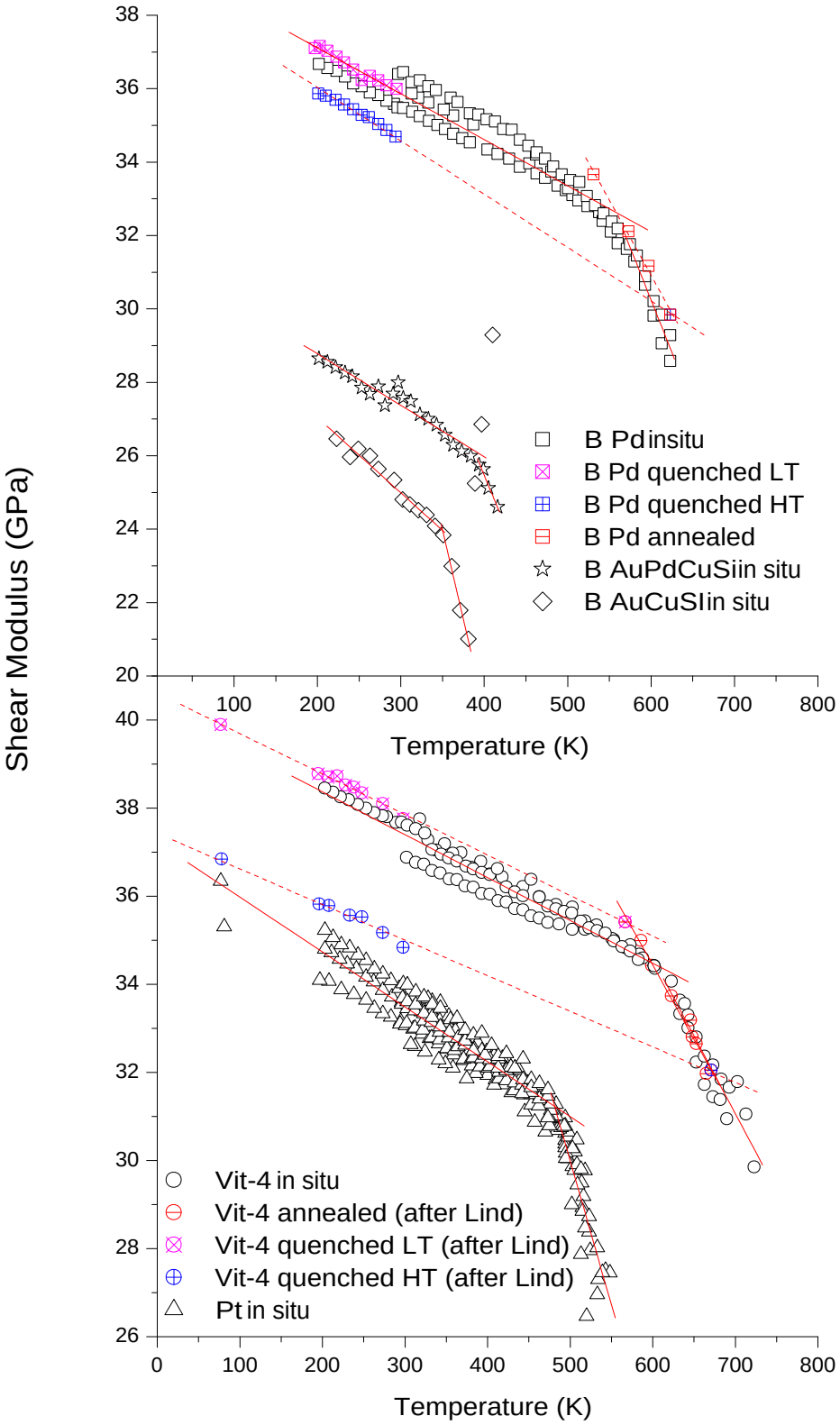

Figure 5.2: *In situ* Au-1 (open diamonds), Au-2(stars), Pd (squares), Pt (triangles), Vit-4 (circles); *ex situ* data shown by corresponding symbol with line through it.

5.5.1 Comparison Between *In Situ* and *Ex Situ* Measurements

As can be seen in Table 5.1 and in Figure 5.2 there is strong correlation between the shear modulii as measured *ex situ* and *in situ*. As previously demonstrated for Vit-4 (36), reversibility of the annealed and quenched samples was shown for the Pd alloy. All of the samples show a strong dependence of G on temperature above the glass transition temperature, while exhibiting an essentially Debye-Gruinesen (or purely thermal expansion) effect in the region below T_g. Since the ultrasonic signal exists at temperatures as high as 420C, and the *in situ* and *ex situ* data (for Vit-4 and Pd in their respective systems) are essentially the same, this demonstrates that the dependence of G on temperature is a true temperature effect and not simply an acoustical attenuation (or damping) effect at high temperature. Experimentally there is a point beyond which the ultrasonic signal no longer exists (it is damped out) because the frequency of the measurement is on the same timescale as the α relaxations in the liquid. Figure 5.1(a) shows sample ultrasonic reflection waveforms captured from the *end of notch in situ* measurement of Vit-4 at 30C, 300C, and 400C. The amplitudes of the waveforms were not altered, they have only been shifted in order to display all waveforms on the same graph. These waveforms all have the same shape and roughly the same amplitude, demonstrating that no errant effects due to signal attenuation are occurring at these temperatures. The small differences between the various heating and cooling cycles in the measurement of the alloys are representative of slight configurational differences due to very small variations in

cooling rate.

Comparing the $\frac{dG}{dT}$ slopes between the various alloys, we see that, as expected, the trend in slope below T_g closely parallels the trend in thermal expansion coefficients: a lower CTE corresponds to smaller $\frac{dG}{dT}$ slope below T_g. Interestingly, this trend is also followed in the region above T_g. However, as can be seen above T_g there is a distinct difference in $\frac{dG}{dT}$ slope between the alloys; Au-1 has the strongest G dependence on T, while Vit-4 has the weakest.

The fact that these slopes from the *in situ* and *ex situ* measurements align means that the effect that we are seeing, of G rapidly decreasing above .9 T_g, is truly a configurational effect of the equilibrium liquid and not a dynamic relaxation effect, or an acoustical absorbtion effect. Essentially, the previously performed *ex situ* measurements demonstrating the reversibility of the shear modulus are the absolute proof that what is seen is truly a configurational property of the equilibrium liquid.

5.5.2 Updated Viscosity Model

The following viscosity model was introduced by Johnson et al. (6):

$$\frac{\eta}{\eta_o} = exp\left[\frac{W(T)}{k_B T}\right] = exp\left[\frac{W_g}{k_B T}\left(\frac{G_e}{G_g}\right)^{1/q}\right] \tag{5.1}$$

where η is the viscosity at temperature, T, η_o is the high temperature limit of the viscosity, $W(T)$ is the energy barrier to shear flow, k_B is Boltzmann's constant, $q = \frac{n}{n+p}$ where n is a reduced elastic index and p is a STZ volume softening index. It was found that for Equation 5.1 the correlation is best when $n = p$.(6) G_e is the

equilibrium value of G at T, and G_g is the equilibrium value of G at T_g. $W(T) = W_g(G_e/G_g)(\Omega/\Omega_g)$ where Ω_g is the volume of a STZ and W_g is the flow barrier of the frozen configuration at T_g. $W_g = (8/\pi^2) * \gamma_c * G_g * \Omega_g$ where γ_c is the shear strain limit of the material, and a universal constant of 0.036 +/- .002.(35) As per the rheologic definition of a glass n_g was considered to be 10^{12} Pa-s and n_o was taken as the Plank limit, or $4 * 10^{-5}$ Pa-s.

While this paper makes an attempt at further elucidating the shape of G(T) in the supercooled liquid, it does not conclusively do so. We will take an exponential decay of the form (noting that other decaying forms could be used).(6)

$$\frac{G_e}{G_g} = exp\left[n\left(1 - \frac{T}{T_g}\right)\right] \tag{5.2}$$

The only "unknown" in Equation 5.2 is the parameter n.(6, 36) Having experimental G(T) data enables us to fit using Equation 5.2 to determine the parameter n, or to use Equation 5.2 in Equation 5.1 and fit viscosity data by Equation 5.1.

According to Johnson, the Angell fragility is related to the parameter n in the following way:

$$m = (1 + 2n)log(\frac{n_g}{n_o}). \tag{5.3}$$

Figure 5.3 shows previously published viscosity data for the Pd alloy and Vit-4 and the *in situ* $\frac{dG}{dT}$ data converted to viscosity with fits by Equation 5.2(the fitting parameters can be found in Table 5.1). A higher n corresponds to a higher Angell

fragility, as can be seen from Table 5.1; the trend in n-parameters from smallest to largest is: Vit-4, Au-2, Pd, Pt, Au-1. In Figure 5.3 the viscosity calculated from the *in situ* data on the Pd alloy matches extremely well with the viscosity measured by Fan et al. (n-parameter 1.150 ($\pm$0.033)). The fit of the viscosity calculated from Vit-4 does not match quite as well with the viscosity measured by Busch et al., but is still a reasonably good fit to within error bars (Busch n parameter = 0.572 ($\pm$0.015)).

When fitting with Equation 5.2 a one- or two-parameter fit can be used: in the one-parameter fit, the high temperature limit of the viscosity is fixed at theoretical limit of $4 * 10^{-5}$; in the two-parameter fit the high temperature limit of the viscosity can also be varied. Using the two-parameter fit the n_os fit to the data varied from the theoretical limit by no more than a factor of two. It is important to note that in this paper the Johnson-viscosity theory has only been shown to hold for the lower temperature region of the supercooled liquid, where the liquid behaves as a Newtonian fluid. For the alloys studied in this paper no extremely high temperature data ($>$ 900K) exists for either the viscosity or the shear modulus.

Using the method of predicting the liquid fragility from the shear modulus shows that G is a meaningful parameter for probing the rheologic properties of a metallic glass. The shear modulus data necessary for this can be accessed either by annealing and quenching the samples, or by the recently developed, relatively simple *in situ* measurement. These measurements are much simpler to perform than the traditional methods of measuring viscosity and give quite good results.

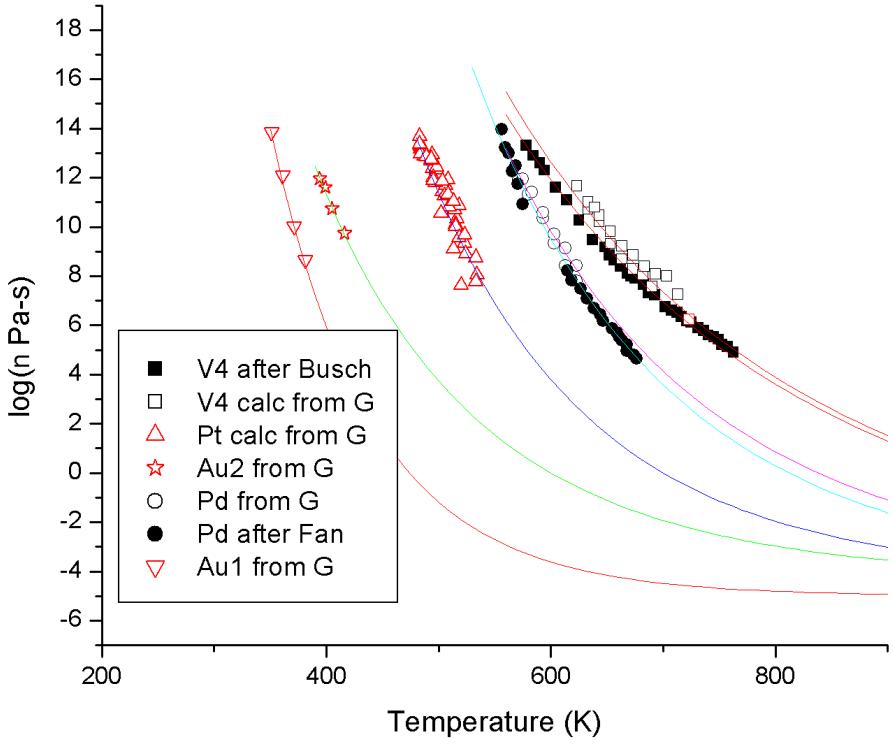

Figure 5.3: *In situ* shear modulus data converted to viscosity using Equation 5.3. Open symbols represent data converted from shear modulus; filled symbols represent measured viscosity data. Both n and n_o were used as fitting parameters, and n can be found in Table 5.1. All fits have an $R^2 > .9$.

Chapter 6

Miscellaneous Experiments

6.1 Control of Elastic Properties by Cooling Rate in Vitreloy-4

The possibility of controlling the elastic properties of Vitreloy 4 by different cooling rates was studied. This alloy was chosen since extensive data is available for it, it is a good glass former, and it is capable of being cast into a wide range of sample shapes and dimensions.

6.1.1 Experimental

Using copper-mold casting, 3-mm, 1-mm, and half-mm rectangular samples of Vitreloy-4 were cast, a .053 mm sample was fabricated in the splat quencher. The density of each sample was measured according to American Society for Testing of Materials (ASTM) standard C 693-93. The elastic properties of each sample were then measured ultrasonically using the pulse-echo technique described elsewhere in this thesis. For the splat-sample, the sound velocity was measured using the through-transmission

technique.

6.1.1.1 Ultrasonic Measurements on Very Thin Samples

Performing ultrasonic measurements on very thin samples (thicknesses less than .5 mm) can be questionable, depending on the frequency of the transducer. For ultrasonic waves, $\lambda = v/\nu$, where λ is the wavelength, v is the speed, and ν is the frequency. In metallic glasses, typical shear sound velocities are 2500 m/s; with a transducer of frequency 25 MHz, the typical wavelength of a shear ultrasonic signal is .1mm.

Many problems are associated with using a measuring tool that is the same length-scale as the item that you are measuring. To avoid this problem when measuring sound velocities in metallic glasses it is ideal for the section of the sample being measured to be a minimum of 3–5 times the typical wavelength of sound in that material. Additionally, when calculating the elastic properties from the sound travel time, all measuring errors on a small sample are proportionally larger than on a large sample, since they are a larger percentage of the quantity being measured. (See Appendix D for more details on how to calculate and propagate the error in ultrasonic calculations.)

Thus, the .053 mm splat produced is potentially shorter than the wavelength of sound used to measure it. However, reasonable, reproducible data was produced using the through-transmission technique.

6.1.2 Results and Discussion

The cooling rates of the various dimensions of cast-alloys were calculated according to the method presented by Liu and Johnson in 1995(75):

$$\frac{dT}{dt} = \frac{T_m - T_g}{\tau} = \frac{K(T_m - T_g)}{CR^2}. \tag{6.1}$$

T_m is the melting point of the alloy, K = thermal conductivity, C = heat capacity per unit volume, R = typical sample dimension, and τ = the total cooling time to reach T_g. τ is of the order,

$$\tau \sim \frac{R^2}{\kappa}. \tag{6.2}$$

Taking $(T_m - T_g) \sim 400$ Kelvin, K = 0.1 $\frac{W}{cmsK}$, C = 4 $\frac{J}{cm^3K}$ then for a typical metallic glass:

$$\frac{dT}{dt} = \frac{10}{R^2(\text{incm})}. \tag{6.3}$$

From the experiments in Chapter 3 it was seen that samples annealed at different temperatures around T_g had different room temperature shear modulii. These values directly corresponded to the temperature from which the sample was quenched (and thus is partially related to the cooling rate/when the sample "fell out of equilibrium"). It was hypothesized that samples of different sizes (reflecting different cooling rates) would fall out of equilibrium in the supercooled liquid at different temperatures — thus yielding different shear modulii. The thinner the sample, the higher this falling

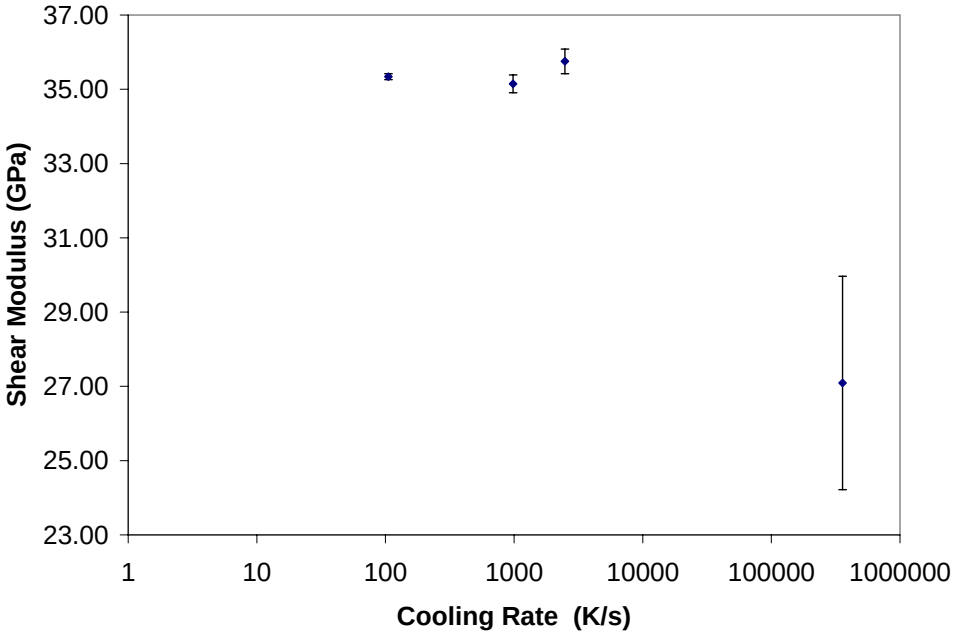

Figure 6.1: Shear modulus vs. cooling rate for different samples of Vit-4

sample thickness (mm)	est. cooling rate (K/s)	density (g/cm^3)	G (GPa)	K (GPa)	v
3	105	5.938	35.34 (±0.08)	110.26 (±0.36)	0.355 (±0.001)
1	980	5.948	35.15 (±0.24)	110.20 (±0.89)	0.356 (±0.001)
.5	2480	5.900	35.75 (±0.33)	ND	ND
0.053	357407	6.003	27.09 (±2.87)	ND	ND

Table 6.1: Summary of Vitreloy-4 cooling rate estimated cooling rates and experimental elastic property results. ND = no data available.

out of equilibrium temperature would be. However, as can be seen from Table 6.1 and Figure 6.1 there is no obvious trend in the data. The only conclusion to be drawn from the data is that the splat sample (.053 mm) has a much lower G, and is much more "shear soft" than the other samples. It appears that many other factors come into play in the as-cast samples: ranging from the rheological properties of filling a copper mold, to the variation of cooling rate from the center of the sample to the edges, to strain rate differences (the splat is subjected to much higher strains than the casting in the copper mold). Thus, the best way to accurately compare cooling-rate differences in the mechanical properties of bulk metallic glasses appears to anneal samples of the same geometry and quench them. However the maximum and minimum quenching rates achievable on a 1 mm sample are experimentally limited, and it is virtually impossible to achieve such a high rate of quenching as in a splat-quenched sample, other than by melt spinning or splat quenching.

6.2 Cavitation in Glycerol

Glycerol is an organic glass with the chemical formula of $HOCH_2CH(OH)CH_2OH$. Glycerol has a glass transition temperature of approximately 225K. At room temperature glycerol exists as a colorless, odorless, clear, and viscous liquid.

Elastic property measurements in Glycerol have been performed through Brilluion scattering.(76) In 1986 Jeong et al. studied the temperature dependence of the longitudinal sound speed and attenuation in glycerol through the glass transition.(77)

Initially, the goal was to measure the *in situ* elastic properties of glycerol. It was thought that it would be relatively simple to obtain contact between the glycerol and ultrasonic transducer and we would not have to worry about the problems associated with high-temperature ultrasonic measurement. It was quickly discovered that it is *very* difficult to get glycerol to vitrify, but that cavitation of voids easily occurs.

Cavitation is when there is a large negative pressure inside a liquid causing a pressure gradient and a resulting void to form. Cavitation of voids is a relatively common problem when casting larger-diameter metallic glass samples, and thus understanding the behavior and potentially being able to model the formation of voids is of interest.

6.2.1 Experimental

It is very difficult to achieve clean vitrification in glycerol. Initially, glycerol was poured into quartz tubes, and the tubes were swirled in a tub of liquid nitrogen to quench the glycerol into a glassy state. The glycerol crystallized instead of vitrifying. With any moisture content, even as little as available in the air of Southern California,

the ability of glycerol to vitrify rapidly degrades. In subsequent trials the glycerol was kept out of air and the samples were degassed by attaching the glycerol-containing tube to a vacuum system and heating the glycerol above the boiling point of water.

Once relatively clean vitrification of glycerol was achieved, it was then noted that the glycerol has a tendency to cavitate and that it was a rare occurrence for the glycerol *not* to cavitate. Due to the incessant cavitation, it was impossible to get a clean sound velocity signal through the sample. Thus, the focus of the experiment was changed from attempting to perform *in situ* ultrasonic measurements on glycerol to trying to study the cavitation behavior.

Since glycerol is a clear liquid, it is possible to videotape or photograph the cavitation. A DVD camera was set up a fixed distance from a background with a ruler. A beaker with warm water maintained at ($\sim$ 50C) was on a hotplate; when the glycerol tube was removed from the liquid nitrogen it was placed inside of this beaker so that condensation would not form on the outside of the tube and photographs/video could be taken.

Then the test-tube setup for creating cavitation voids in the glycerol was modified. Quartz tubes that were approximately 5 mm in inner diameter and 12 inches long were used. A copper-plug that slip fit into the tube was made, the bottom of the plug was polished to a 2-micron finish, and the level of the glycerol in the tube went above the top of the "plug". This plug was inserted to help the cooling of the "gauge section" at the bottom of the tube occur more uniformly from top to bottom. Without the plug, a downward shaped vortex from the surface of the glycerol tends to form. A

schematic of this copper-plug and tube design can be seen in Figure 6.2.

6.2.2 Results and Discussion

A series of glycerol tubes with copper plugs were swirled in a container of liquid nitrogen for 90 seconds. The tubes were immediately placed into the viewing chamber and videotaped. The size of the cavitation bubble was recorded as well as the time for the sample to reheat enough for the cavitation to dissipate. Samples were quenched from two different starting temperatures: room temperature (25 C) and boiling water (100C). The hypothesis was that different size voids would cavitate when quenched from different temperatures. It was expected that larger bubbles would cavitate when quenched from higher temperatures because larger temperature and pressure gradients across the sample would be generated.

The fact that there were no visible air-bubbles prior to quenching, and the fact that the cavitation voids would shrink upon re-heating of the samples, necessarily implies that what is occurring is indeed cavitation (and not merely air-bubbles trapped in the sample). Also, the nucleation of the cavities is most likely homogeneous and not heterogeneous since the voids would cavitate away from any hard surfaces and the glycerol was theoretically free of extraneous particles.

Figure 6.3 shows the results from a series of preliminary cavitation experiments of average cavitation void diameter vs. the initial temperature from which the glycerol was quenched. While there appears to be a slight difference in the average diameter of the voids, it is not significant. Due to the loss of the video-taping equipment as well

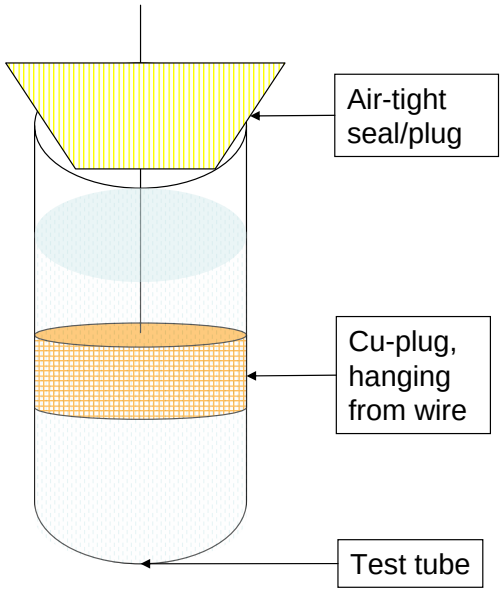

Figure 6.2: Schematic of glycerol cavitation setup

as the long times required to de-gas the glycerol, the experiments were discontinued.

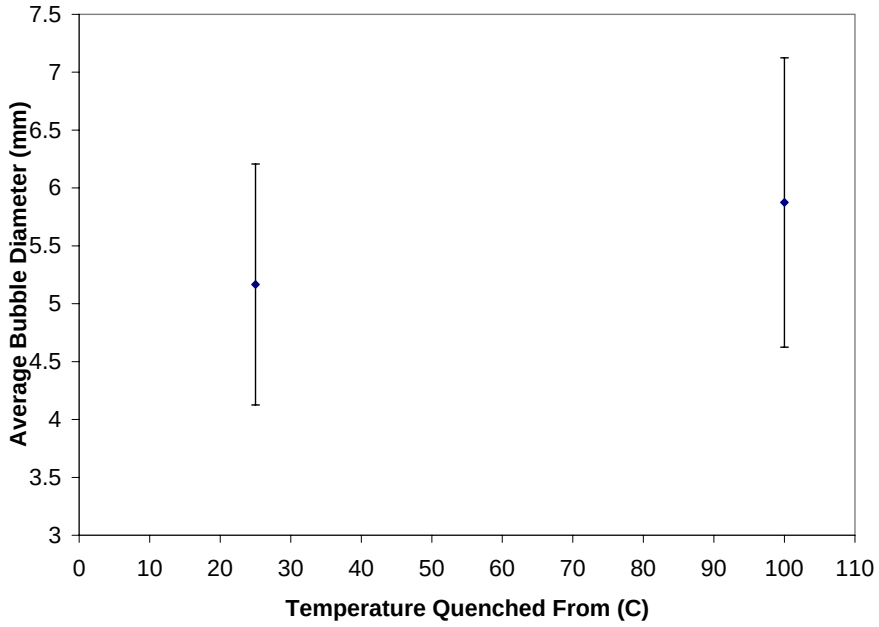

Figure 6.3: Cavitation results

Chapter 7

Summary and Future

7.1 Conclusions

In this thesis it was demonstrated that it is possible to access the equilibrium state of the supercooled liquid region of a bulk metallic glass through two methods. First, it is possible to anneal samples in the super-cooled liquid region (SCLR) and then rapidly quench them to room temperature. The properties measured at room temperature are directly correlated to the configuration state of the sample at high temperature. Second, with the appropriately shaped sample, as well as high enough frequency transducers, it is possible to measure the *in situ* sound velocities of glasses in the SCLR.

A variety of alloy systems with different Angell fragilities were studied: Zr, Pd, Pt, Au, and Au. In the Vit-4 and Pd systems both the *in situ* and *ex situ* data corroborate one another. Reversibility of the shear modulus between different temperatures was shown in both the *in situ* and *ex situ* experiments. There is a distinct change or "softening" in shear modulus seen above the glass transition temperature as the dependence of the elastic properties changes from a purely thermal-expansion

dependence to a configurational potential energy/entropy dependence. The results show that both methods of measurement are representative of the equilibrium liquid, and that what is being measured is the isoconfigurational shear modulus.

In the recently developed Cooperative Shear Model, the barrier height to configurational change is hypothesized to be directly proportional to the shear modulus.(35) Utilizing this barrier height in the general formulation of viscosity, a relationship between shear modulus and viscosity has been established.

7.1.1 The Big Picture

While interesting and novel, the experimental work presented in this thesis is better understood in the context of the "big picture." In this thesis we demonstrated how to measure *in situ* elastic properties of bulk metallic glasses below and through the glass transition region and we presented results from a variety of systems. By combining ultrasonic G(T) data presented in this thesis with other experiments in both enthalpy recovery and strain rate dependence of G we can get the configurational potential energy dependence of G.(6) In Chapter 3 it was shown that the shear sound velocity, and hence shear modulus, was a reversible property of the equilibrium liquid; this set the stage for testing the hypothesis that the shear modulus may have a unique functional dependence on the configurational energy of the system. Harmon et al. demonstrated that for the liquid of a glassy specimen that both mechanical "relaxation" (via compression) and thermal relaxation (via annealing relaxation measurements) yield essentially the same $\frac{dG}{d\Delta h}$ (or $\frac{dG}{de}$) slope.(7) This implies that the

configurational dependence of these mechanical properties are a unique function of the position in the configurational landscape.

In the Harmon et al. experiments samples of Pt and Pd were deformed at various strain rates at constant temperatures. The ultrasonic properties of the samples at room temperature were then measured. Then the samples were then put in the Differential Scanning Calorimeter and the "recovery enthalpy" was measured for both the deformed samples and the undeformed reference sample. From the recovery enthalpy the amount of stored configurational potential energy was computed.

Table 7.1.1 shows the summary of the $\frac{dG}{d\Delta h}$ slopes from Figure 7.1. The data for Vit-1 and $Pt_{57.2}Ni_{5.3}Cu_{14.7}P_{22.5}$ are reproduced exactly from that measured by Harmon. However, the data for $Pd_{43}Ni_{10}Cu_{27}P_{20}$ was adjusted by the Debye-Gruinesen parameter measured in this thesis (presented in Chapter 5)and not the one utilized in the Harmon thesis (from (78)).

system	dG/dΔh (GPa/$\frac{MJ}{m^3K}$)
Vit	-0.01695 ±0.00123
$Pt_{57.2}Ni_{5.3}Cu_{14.7}P_{22.5}$	-0.03105 ±0.00213
$Pd_{43}Ni_{10}Cu_{27}P_{20}$	-0.02305 ±0.00225

Table 7.1: Summary of Slopes from Figure 7.1

system	dG/dT (GPa/K)	dΔh/dT (MJ/m^3K)	dG/dΔh (GPa/$\frac{MJ}{m^3K}$)
Vit-4	-0.0350	1.77*	-0.0198
$Pt_{57.2}Ni_{5.3}Cu_{14.7}P_{22.5}$	-0.08**	2.56**	-0.0313
$Pd_{43}Ni_{10}Cu_{27}P_{20}$	-0.0527	2.5**	-0.021

Table 7.2: * = data from (2); ** = from (7)

By comparing the $\frac{dG}{d\Delta h}$ slopes given in Tables 8.1 and 8.2 we see that to within

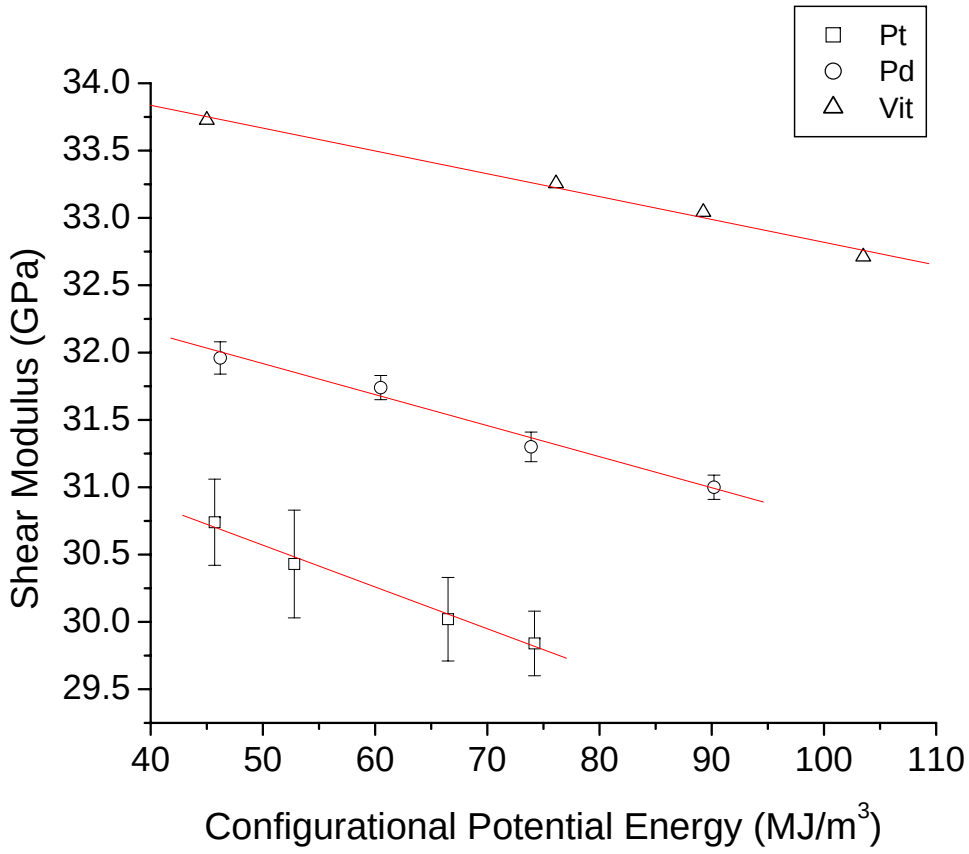

Figure 7.1: Figure similar to that from (6), raw data taken from (7). Shear modulus vs. configurational potential energy for mechanically deformed glassy/liquid specimens

error the slopes of G from thermal relaxation and mechanical relaxation are very similar. This implies that G is a unique function of the configurational potential energy landscape, or that each configuration of a glass (or even the crystalline form of the glass) has a unique shear modulus.

Figure 7.2 depicts the *in situ* data measured in this thesis as well as additional data recently measured by Wang for a Cerium-based glass.(8) This figure leads us to believe that there might be a correlation between the shear modulus and the glass transition temperature of the alloy. Noting that the Ce-based alloy has a much larger atomic volume than any of the alloys measured in this thesis, the following correlation was proposed:

$$\frac{Gv}{k_b} \propto T_g. \tag{7.1}$$

Where G is the shear modulus, v is the atomic volume, and k_B is Boltzmann's constant.

Or in other words that

$$\frac{Gv}{k_b T_g} = constant. \tag{7.2}$$

The shear modulus, G, can be thought of as an energy density posessing units of [J/m^3], the atomic volume has units of [m^3/atom], and Boltzmann's constant has units of [J/K]. Thus the ratio $\frac{Gv}{k_b}$ has units of [K/atom] or essentially temperature.

Taking additional room temperature data for an iron-based glass, as well as G(T) data for silica (SiO_2), an organic glass, Figure 7.3 was generated using Equation

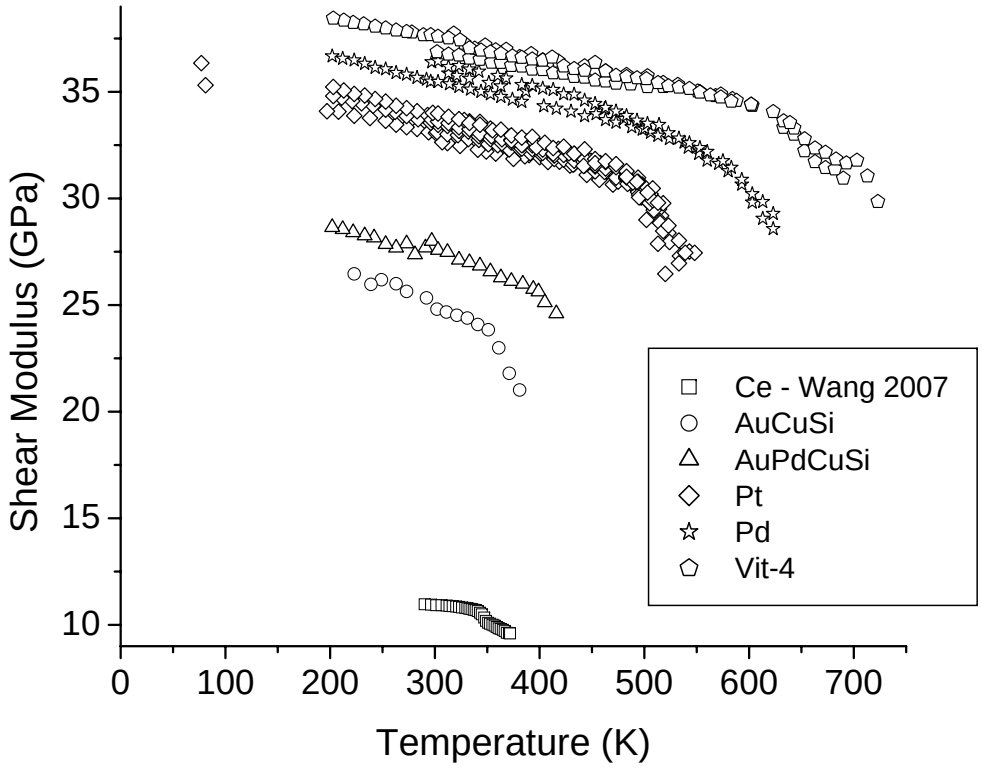

Figure 7.2: Summary of *in situ* data measured in this thesis as well as Cerium-based-alloy data from Reference (8)

7.1.(79)(80) As can be seen from Figure 7.3 there is a strong, nearly linear, correlation between the proposed ratio, $\frac{Gv}{k_B}$, and the glass transition temperature of the alloys. The raw data and calculated quantities used in Figure 7.3 can be found in Appendix A.

The equation for the linear fit in Figure 7.3 is:

$$T_g = 67.56 + .01198 * \frac{Gv}{k_B} \tag{7.3}$$

with an R^2 value of .98.

This is a novel correlation from which it is possible to predict the glass transition temperature from the elastic properties and atomic volume of a glass. This correlation can potentially be used to help guide the design of new bulk metallic glasses with specific glass transition temperatures.

7.2 Possible Future Experiments

7.2.1 Pure Shear

The concept of measuring *in situ* elastic properties via a notched sample opens up many potential future experiments. An experiment proposed, in very rough form, by Professor Johnson would be to study the shear modulus *in situ* in a metallic glass sample under pure shear. One possible geometry enabling this would be a cylinder with a large diameter but relatively small wall-thickness, that would approximately replicate pure shear in the wall-thickness area when placed in torsion. Another pos-

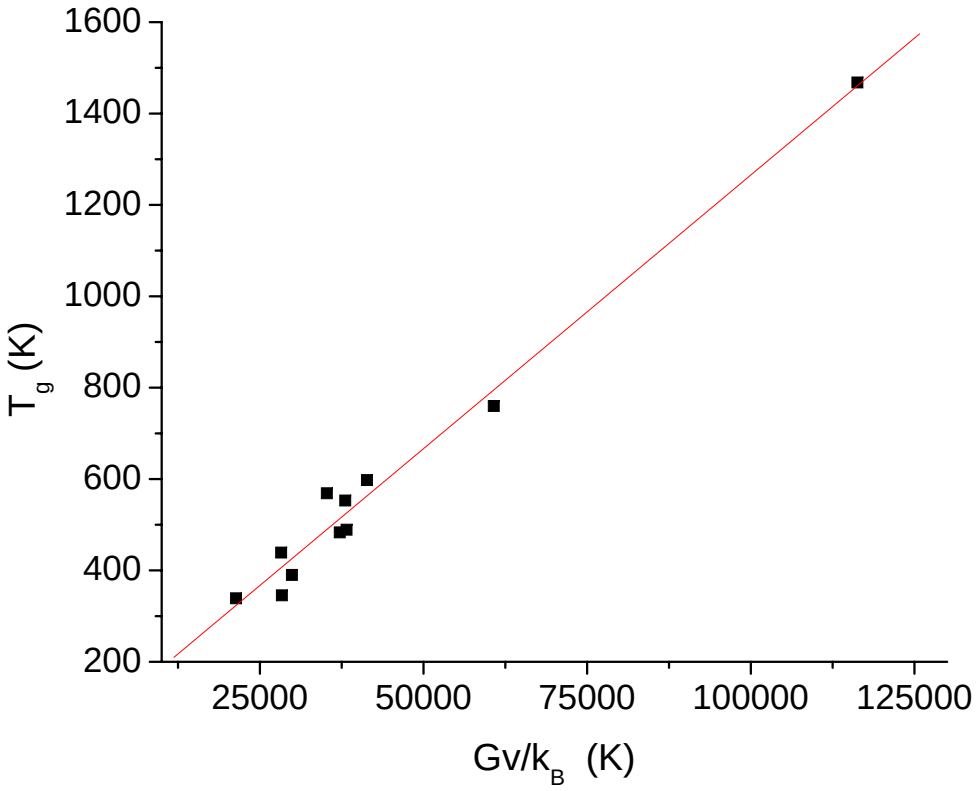

Figure 7.3: Correlation between shear modulus, atomic volume, Boltzmann's constant, and the glass transition temperature. The R^2 for the linear fit found in 7.3 is .98, the slope of the fit is .01198.

sible geometry, utilizing the "notch" concept, is pictured in Figure 7.4. The sample is designed with "legs" that stick up and down so the sample can be placed in compression. The inner area between the "notches" will essentially be in pure shear, and a transducer can be placed to measure width-wise across the sample in the region between the 2 notches. Then the *in situ* behavior of the shear sound velocity can be studied. Additionally, the polarization of the shear wave and how this responds to the current state of stress in the sample can be studied.

7.2.2 The Undercooled Liquid, From High Temperature Down

The true challenge is to experimentally measure the shear sound velocity of glassy samples completely through the undercooled liquid to try and determine the exact shape of the $C_s(T)$ or $G_e(T)$ curves. In this thesis it was shown that the supercooled liquid region can be accessed in an *ex situ* manner by annealing samples in the SCLR and then rapidly quenching them to freeze in the configurational state. Experimentally the fundamental limitation of this technique is how quickly the quenching can happen, at a certain limit (approximately 50 degrees above T_g) the rate at which a millimeter-sized sample can be quenched in the laboratory is no longer faster than the relaxation timescale in the sample; thus the true configurational state of the alloy is not captured. The second technique introduced in this thesis was measuring the *in situ* shear sound velocity in a long-rod sample with a reflective notch cut into it. The fundamental limitations of this technique are having to use alloys capable of being cast into rods greater than four-millimeters in diameter and that the shear

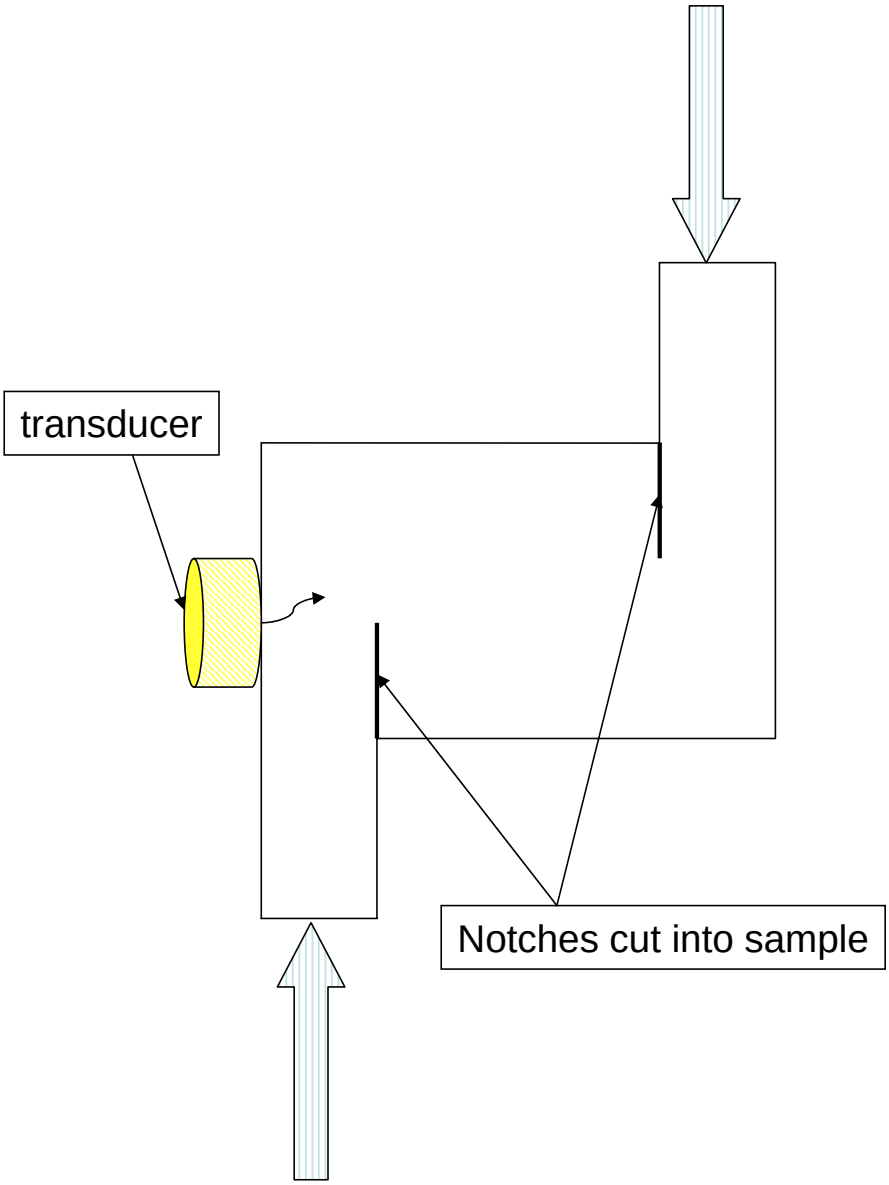

Figure 7.4: Pure shear: by placing the sample in compressing where the arrows are a "gauge" section of pure shear between the notches can be created.

sound velocity attenuated out at temperatures 70–100K above the glass transition temperature when using a 25-MHz transducer.

With a high-enough frequency transducer it would be possible to both probe higher into the SCLR as well as potentially completely melt the sample (as in Electrostatic Levitation Experiments(81)) and then undercool the liquid into the glassy region. Using a very high frequency transducer it might be possible to measure elastic properties in this undercooled liquid region.

7.2.3 Frequency Dependence of the Elastic Properties in the SCLR

Another interesting project to tackle would be to study the frequency dependence of the elastic properties in the supercooled liquid region. This could either be done by doing a series of measurements with transducers of varying frequencies, or by obtaining a transducer with a tuneable frequency range. From the acoustic attenuation, more information could be gathered about the β-relaxation, or the "slow" relaxations of the liquid.

7.2.4 Other Elastic Properties

It would be of value to perform *in situ* longitudinal sound velocity measurements of the BMGs studied in this thesis. Due to material availability constraints *in situ*, longitudinal measurements were not performed. The palladium- and platinum-based glassy samples were recast a few times for repeated *in situ* shear measurements,

however it is believed that after a few recastings a significant amount of phosphorous is lost and the alloy composition has changed slightly. Therefore the samples were not used for longitudinal measurements.

7.2.5 Viscosity/Shear Modulus Connection

To further study the viscosity/shear modulus connection proposed in this thesis and elsewhere it would be beneficial to study a glass for which good viscosity data exists for both low temperature (via parallel plate rheometry and beam bending) and high temperature (via electrostatic levitation). It would also be beneficial to be able to probe further into the SCLR, which could most likely be accomplished with higher frequency transducers. An appropriate alloy for this would be Gang Duan's GHDT (Gang's High Delta-T) alloy; there exists good viscosity data for it, and it should be simple to make a sample with the appropriate geometry for *in situ* notched measurements.

Appendix A

Raw Data Used Throughout Thesis

This appendix contains the raw data for the graphs provided throughout this thesis.

time (s)	temp (K)	ρ $\frac{g}{cm^3}$	G (GPa)	error	K (GPa)
0	652	6.038	32.73329	0.52	109.28749
900	569	6.054	34.48983	0.51	110.55314
1800	569	6.054	34.58984	0.5	110.65314
2700	567	6.044	34.60807	0.38	110.46677
3600	567	6.036	34.61807	0.25	110.36677
5400	567	6.063	34.89807	0.38	110.86677
7200	567	6.041	34.73806	0.23	110.36677
10800	567	6.027	34.80806	0.38	110.16677
14400	567	6.02	34.81807	0.23	110.26676
21600	567	6.084	35.19807	0.21	111.46677
36000	567	6.073	35.30806	0.16	111.46677
–	–	–	–	–	–
36900	648	6.073	32.80975	0.23	109.97475

Table A.1: Vitreloy-4 *ex situ* data used in Chapter 3 for relaxation figure

It is thought that the relaxation time for (*) the sample quenched from 671K is faster than the time it took to quench the sample, therefore this point was excluded from computations in the thesis.

	temp K	ρ $\frac{g}{cm^3}$	G GPa	K GPa
quenched from around T_g	567	6.08	35.41 ±0.19	110.89 ±0.72
	586	6.087	34.99 ±0.16	111.14 ±0.71
	599	6.057	34.43 ±0.14	110.55 ±0.59
	623	6.031	33.74 ±0.229	108.90 ±0.848
	646	6.026	33.19 ±0.13	108.34 ±0.58
	648	6.073	32.81 ±0.25	110.01 ±0.96
	653	6.059	32.65 ±0.33	108.76 ±0.96
	665	6.004	31.97 ±0.1	106.91 ±0.4
	671*	6.041	32.05 ±0.35	108.25 ±1.18
quenched from 579 K *in situ* low T measurement	298	6.073	37.76 ±0.16	112.95 ±0.69
	273	6.078	38.1 ±0.19	113.68 ±0.76
	248	6.083	38.34 ±0.2	113.09 ±0.85
	238	6.085	38.47 ±0.18	113.73 ±0.81
	228	6.087	38.52 ±0.42	113.86 ±0.85
	218	6.089	38.73 ±0.71	113.74 ±1
	207	6.092	38.7 ±0.3	114.07 ±0.76
	195	6.094	38.78 ±0.24	114.09 ±0.84
	77	6.118	39.89±0.25	114.87 ±0.8
quenched from 663 K *in situ* low T measurement	298	5.981	34.84 ±0.20	109.60 ±0.82
	273	5.986	35.17 ±0.21	109.53 ±0.82
	248	5.991	35.53 ±0.18	109.76 ±0.90
	233	5.994	35.57 ±0.20	109.90 ±0.85
	208	5.999	35.79 ±0.19	110.29 ±0.84
	196	6.001	35.82 ±0.20	110.30 ±0.90
	78	6.025	36.84 ±0.20	110.82 ±0.97

Table A.2: Vitreloy-4 *ex situ* data used in Chapter 3

	temp (K)	G (Gpa)
Pd quenched from 300C	295	35.99264
	283	36.09144
	273	36.22839
	263	36.34365
	253	36.2361
	243	36.51842
	232	36.71022
	223	36.8711
	212	37.03427
	203	37.16012
	197	37.09981
Pd quenched from 350C	294	34.68757
	283	34.86785
	273	35.03373
	262	35.22399
	253	35.28259
	243	35.4391
	232	35.5652
	222	35.69034
	210	35.80849
	201	35.86703
Pd quenched around Tg	531	33.66
	573	32.11
	597	31.17
	623	29.84

Table A.3: Raw data for *ex situ* measurement of $Pd_{43}Ni_{10}Cu_{27}P_{20}$. Data utilized in Chapter 3

	temp (K)	G (Gpa)
$Au_{52}Pd_{2.3}Cu_{29.2}Si_{16.5}$	291	27.68
	281	27.38
	273	27.89
	263	27.7
	253	27.87
	242	28.19
	233	28.3
	222	28.45
	212	28.6
	202	28.7
	273	27.69
	303	27.58
	312	27.48
	323	27.11
	333	26.98
	343	26.81
	353	26.54
	363	26.25
	373	26.08
	384	25.95

Table A.4: $Au_{52}Pd_{2.3}Cu_{29.2}Si_{16.5}$ *in* data used in Chapter 4

temp (K)	G (Gpa)	K (GPa)
292	25.37 (±1.6)	135.94 (±11.12)
273	25.64 (±1.7)	142.77 (±11.58)
263	25.9979 (±1.70)	139.59 (±11.47)
249	26.19 (±1.70)	139.18 (±11.61)
239	25.97 (±1.69)	138.28 (±11.34)
223	26.46 (±1.76)	141.11 (±11.70)
209	28.05 (±1.81)	136.91(11.44±)
196	28.29 (±1.83)	137.24 (±11.47)
302	24.81 (±1.60)	
311	24.67 (±1.60)	
321	24.51 (±1.59)	
331	24.39 (±1.57)	
341	24.09 (±1.56)	
351	23.84 (±1.54)	
361	22.99 (±1.49)	
371	21.79 (±1.41)	
381	21.01 (±1.36)	
389	25.24 (±1.63)	
397	26.86 (±1.99)	
410	29.29 (±3.29)	

Table A.5: $Au_{55}Cu_{25}Si_{20}$ *in* data used in Chapter 4

	temp (K)	G (Gpa)
below RT measure 1	292	35.58364
	283	35.66533
	273	35.81919
	263	35.89503
	253	36.06713
	243	36.13861
	233	36.32636
	223	36.486
	212	36.56275
	202	36.67337

Table A.6: Raw data for first low temperature *insitu* measurement of $Pd_{43}Ni_{10}Cu_{27}P_{20}$ using a notched-sample. Data utilized in Chapter 5

	temp (K)	G (Gpa)
up 1	296	35.48937
	303	35.47411
	314	35.36828
	323	35.24654
	334	35.11909
	344	35.00978
	353	34.89684
	363	34.77235
	374	34.64708
	383	34.53992
	404	34.33766
	416	34.21947
	430	34.08778
	443	33.87088
	454	33.96243
	463	33.68667
	473	33.56636
	488	33.35281
	498	33.23855
	506	33.09554
	513	32.95087
	524	32.79779
	538	32.63421
	553	32.21432
	571	31.63317
	580	31.28962
	593	30.65796
	603	29.81559
	613	29.05621
	623	28.57605
down 1	560	31.78526
	552	32.10213
	542	32.39524
	500.5	33.28298
	480.5	33.73789
	462	34.19926
	387	35.02436
	363	35.2689
	351.5	35.43088
	333	35.62118
	321	35.75765
	313	35.86724

Table A.7: Raw data for first *insitu* measurement of $Pd_{43}Ni_{10}Cu_{27}P_{20}$ Data utilized in Chapter 5

	temp (K)	G (Gpa)
	297	36.39947
	303	36.44485
	313	36.17474
	323	36.22495
	333	36.06041
	342	35.95741
	360	35.75488
	368	35.63684
	383	35.32959
	393	35.29509
	403	35.16167
	413	35.10182
	423	34.8979
	433	34.87874
	443	34.60229
	453	34.44337
up 2	463	34.2593
	473	34.08893
	483	33.87924
	493	33.66119
	503	33.51196
	514	33.46017
	523	33.0706
	533	32.82103
	543	32.60297
	553	32.37355
	560	32.1922
	575	31.76172
	583	31.44908
	593	30.88289
	603	30.21278
	613	29.84333
	623	29.28684

Table A.8: Raw data for second *insitu* measurement of $Pd_{43}Ni_{10}Cu_{27}P_{20}$ Data utilized in Chapter 5

	temp (K)	G (Gpa)
first-heat	302	36.87562
	313	36.76262
	323	36.72329
	333	36.57658
	343	36.51878
	354	36.3852
	363	36.37439
	373	36.23046
	383	36.20117
	393	36.05788
	403	36.04086
	413	35.88966
	423	35.86733
	433	35.71716
	443	35.68298
	453	35.54845
	463	35.50202
	473	35.40168
	487	35.36307
	503	35.23982
	518	35.24286
	553	35.00363
	568	34.81916
	584	34.67866
	603	34.35931
	633	33.3271
	643	33.00926
	653	32.2301
	663	31.72159
	673	31.44534
	682	31.37942
	690	30.9452

Table A.9: Raw data for first heat up *insitu* measurement of Vit-4 Data utilized in Chapter 5

	temp (K)	G (Gpa)
first-cool	602	34.41919
	588	34.59234
	573	34.89462
	551	35.03606
	532	35.34191
	518	35.43351
	503	35.74916
	483	35.81062
	463	35.98399
	443	36.21371
	418	36.43832
	403	36.49755
	392	36.78876
	381	36.65106
	368	36.98883
	358	36.97014
	348	37.18894
	338	37.04135
	328	37.27681
	318	37.74707
below RT	289	37.67488
	278	37.79953
	273	37.8234
	263	37.89281
	253	37.99392
	243	38.07541
	232	38.18568
	222	38.25257
	213	38.35791
	203	38.44957

Table A.10: Raw data for first-cool down *insitu* measurement of Vit-4 Data utilized in Chapter 5

	temp (K)	G (Gpa)
second heat	296	37.67649
	303	37.60464
	313	37.52503
	324	37.43163
	333	37.05758
	344	36.95239
	353	36.86785
	363	36.79318
	374	36.67642
	383	36.61338
	393	36.53564
	403	36.48232
	412	36.62466
	423	36.20803
	433	36.08934
	443	36.00677
	453	36.37551
	463	35.97897
	473	35.76807
	483	35.70824
	493	35.65238
	502	35.61342
	513	35.42794
	523	35.28185
	533	35.21466
	543	35.15443
	553	34.98145
	563	34.85331
	573	34.75314
	583	34.55588
	602	34.41189
	623	34.0678
	633	33.63608
	643	33.29753
	653	32.79695
	663	32.36095
	673	32.16158
	683	31.84416
	693	31.66044
	703	31.78825
	713	31.04972
	723	29.85022

Table A.11: Raw data for second *insitu* measurement of Vit-4 Data utilized in Chapter 5

	temp (K)	G (Gpa)
below RT	295	33.15869
	283	33.25892
	273	33.339
	263	33.45884
	253	33.6449
	238	33.77207
	223	33.87518
	208	34.07141
	197	34.09158
	81	35.30846
up 1	294	33.10209
	301	33.0627
	310	32.9885
	321	32.87135
	330	32.76817
	341	32.64994
	351	32.53283
	359	32.39799
	371	32.27397
	381	32.15208
	390	32.03416
	400	31.93798
	410	31.83241
	419	31.72435
	433	31.61566
	444	31.49529
	455	31.30687
	465	31.26048
	474	31.00978

Table A.12: Raw data for second *insitu* measurement of Pt Data utilized in Chapter 5

	temp (K)	G (Gpa)
down 1	477	31.14015
	466	31.41289
	457	31.5812
	449	31.75848
	441	31.8842
	429	32.08582
	420	32.18004
	410	32.32504
	401	32.45612
	390	32.58112
	380	32.71501
	371	32.79527
	360	32.92986
	350	33.02791
	339	33.16717
	330	33.26739
	320	33.37782
	311	33.46876
	305	33.53416
up 2	304	33.53587
	312	33.49373
	323	33.39058
	332	33.34468
	342	33.16837
	351	33.12906
	361	32.94601
	371	32.89588
	380	32.7076
	388	32.67507
	399	32.47483
	408	32.36843
	418	32.32019
	428	32.10372
	438	32.04965
	448	31.75807
	458	31.65922
	468	31.36342
	476	31.2868

Table A.13: Raw data for second *insitu* measurement of Pt Data utilized in Chapter 5

	temp (K)	G (Gpa)
down 2	470	30.64872
	457	30.87306
	445	31.10677
	429	31.54443
	408	31.71097
	386	31.97689
	375	31.85923
	358	32.10225
	349	32.20224
	341	32.28284
	324	32.46444
	312	32.59524
	307	32.63617
up 3	302	33.1143
	312	33.00739
	322	32.96685
	332	32.78485
	342	32.74542
	351	32.5441
	360	32.49815
	371	32.29783
	381	32.31547
	391	32.12847
	401	32.09898
	414	31.85397
	423	31.81537
	432	31.58593
	443	31.54444
	453	31.26734
	462	31.24339
	475	30.79009
below RT	296	33.59248
	284	33.71287
	273	33.86548
	262	34.05617
	253	34.16542
	241	34.34757
	230	34.46097
	221	34.57061
	211	34.72467
	203	34.80179

Table A.14: Raw data for second *insitu* measurement of Pt Data utilized in Chapter 5

	temp (K)	G (Gpa)
recast up 1	296	33.54912
	303	33.45035
	312	33.4017
	323	33.16849
	332	33.1374
	342	32.91724
	353	32.78322
	364	32.58778
	373	32.62445
	383	32.33864
	393	32.31097
	403	32.1343
	414	32.00841
	423	32.07532
	433	31.76648
	442	31.71531
	453	31.50244
	463	31.40298
	473	30.97441
below RT	293	33.90852
	283	34.08923
	273	34.23272
	263	34.34678
	253	34.54364
	243	34.66153
	233	34.82639
	223	34.90266
	213	35.06396
	203	35.22892
	77	36.34599

Table A.15: Raw data for second *insitu* measurement of Pt Data utilized in Chapter 5

	temp (K)	G (Gpa)
up	298	33.68044
	297	33.68395
	303	33.61008
	313	33.5342
	323	33.33642
	333	33.24906
	343	33.03549
	354	32.91378
	364	32.77534
	373	32.75658
	384	32.51865
	393	32.49399
	403	32.29044
	413	32.30473
	423	32.04259
	433	32.09641
	443	31.83423
	453	31.84619
	463	31.70828
	473	31.46491
down	453	31.54883
	442	31.52425
	428	32.1221
	413	32.09741
	397	32.39583
	383	32.49536
	373	32.71111
	353	33.27713
	343	33.59026
	333	33.61646
	328	33.67586

Table A.16: Raw data for second *insitu* measurement of Pt Data utilized in Chapter 5

	temp (K)	G (Gpa)
up	298	34.01433
	303	33.98378
	313	33.83026
	323	33.71702
	333	33.54035
	343	33.45704
	355	33.19669
	363	33.22613
	373	32.95389
	383	32.85135
	393	32.89061
	405	32.61134
	413	32.36073
	423	32.42679
	433	32.09758
	443	32.30637
	453	31.65473
	463	31.74866
	473	31.60882

Table A.17: Raw data for second *insitu* measurement of Pt Data utilized in Chapter 5

Appendix B

Adhesive Charts

Adhesive test results

Material	Manufacturer	Transmit?	Low T °C	High T °C	Removal
super glue	Krazy	yes	25	50	acetone, force
crystal bond		yes	25	70	acetone or heat
SuperLock 2277	Devcon	yes	25	50	acetone, heat
SuperLoc 2609	Devcon	yes	25	50	acetone, heat
Mylar A	Dupont-Teijin polymer	yes	25	100	heat
High Quality S-250A Clear Sanding Resin with catalyst	Big Swell	yes	0	150	acetone, cold
Torr-Seal	Varian	yes	-195.8	50	acetone, force, prolonged exposure to LN2

Table B.1: Tested Adhesives and Cements that Work

Material	Manufacturer	Transmit?	Removal
candle wax		No	force, heat
Structural Adhesive	Scotch-Weld	No	
The Welder	NY Bronze Powder Co.	No	
2216	3M Scotch Weld	No	
101Br Ultra-Copper High Temp RTV Silicone	Permatex	No	
UHU	Alles-Kleber	No	
S00601 Red Insulating Varnish	Sherwin-Williams	No	
Resbond 907GF adhesive sealing putty	Cotronics	No	
Resbond 907 Green Thread Locking	Cotronics	No	
Resbond 797	Cotronics	No	force
Resbond 940LE	Cotronics	No	
In solder		no, would not wet quartz	

Table B.2: Tested Adhesives and Cements that Do Not Work

Appendix C

Catalogue of Ultrasonic Measured Properties for Glasses

Unless otherwise noted, the results presented in this table are for "as-cast" alloys, most of these alloys were cast by copper-mold casting in the"casting box" in Keck 320. The density of the samples was measured via Archimedes principle according to American Society for Testing of Materials (ASTM) standard C 693-93, on occasion the density was estimated from that of the pure elements. To my best knowledge the alloys in the following table were glassy at the time of measurement.

Alloy	d (mm)	ρ $\frac{g}{cm^3}$	G GPa	K GPa	ν	C_s $\frac{m}{s}$	C_l $\frac{m}{s}$
$Zr_{55}Be_{25}Cu_{20}$	1	6.245 (0.104)	33.72 (0.82)	108.05 (2.75)	0.359 (0.004)	2323.7 (29.2)	4949.7 (14.6)
$Zr_{60}Be_{27.5}Cu_{12.5}$		6.049 (0.040)	32.75 (0.33)	120.19 (1.32)	0.375 (0.002)	2326.9 (12.7)	5204.8 (14.8)
$Zr_{55}Be_{27.5}Cu_{17.5}$		6.212 (0.024)	33.80 (0.13)	108.62 (0.64)	0.359 (0.001)	2332.5 (1.8)	4973.8 (5.0)
$Zr_{57.5}Be_{22.5}Cu_{20}$		6.279 (0.026)	30.92 (0.14)	106.17 (0.64)	0.367 (0.001)	2219.0 (3.4)	4845.0 (2.9)
$Zr_{57.5}Be_{25}Cu_{17.5}$		6.195 (0.011)	31.54 (0.07)	105.09 (0.31)	0.364 (0.000)	2256.5 (2.6)	4873.7 (3.9)
$Zr_{57.5}Be_{27.5}Cu_{15}$		6.142 (0.024)	32.50 (0.13)	105.63 (0.67)	0.360 (0.001)	2300.2 (2.1)	4924.7 (7.0)
$Zr_{60}Be_{20}Cu_{20}$		6.454 (0.016)	30.30 (0.09)	106.05 (0.49)	0.370 (0.001)	2166.6 (2.4)	4763.5 (7.0)
$Zr_{65}Be_{15}Cu_{10}$		5.952 (0.168)	30.53 (0.87)	103.11 (4.15)	0.365 (0.007)	2264.7 (8.1)	4915.4 (7.4)
$Ti_{45}Zr_{20}Be_{35}$		4.587 (0.023)	35.70 (3.60)	95.40 (16.83)	0.334 (0.028)	2789.8 (198.4)	5583.4 (453.6)
$Ti_{30}Zr_{35}Be_{35}$		4.906 (0.057)	36.37 (0.56)	111.37 (2.75)	0.353 (0.004)	2722.8 (19.6)	5708.6 (49.3)
$Ti_{11}Zr_{54}Be_{22.5}Cu_{12.5}$		5.991 (0.009)	30.29 (0.07)	103.48 (0.31)	0.367 (0.000)	2248.4 (2.7)	4900.3 (5.0)
$Ti_{9}Zr_{51}Be_{25}Cu_{15}$		5.972 (0.010)	31.76 (0.07)	104.29 (0.34)	0.362 (0.001)	2306.1 (2.5)	4955.1 (5.7)
$Ti_{30}Zr_{35}Be_{27.5}Cu_{7.5}$		5.424 (0.014)	31.83 (0.10)	102.89 (0.47)	0.360 (0.001)	2422.7 (3.2)	5176.5 (6.9)
$Ti_{45}Zr_{20}Be_{30}Cr_{5}$		4.764 (0.034)	39.23 (0.81)	114.51 (3.71)	0.346 (0.005)	2869.5 (39.6)	5917.3 (85.9)
$Cu_{40}Zr_{50}Ag_{10}$	1.7365 (0.0015)	7.554 (0.046)	31.56 (0.20)	117.2 (1.0)	0.376 (0.001)	2044.0 (2.1)	4591.4 (4.6)
$Zr_{55}Be_{20}Cu_{25}$	1.3911 (0.0015)	6.465 (0.044)	33.50 (0.23)	112.4 (1.2)	0.364 (0.002)	2276.3 (3.1)	4929.0 (12.5)
$Zr_{55}Be_{22.5}Cu_{22.5}$	2.1196 (0.0034)	6.369 (0.021)	33.13 (0.13)	109.0 (3.7)	0.362 (0.005)	2280.7 (3.9)	4904.4 (82.5)
$Zr_{52.5}Be_{20}Cu_{27.5}$	1.3119 (0.0022)	6.476 (0.054)	34.37 (0.36)	113.9 (1.6)	0.363 (0.002)	2303.9 (10.3)	4966.7 (16.7)
$Zr_{52.5}Be_{22.5}Cu_{25}$	1.6713 (0.0000)	6.407 (0.024)	33.84 (0.14)	110.1 (0.6)	0.361 (0.001)	2298.4 (3.0)	4922.3 (4.5)
$Zr_{52.5}Be_{25}Cu_{22.5}$	1.4084 (0.0055)	6.280 (0.023)	35.02 (0.24)	111.5 (1.1)	0.358 (0.002)	2361.4 (9.8)	5019.5 (20.8)
$Zr_{52.5}Be_{27.5}Cu_{20}$	2.3216 (0.0000)	6.178 (0.089)	36.10 (9.97)	110.1 (10.2)	0.352 (0.021)	2417.3 (471.4)	5061.1 (3.0)

Table C.1: Ultrasonic Material Properties of Zr-Be based alloys created by Gang Duan

Alloy	d (mm)	ρ $\frac{g}{cm^3}$	G GPa	K GPa	ν	C_s $\frac{m}{s}$	C_l $\frac{m}{s}$
dg269		6.414 (0.029)	36.57 (0.24)	117.95 (0.89)	0.359 (0.001)	2387.9 (8.1)	5098.3 (9.1)
dg303		5.359 (0.010)	34.04 (0.09)	105.08 (0.40)	0.354 (0.001)	2520.4 (3.7)	5298.9 (7.1)
dg302		5.931 (0.012)	28.50 (0.10)	100.04 (0.45)	0.370 (0.001)	2192.3 (4.4)	4824.6 (8.6)

Table C.2: Unpublished alloy results from Gang Duan

Appendix D

Error Propagation

This section briefly demonstrates how to calculate error propagation through ultrasonic measurements. It is important to note that measurement errors in parameters like sample thickness and density can have large effects on the final value determination.

This is by no means a comprehensive introduction to either statistics or error, but simply a quick overview explaining how the error was calculated in this thesis. For more complete introduction to error and statistical analysis the books by Bevington and Skoog are referenced for the reader. (82, 9)

D.1 Basic Concept of Error

Typically quantities are measured in the laboratory, and then these quantities are used to calculate things of interest (e.g. shear modulus, bulk modulus). When measuring a quantity in the laboratory, there are two main types of uncertainty: instrumental and statistical. Instrumental uncertainty are fluctuations in readings of an instrument due to either the human effect, imperfections in the equipment or some combination

of both. Statistical uncertainty

D.2 Basic Formula

$$\lambda f = \sqrt{\sum_{i=1}^{n} \left[\frac{\partial f}{\partial x_i} \lambda x_i \right]^2} \tag{D.1}$$

$f = f(x_1, x_2, x_3, ..., x_n)$ λf = error in f λx_i = error in x_i

Type of Calculation	Example	Standard Deviations
addition or subtraction	$y = a + b - c$	$s_y = \sqrt{s_a^2 + s_b^2 + s_c^2}$
multiplication or division	$y = a \cdot b/c$	$\frac{s_y}{y} = \sqrt{(\frac{s_a}{a})^2 + (\frac{s_b}{b})^2 + (\frac{s_c}{c})^2}$
exponentiation	$y = a^x$	$\frac{s_y}{y} = \sqrt{x \frac{s_a}{a}}$
logarithm	$y = \log_{10} a$	$s_y = 0.434 \frac{s_a}{a}$
antilogarithm	$y = antilog_{10} a$	$\frac{s_y}{y} = 2.303 s_a$

Table D.1: Error Propagation in Arithmetic Calculations table reproduced from (9)

D.3 Density

from American Society for Testing of Materials (ASTM) standard C-693

$$\rho = \frac{W_a \rho_w - W_w \rho_a}{W_a - W_w} \tag{D.2}$$

W_a is the weight of the sample in air, W_w is the weight of the sample in water, ρ_w is the density of the water, and ρ_a is the density of the air.

D.4 Shear Modulus

The shear sound velocity as defined in Section 1.2 is :

$$C_t = \sqrt{\frac{\mu}{\rho}} = \sqrt{\frac{G}{\rho}} \tag{D.3}$$

The error in measurement, λ_{C_t}, for the shear sound velocity is

$$\lambda_{C_t} = C_t \sqrt{\left(\frac{\lambda_d}{d}\right)^2 + \left(\frac{\lambda_{t_s}}{t_s}\right)^2} \tag{D.4}$$

where C_t is the calculated shear sound velocity, d is the measured thickness of the sample, λ_d is error in the measured thickness of the sample, t_s is the measured time for the signal to travel through the sample and λ_{t_s} is the measured error for the shear traveling time

$$\lambda_G = G \sqrt{2\left(\frac{\lambda_{C_t}}{C_t}\right)^2 + \left(\frac{\lambda_\rho}{\rho}\right)^2} \tag{D.5}$$

Following Equation D.1 the error can be propagated very easily for the longitudinal sound velocity, bulk modulus, Possion ratio, and any other quantity for which calculation is desired.

Appendix E

Matlab Script

This the the Matlab program and function referred to in Section 2.1. The function estimate delay ft may be used independently of the main program. The inputs to the function are two 2x2 arrays of times and voltages, and the outputs are the cross-correlated time to overlap the two input arrays; this is also displayed in a graph for a visual check to ensure the cross-correlation was indeed successful. To use the main program, the files must be names sequentially; the the program utilized the function to process a batch of stored wavefunctions. The purpose of the fast fourier transform in the estimate delay function is to provide a quick check that the signal captured was indeed the intended signal - the FFT spectrum should be centered around the operating frequency of the transducer; if the FFT is not found to be so, most likely the measurement should be discarded and taken again.

```
0001 close all;
0002 clear all;
0003 format long;
0004
0005 outputfilename =input('Please enter full path name for output: ','s');
0006
0007 outfile = fopen(outputfilename, 'at');
0008 fprintf(outfile, '\n\n');
0009 fprintf(outfile, 'name       average round trip delay time     stdev\n\n')
```

```
0010
0011 firstwave = input('Enter full path of 1st reflec.,non-seq. part: ', 's');
0012
0013 totalmeas = input('Please enter total number of measurements: ');
0014 numreflec = input('Please enter number of reflections: ');
0015
0016 %file read in loop created by N. Lundbliggity!
0017
0018 for i = 1:totalmeas
0019     for j = 1:numreflec
0020
0021
0022 filenamestring = ['''' firstwave num2str(i) '_R' num2str(j) ''''];
0023 eval(['array' num2str(i) '_' num2str(j) ' = spcread(' filenamestring ');'])
0024
0025
0026     end
0027 end
0028
0029 n = 1;
0030 for i = 1:totalmeas
0031      for j = 2:numreflec
0032
0033        [delay(n)] = (eval(['estimate_delay_ft(array' num2str(i) '_1'  ',arr
0034            num2str(i) '_' num2str(j) ');' ]))/(j-1);
0035         n = n+1;
0036      end
0037 end
0038
0039 avg = mean(delay)
0040 stdev = std(delay)
0041
0042 fprintf(outfile, '%s                    %f              %f\n',firstwave,
0043 avg, stdev);
0044
0045 fclose(outfile);
```

Function Estimate Delay FT that is called by main program

```
0001 function timeDelay = estimate_delay(X,Y)
0002
0003 % make sure that X is the input
0004 if (X(1,1) > Y(1,1))
0005    temp = Y;
```

```
0006     Y = X;
0007     X = temp;
0008 end
0009
0010 % compute the total length of the vectors
0011 totalSamples = max(length(X), length(Y));
0012 timeStep = X(2,1)-X(1,1);
0013
0014 % compute the cross-correlation and find the max
0015 Z = xcorr(X(:,2), Y(:,2));
0016 [maxZ, maxInd] = max(Z);
0017
0018 % compute the associated time-delay
0019 indexDelay = totalSamples - maxInd;
0020 timeDelay = indexDelay*timeStep + Y(1,1) - X(1,1);
0021
0022 % plot stuff
0023 plotMyStuff(X,Y,Z,indexDelay, timeDelay);
0024
0025 function [ ] = plotMyStuff(X,Y,Z,indexDelay, timeDelay)
0026
0027 % plot the input
0028 figure(1)
0029 subplot(2,2,1)
0030 plot(X(:,1), X(:,2))
0031 xlabel('time')
0032 ylabel('amplitude')
0033 title('Input Waveform')
0034
0035 % plot the received wave
0036 subplot(2,2,2)
0037 plot(Y(:,1), Y(:,2))
0038 xlabel('time')
0039 ylabel('amplitude')
0040 title('Received Waveform')
0041
0042 % plot the correlation analysis
0043 subplot(2,2,3)
0044 plot([1:length(Z)]-length(X), Z)
0045 xlabel('offset')
0046 ylabel('correlation')
0047 title('Signal Cross-Correlation')
0048
0049 % plot the alleged overlap
```

```
0050 subplot(2,2,4)
0051
0052 if (indexDelay >= 0)
0053     plot(X(:,2))
0054     hold on
0055     plot(Y(indexDelay+1:end,2),'r')
0056 else
0057     plot(X(abs(indexDelay):end,2))
0058     hold on
0059     plot(Y(:,2),'r')
0060 end
0061
0062 xlabel('shifted time')
0063 ylabel('amplitude')
0064 title(['Optimal Time-Delay: ', num2str(timeDelay), 'ms'])
0065 legend('Input', 'Received')
0066 hold off
0067
0068
0069
0070 A = fft(X(:,2));
0071 As = A.*conj(A);
0072 B = fft(Y(:,2));
0073 Bs = B.*conj(B);
0074
0075 ts = round((X(2,1)-X(1,1))*10)/10;
0076 freqstep = 1/(ts*10^-6*length(X));
0077 freq = (1:freqstep:(length(X)*freqstep));
0078
0079 figure(2)
0080 subplot(2,1,1)
0081 plot(freq(1:50),As(1:50));
0082 xlabel('R1 frequency');
0083
0084 subplot(2,1,2)
0085 plot(freq(1:50),Bs(1:50));
0086 xlabel('R2 frequency');
```

Bibliography

[1] J. Schroers, B. Lohwongwatana, W.L. Johnson, and A. Peker. Gold based bulk metallic glass. *Applied Physics Letters*, 87:061912, 2005.

[2] R. Busch, E. Bakke, and W.L. Johnson. Viscosity of the supercooled liquid and relaxation at the glass transition of the $zr_{46.75}ti_{8.25}cu_{7.4}ni_{10}be_{27.5}$ bulk metllic glass forming alloy. *Acta Materialia*, 46:4725, 1998.

[3] P. Debenedetti and F. Stillinger. Supercooled liquids and the glass transition. *Nature*, 410:259, 2001.

[4] R. Busch, J. Schroers, and W.H. Wang. Thermodynamics and kinetics of bulk metallic glass. *Materials Research Society Bulletin*, 32:620–623, 2007.

[5] G. J. Fan, H.-J. Fecht, and E. J. Lavernia. Viscous flow of the pd43ni10cu27p20 bulk metallic glass-forming liquid. *Applied Physics Letters*, 84:487–489, 2004.

[6] W.L. Johnson, M.D. Demetriou, J.S. Harmon, M.L. Lind, and K. Samwer. Rheology and ultrasonic properties of metallic glass-forming liquids: A potential energy landscape perspective. *Materials Research Society Bulletin*, 32:644–650, 2007.

[7] J.S. Harmon. *Experimental Studies of Elasticity, Plastic Flow, and Anelasticity in Metallic-Glass-Forming-Liquids*. PhD thesis, California Institute of Technology, May 2007.

[8] B. Zhang, H. Y. Bai, R. J. Wang, and Y. Wu andW. H. Wang. Shear modulus as a dominant parameter in glass transitions: Ultrasonic measurement of the temperature dependence of elastic properties of glasses. 76:012201, 2007.

[9] Douglas A. Skoog, Donald M. West, and F. James Holler. *Fundamentals of Analytical Chemistry*. Saunders College Publishing, Fort Worth, TX, 7th edition, 1992.

[10] W. Klement, R.H. Willens, and P. Duwez. Non-crystalline structure in solidified gold-silicon alloys. *Nature*, 187:869–870, 1960.

[11] H.S. Chen. *Acta Metallurgica*, 22:1505, 1974.

[12] A. E. Inoue, T. Zhang, and T. Masumoto. Production of amorphous cylinder and sheet of la55al25ni20 alloy by a metallic mold casting method. *Materials Transactions, JIM*, 31:425, 1990.

[13] N. Nishiyama and A. Inoue. Glass-forming ability of bulk $pd_40ni_10cu_30pd_20$ alloy. *Materials Transactions, JIM*, 37:1531–1539, 1996.

[14] A. Inoue, N. Nishiyama, and H. Kimura. Preparation and thermal stability of bulk amorphous $pd_40ni_10cu_30pd_20$ alloy 72 mm in diameter. *Materials Transactions, JIM*, 38:179–183, 1997.

[15] A. Inoue, A. Kato, T. Zhang, S.G. Kim, and T. Masumoto. Mg-cu-y amorphous-alloys with high mechanical strengths produced by a metallic mold casting method. *Materials Transactions, JIM*, 32:609–616, 1991.

[16] A. Peker and W. L. Johnson. A highly processable metallic glass: Zr41.2ti13.8cu12.5ni10.0be22.5. *Applied Physics Letters*, 63:2342, 1993.

[17] G. Duan, D.H. Xu, and W.L. Johnson. High copper content bulk glass formation in bimetallic cu-hf system. *Metallurgical and Materials Transactions A — Physical Metallurgy and Materials Science*, 36A:455–458, 2005.

[18] D. Turnbull and J.C. Fisher. Rate of nucleation in condensed systems. *The Journal of Chemical Physics*, 17:71–73, 1949.

[19] D. Turnbull. Kinetics of heterogeneous nucleation. *The Journal of Chemical Physics*, 18:198–203, 1950.

[20] G. Duan. Bulk metallic glasses with benchmark thermoplastic processability. *Advanced Materials*, page DOI: 10.1002/adma.200700969, 2007.

[21] J. Schroers, Q. Pham, A. Peker, N. Paton, and R.V. Curtis. Blow molding of bulk metallic glasses. *Scripta Materialia*, 57:341–344, 2007.

[22] Peter J. Shull. *Nondestructive Evaluation Theory, Techniques, and Applications.* Marcel Dekker, Inc., New York, 2002.

[23] M. Goldstein. Viscoius liquids and the glass transition: A potential energy barrier picture. *The Journal of Chemical Physics*, 51:3728–3739, 1969.

[24] F.H. Stillinger and T.A. Weber. Hidden structure in liquids. *Physical Review A*, 25:978–989, 1982.

[25] F. Sciortino. Potential energy landscape description of supercooled liquids and glasses. *J. Stat. Mech*, page P05015, 2005.

[26] J.P.K. Doye and D.J. Wales. Saddle points and dynamics of lennard-jones clusters, solids, and supercooled liquids. *The Journal of Chemical Physics*, 116:3777–3788, 2002.

[27] D.J. Wales. A microscopic basis for the global appearance of energy landscapes. *Science*, 293:2067–2070, 2001.

[28] D.L. Malandro and D.J. Lacks. Relationships of shear-induced changes in the potential energy landscape to the mechanical properties of ductile glasses. *The Journal of Chemical Physics*, 110:4593–4601, 1999.

[29] D.L. Malandro and D.J. Lacks. Volume dependence of potential energy landscapes in glasses. *The Journal of Chemical Physics*, 107:5804–5810, 1997.

[30] A.S. Argon. Plastic deformation in metallic glasses. *Acta Metallurgica*, 27:47–58, 1979.

[31] A.S. Argon and L.T. Shi. Development of visco-plastic deformation in metallic glasses. *Acta Metallurgica*, 31:499–507, 1983.

[32] F. Spaepen. A mictoscopic mechanism for steady state inhomogeneous flow in metallic glasses. *Acta Metallurgica*, 25:407–415, 1977.

[33] M.L. Falk and J.S. Langer. Dynamics of viscoplastic deformation in amorphous solids. *Physical Review E*, 57:7192–7205, 1998.

[34] J.S. Langer. Dynamics of shear-transformation zones in amorphous plasticity: Formulation in terms of an effective disorder temperature. *Physical Review E*, 70:041502, 2004.

[35] W.L. Johnson and K. Samwer. A universal criterion for plastic yielding of metallic glasses with a (t/t-g)(2/3) temperature dependence. *Physical Review Letters*, 95:195501, 2005.

[36] M.L. Lind, G. Duan, and W.L. Johnson. Isoconfigurational elastic constants and liquid fragility of a bulk metallic glass forming alloy. *Physical Review Letters*, 97:015501, 2006.

[37] C.A Angell. Spectroscopy simulation and scattering, and the medium range order problem in glass. *Journal of Non-Crystalline Solids*, 73:1, 1985.

[38] S.M. Rekhson. *Glass: Science and Technology, Viscoelasticy of Glass*. Academic Press Inc., London, 1986.

[39] J.C. Dyre. Colloquium: The glass transition and elastic models of glass-forming liquids. *Reviews Of Modern Physics*, 78:953–972, 2006.

[40] R. Busch, W. Liu, and W.L. Johnson. Thermodynamics and kinetics of the mg65cu25y10 bulk metallic glass forming liquid. *Journal of Applied Physics*, 83:4134–4141, 1998.

[41] DN Perera. Compilation of the fragility parameters for several glass-forming metallic alloys. *Journal Of Physics-Condensed Matter*, 11:3807–3812, 1999.

[42] W.H. Wang. Correlations between elastic moduli and properties in bulk metallic glasses. *Journal of Applied Physics*, 99:093506, 2006.

[43] H.S. Chen, J.T. Krause, and E. Coleman. Elastic constants, hardness and their implications to flow properties of metallic glasses. *Journal of Non-Crystalline Solids*, 18:157–171, 1974.

[44] N. Morito and T. Egami. Correlation of the shear modulus and internal friction in the reversible structural relaxation of a glassy metal. *Journal of Non-Crystalline Solids*, 61-62:973, 1984.

[45] E.F. Lambson, W.A. Lambson, J.E. Macdonald, M.R. Gibbs, G.A. Saunders, and D. Turnbull. Elastic behavior and vibrational anharmonicity of a bulk pd40ni40p20 metallic glass. *Physical Review B*, 33:2380–2385, 1986.

[46] L.G. Hwa, W.C. Chao, and S.P. Szu. Temperature dependence of elastic moduli of lanthanum gallogermanate glasses. *Jounral of Materials Science*, 37:3423–3427, 2002.

[47] T. Ichitsubo, E. Matsubara, S. Kai, and M. Hirao. Ultrasound-induced crystallization around the glass transition temperature for pd40ni40p20 metallic glass. *Acta Materialia*, 52:423–429, 2004.

[48] T. Ichitsubo, S. Kai, H. Ogi, M. Hirao, and K. Tanaka. Elastic and anelastic behavior of zr55al10ni5cu30 bulk metallic glass around the glass transition temperature under ultrasonic excitation. *Scripta Materialia*, 49:267–271, 2003.

[49] T. Ichitsubo, E. Matsubara, K. Anazawa, and N. Nishiyama N. Crystallization accelerated by ultrasound in pd-based metallic glasses. *JOURNAL OF ALLOYS AND COMPOUNDS*, 434:194–195, 2007.

[50] L.M. Wang, W.H. Wang, R.J. Wang, Z.J. Zhan, D. Y. Dai, L.L. Sun, and W.K. Wang. Ultrasonic investication of pd39ni10cu30p21 bulk metallic glass upon crystallization. *Applied Physics Letters*, 77:1147, 2000.

[51] Z.X. Wang, R.J. Wang, and W.H. Wang. Elastic properties of cu60zr20hf10ti10 bulk metallic glass under high pressure. *Materials Letters*, 60:831–833, 2006.

[52] B. Zhang, R.J. Wang, and W.H. Wang. Response of acoustic and elastic properties to pressure and crystallization of ce-based bulk metallic glass. *Physical Review B*, 70:104205, 2005.

[53] L.M. Wang, L.L. Sun, W.H. Wang, R.J. Wang, Z.J. Zhan, D.Y. Dai, and W.K. Wang. Elastic constants of pd39ni10cu30p21 bulk metallic glass under high pressure. *Applied Physics Letters*, 77:3734, 2000.

[54] S. Tamura, M. Fukuhara, and A. Inoue. Changes in mechanical properties of zr-based bulk metallic glass under linear heating and cooling. *Journal of Applied Physics*, 101:073520, 2007.

[55] V.N. Novikov and A.P. Sokolov. Correlation of fragility and poisson's ratio: Difference between metallic and nometallic glass formers. *Physical Review B*, 74:064203, 2006.

[56] V.N. Novikov and A.P. Sokolov. Poisson's ratio and the fragility of glass-forming liquids. *Nature*, 431:961–963, 2004.

[57] S.N. Yannopoulos and G.P Johari GP. Glass behaviour — poisson's ratio and liquid's fragility. *Nature*, 442:E7–E8, 2006.

[58] D.P. Almond and S. Blairs. An apparatus employing the pulse-echo overlap technique for the measurement of sound velocities in liquid metals. *Journal of Physics E: Scientific Instruments.*, 13:964–968, 1980.

[59] J.T. Krause. Differential path method for measuring ultrasonic velocities in glasses at high temperatures. *Journal of the Acoustical Society of America*, 35:1, 1963.

[60] A.J. Drehman, A.L. Greer, and D. Turnbull. Bulk formation of a metallic glass: Pd40ni40p20. *Applied Physics Letters*, 41:716–717, 1982.

[61] K. Samwer, R. Busch, and W.L. Johnson. Change in compressibility at the glass transition and the prigogine-defay ratio in zrticunibe alloys. *Physical Review Letters*, 82:580, 1999.

[62] F.H. Stillinger. A topographic view of supercooled liquids and glass formation. *Science*, 267:1935, 1995.

[63] T. Waniuk, J. Schroers, and W. L. Johnson. Timescales of crystallization and viscous flow of the bulk glass formning zr-ti-ni-be alloys. *Physical Review B*, 67:184203, 2003.

[64] E. Schreiber, O. Anderson, and N. Soga. *Elastic Constants and Their Measurement*. McGraw-Hill, New York, 1973.

[65] R. Busch and W.L. Johnson. The kinetic glass transition of the zr46.75ti8.25cu7.5ni10be27.5 bulk metallic glass former-supercooled liquids on a long time scale. *Applied Physics Letters*, 72:2695, 1998.

[66] A. Masuhr. *Viscous Flow and Crystallization of Bulk Metallic Glass Forming Liquids*. PhD thesis, California Institute of Technology, 1999.

[67] Y Qi, T Cagin, WL Johnson, and WA Goddard. Melting and crystallization in ni nanoclusters: The mesoscale regime. *Journal Of Chemical Physics*, 115:385–394, 2001.

[68] J.C. Dyre, N.B. Olsen, and T. Christensen. Local elastic expansion model for viscous-flow activation energies of glass-forming molecular liquids. *Physical Review B*, 53:2171–2174, 1996.

[69] J.S. Harmon, M.D. Demetriou, W.L. Johnson, and M. Tao. Deformation of glass forming metallic liquids: configurational changes and their relation to elastic softening. *Applied Physics Letters*, 90:131912, 2007.

[70] J.S. Harmon, M.D. Demetriou, and W.L. Johnson. Rheology and ultrasonic properties of pt57.5ni5.3cu14.7p22.5 liquid. *Applied Physics Letters*, 90:171923, 2007.

[71] B. Lohwongwatana. *Development, characterization, and applications of gold and platinum bulk metallic glasses*. PhD thesis, California Institute of Technology, May 2007.

[72] M.D. Demetriou, J.S. Harmon, M. Tao, G. Duan, K. Samwer, and W.L Johnson. Cooperative shear model for the rheology of glass-forming metallic liquids. *Physical Review Letters*, 97:065502, 2006.

[73] D.Q Zhao W.H. Wang B. Zhang, M.X. Pan. Soft bulk metallic glasses based on cerium. *Applied Physics Letters*, 85:61–63, 2004.

[74] G. Duan, M.L. Lind, M.D. Demetriou, and W.L. Johnson. Strong configurational dependence of elastic properties for a binary model metallic glass. *Applied Physics Letters*, 89:151901, 2006.

[75] X.H. Liu and W.L. Johnson. Formation of ti-zr-cu-ni bulk metallic glasses.

[76] W.T Grubbs and R.A. Macphaii. Dynamics in supercooled glycerol by high-resolution stimulated brillouin gain spectroscopy. *Journal of Chemical Physics*, 100:2561–2570, 1994.

[77] Y.H. Jeong, S.R. Nagel, and S. Bhattacharya. Ultrasonic investigation of the glass transition in glycerol. *Physical Review A*, 34:602–608, 1986.

[78] N. Nishiyama, A. Inoue, and J.Z. Jiang. *Applied Physics Letters*, 78:1985, 2001.

[79] X.J. Gu XJ, S.J. Poon, and G.J. Shiflet. Mechanical properties of iron-based bulk metallic glasses. *JOURNAL OF MATERIALS RESEARCH*, 22:344–351, 2007.

[80] A. Polian, D. Vo-Thanh, and P. Richet. Elastic properties of a-sio2 up to 2300k from brillouin scattering measurements. *Europhys. Lett.*, 57:375381, 2002.

[81] S. Mukherjee. *Study of crystallization behavior, kinetics and thermodynamics of bulk metallic glasses using noncontact electrostatic levitation technique*. PhD thesis, California Institute of Technology, January 2005.

[82] P.R. Bevington and D.K. Robinson. *Data Reduction and Error Analysis for the Physical Sciences*. McGraw-Hill, Boston, MA, 2nd edition, 1992.